Master's Thesis: Mechanisms of cerebral artery compliance at sea-level and following acclimatization to high altitude.

by

Destiny Underwood

A Thesis Submitted in Partial Fulfillment of the

Requirements for the Degree of

MASTER OF SCIENCE

in the Department of Exercise Science, Physical & Health Education

University of Victoria

We acknowledge and respect the Lək^{w}əŋən (Songhees and Esquimalt) Peoples on whose territory the university stands, and the Lək^{w}əŋən and W̱ SÁNEĆ Peoples whose historical relationships with the land continue to this day.

Master's Thesis: Mechanisms of cerebral artery compliance at sea-level and following acclimatization to high altitude.

by

Destiny Underwood
B.Sc., Camosun College, 2022.

Supervisory Committee

Dr. Kurt Smith, Supervisor
Department of Exercise Science, Physical & Health Education

Dr. David Kennedy, Departmental Member
Department of Exercise Science, Physical & Health Education

Abstract

Brain health is dependent on adequate cerebral blood flow (CBF) delivered through healthy compliant vessels that buffer pulsatile hemodynamic stress. Pharmacological interventions at sea-level (SL) and high altitude (HA, 5050m) that increase and lower CBF provide a useful experimental design to assess the mechanisms involved in buffering cerebrovascular hemodynamic stress. We characterized pulsatile hemodynamic damping factors (DFi), as an index of cerebral hemodynamic stress. DFi was calculated from pulsitility (PI) in the internal carotid (ICA) and middle cerebral arteries (MCA) at SL and HA following pharmacological attempts to increase (SL=Dobutamine, DOB; HA = DOB+Actetazolamide, DOB+ACZ) and decrease (Indomethacin; INDO) CBF in healthy lowlander adults (n=12, 4 females). Cerebrovascular hemodynamics in the ICA (flow [Q_{ICA}], PI_{ICA}) and MCA (velocity [MCA_v], PI_{MCA}) were measured using ultrasound; DFi=PI_{ICA}:PI_{MCA}. Administration of DOB (2-5µg/kg/min) at SL, DOB+ACZ (5µg/kg/min+10 mg/kg) at HA, and INDO (1.45 mg/kg) at SL and HA were performed on separate days in randomized order. No Q_{ICA} response were observed following DOB, while Q_{ICA} increased following DOB+ACZ (Δ+41±24 $ml.min^{-1}$, p=0.01), and decreased following INDO at SL (Δ-53± 56 $ml.min^{-1}$,p=0.04) and HA (Δ-41± 18 $ml.min^{-1}$, p=0.004). DOB and DOB+ACZ administration differentially altered HR (Δ-3 bpm; Δ+5 bpm, p=0.02), ΔICA_V (Δ-6 ± 10 $cm.s^{-1}$; Δ+10 ± 11 $cm.s^{-1}$; p=0.04), MCAv (Δ+0 ± 10 $cm.s^{-1}$; Δ+17± 5 $cm.s^{-1}$), and PI_{ICA} (Δ+0.4 ± 0.2 a.u; Δ+0.2 ± 0.09 a.u.; p=0.03). DOB reduced DFi (Δ-0.1± 0.05, p=0.02) at SL. Meanwhile DFi following INDO was significantly lower at HA (Δ-0.54± 0.3a.u, p=0.02) but not at SL (Δ-0.26± 0.3 a.u, p=0.18). The results from these two field experiments highlights that reducing CBF via cyclooxygenase inhibition detrimental alters the buffering of

cerebrovascular hemodynamic forces. In contrast, at HA when CBF is increased following DOB+ACZ cerebrovascular hemodynamic regulation was preserved.

Table of Contents

List of Tables

List of Figures

Glossary

ACZ: Acetazolamide

AMS: Acute mountain sickness

B_p: Barometric pressure

C_aO_2: arterial oxygen content

CBF: cerebral blood flow

$CMRO_2$: Cerebral metabolic rate of oxygen

DFi: Damping factor index

DOB: Dobutamine

ECA: External carotid artery

gCBF: Global cerebral blood flow

HA: High altitude

ICA: Internal carotid artery

ICA_v: Internal carotid artery velocity (blood)

ICP: Intracranial pressure

INDO: Indomethacin

MAP: Mean arterial pressure

MCA_v: Middle cerebral artery velocity (blood)

P_aCO_2: Partial pressure of arterial carbon dioxide

P_aO_2: Partial pressure of arterial oxygen

$P_{ET}CO_2$: Partial pressure of end-tidal carbon dioxide

$P_{ET}O_2$: Partial pressure of end-tidal oxygen

PI: Pulsitility

SL: Sea level

VDu: Vascular Duplex ultrasound

Acknowledgements

My journey through academia would not be possible without all the teachers who planted a seed in my mind that I could achieve more than I ever believed. From my middle school teacher Emily Pontus, who supported me throughout my pre-teen angst, to Crystal Anderson whose unwavering support and praise furthered my expectations for my career.

I am grateful to my supervisor Kurt Smith for providing me with a roller coaster of opportunities over two action packed years. I will remember my years as a graduate student in the CHEERs lab fondly. Thank you to all my lab mates with special mention to Tabitha Craig and Brianne Smith for their contributions. Brianne works tirelessly behind the scenes to support all of us in the CHEERs lab.

I would like to acknowledge the contributions of the Centre for Heart, Lunge & Vascular Health for sharing the data from the Everest-K2 expedition, in which my supervisor completed his PhD.

Finally, I extend an enormous thank you to the WSANEC school board, Linda Gladstone, and Denise Sam. Without your funding and support I would not have access to the privilege of education I have enjoyed over the 6 years.

Dedication

To my family and community of friends that supported me while I pursued this dream. A special mention to my cheerleaders; my sister Jacqueline and brother in-law Jake, and my dear friend Holly for those times you urged me on when doubt crept in.

To my partner Reuben for having unwavering faith and weathering the storm of graduate school with me. Thank you for always sharing your laughter, I'm convinced there is no challenge we cannot manage in the face of your unparallel optimism and sense of fun.

To my aunties and uncles who sought to support in different small and large ways, knowing I was working towards my dream.

To my mom, my cheerleader since day one, whose belief in my ability to achieve anything I set my mind to borders on delusion.

Chapter 1 Introduction & Purpose

The brain has a high metabolic demand with limited capacity for fuel storage relative to its size (~2% of total body mass). The resting brain requires 15% of cardiac output and utilizes 20% of total oxygen consumption (Kety & Schmidt., 1948, Koep et al., 2022; Williams & Leggett.,1989). Continuous brain blood flow requires regulation by several integrative systems. Thus, a multi-integrative system supports a continuous brain blood flow, both at rest, and in response to environmental and systemic physiological perturbation. The primary individual stimuli responsible are the partial pressures of arterial oxygen (P_aO_2) and carbon dioxide (P_aCO_2), mean arterial blood pressure (MAP), cerebral metabolism, and the sympathetic nervous system (Willie et al., 2014). This regulation is important for humans' versatility throughout the lifespan, as well as for populations travelling and living in extreme environments like high altitude (HA).

Globally, 500.3 million people live at an altitude of ≥1,500 m, while 81.6 million people live at an altitude of ≥2,500 m (Tremblay & Ainslie, 2021). Ascent to high altitude presents a systemic physiological challenge, initiated by a reduction in barometric pressure (B_p)(Ainslie & Subhadi., 2014; Severinghaus et al., 1963). If the severity of the drop in B_P is sufficient and sustained, P_aO_2 is reduced. Systemic compensations such as increased heart rate and blood pressure, sympathetic nervous excitation, and ventilation can help to re-establish necessary arterial blood gas levels to maintain physiological function (Ainslie & Subhadi., 2014; Willie et al., 2014). However, if reductions in P_aO_2 are significant, this can trigger an increased CBF, which serves to maintain adequate oxygen and nutrient delivery. These factors have been extensively reviewed in previously published research (Ainslie & Subudhi., 2014; Lucas et al., 2011; Willie et al., 2014),

however, what remains to be investigated is how HA cerebrovascular regulation influences pulsatile hemodynamics stressors which are associated with adverse brain function (Ainslie & Ogoh., 2010; Lucas et al., 2011; Ainslie & Subudhi., 2014). Because of difficulties in conducting research at HA, CBF regulation at sea level (344m) is more comprehensively understood compared to regulation at HA. However, overlapping mechanisms promoting vasodilation and vasoconstriction are expected (Ainslie & Subudhi., 2014; Lucas et al., 2011) and likely contribute to changes in pulsatile hemodynamic stress throughout the cerebral vasculature. It is worth investigating if these overlapping regulations result in similar buffering of hemodynamics stress at SL and HA, or whether subtle alterations negatively impact cerebrovascular function at HA compared to SL. Understanding these mechanisms could have important implications for identifying deviations in healthy cerebrovascular function, especially for those living, visiting, and working at HA, and further our insight into healthy responses to HA.

Dysregulation upon ascent to HA increases the risk of developing acute mountain sickness (AMS). Individuals sojourning to HA have a 40-90% chance of developing AMS depending on the specific altitude, the rate of ascent, individual hypoxic sensitivities, and the degree of pre acclimatization (Hackett & Roach., 2001; Luks et al., 2017). Physiological manifestations of AMS such as headache and dizziness may impact systemic factors known to regulate CBF (i.e., metabolism, ventilation, acid base balance, blood pressure regulation). In addition, more than 90% of people ascending to above 5,000 m experience central sleep apnea, which can exacerbate AMS severity. Burgess et al., (2018) investigated the mechanisms of central sleep apnea at altitude by pharmacologically increasing (i.e., acetazolamide and dobutamine) and decreasing (i.e., indomethacin) cerebral blood flow as a means to understand chemoreceptive control during

sleep and found that increasing the removal of locally produced CO_2 from the central chemoreceptors via elevated CBF caused a reduction in hypercapnic ventilatory responses, and subsequently stabilized ventilation. Burgess et al., (2018) found this reduced the severity of central sleep apnea at high altitude. The key component to the Burgess et al., (2018) investigation was the use of three specific medications: 1) Acetazolamide; 2) Dobutamine; 3) Indomethacin.

Acetazolamide (ACZ) is a potent carbonic anhydrase inhibitor and is used to increase ventilation while at HA to mitigate the risk of AMS (Hackett & Roach., 2001). Initially, ACZ was given to stabilize breathing in sleep, as it makes the brain tissue acidotic which stimulates ventilation. Hypoxic induced hyperventilation leads to hypocapnia, reducing the drive to breath, resulting in sleep apnea. Thus, acetazolamide can counter the effects of hyperventilation induced hypocapnia by maintaining the drive to breathe. A side effect of the acidosis is that it causes cerebrovascular vasodilation. It is unclear what impact ACZ has on pulsatile cerebrovascular hemodynamics, but increasing acidosis in the cerebral microvasculature theoretically should cause a reduction in cerebrovascular resistance. Dobutamine (DOB), a beta-1 agonist was used by Burgess et al., (2018) to increase cardiac contractility in combination with ACZ to increase CBF and enhance central chemoreceptor CO_2 wash-out (Burgess et al., 2018). The overall increase in CBF served to stabilize the cerebral CO_2 gradient which has previously been theorized to stabilize ventilation (Hoiland et al., 2018; Hoiland et al., 2015). For the purposes of this thesis, we aimed to investigate how DOB at SL, and DOB+ACZ at HA influence pulsatile cerebrovascular hemodynamics when CBF is pharmacologically increased through upstream cardiac contractility (DOB) and downstream reductions in microvascular resistance (ACZ).

The “tight fit” hypothesis is another theory seeking to explain AMS. What it posits is that some individuals may have a predisposition for AMS because of a lower intracranial reserve volume to compensate for brain swelling at HA (Kallenberg et al., 2007; Ross., 1985). Ultimately, increasing CBF at HA in a brain that has less compensatory volume will enhance AMS symptoms influenced by brain swelling. Indomethacin (INDO), a non-steroidal anti-inflammatory medication that inhibits cyclooxygenase, can lower brain blood flow by up to 30% as a result of increased cerebral vasoconstriction induced by impaired prostaglandin synthesis or potentially another cyclooxygenase mediated pathway. Burgess et al., (2018) hypothesized that this reduction in CBF may mitigate symptoms associated with AMS referencing the “tight fit” hypothesis as the supporting rationale (Lucas., 2016; Suleyman et al., 2010; Summ & Evers., 2013).

The following thesis aims to provide details that help to understand how pharmacological interventions at sea-level (SL) and HA that increase and lower CBF provide an experimental opportunity to assess the mechanisms involved in buffering cerebrovascular hemodynamic stress. This series of experiments seeks to quantify changes in vascular compliance using a damping factor index (DFi) that accounts for pulsatile changes through large extra and intracranial cerebral arteries. We aimed to characterize pulsatile cerebrovascular hemodynamic DFi, as an index of cerebral hemodynamic buffering, by observing pulsitility (PI) in the internal carotid (ICA) and middle cerebral artery (MCA) following pharmacological increases (Experiment 1) and decreases (Experiment 2) in CBF at SL and following acclimation to HA. For experiment 1, DOB (SL) and DOB+ACZ (HA) were administered to increase cardiac output and decrease microvascular resistances. For experiment 2, the effects of CBF reductions

following INDO administration at SL and HA on pulsatile hemodynamic damping in large cerebral arteries are quantified. Specific and comprehensive details pertaining to the regulatory factors involved in cerebrovascular hemodynamic regulation will be reviewed in the following literature review (Chapter 2). Chapter 3 includes a detailed report on the methodology and experimental studies, and the finalized research paper "*Altering hemodynamic mechanisms at sea-level and high altitude"* (Chapter 4) follows. The overall summary includes a discussion (Chapter 5) outlining the primary findings and interpretations along with the strength and limitations of the research, plus conclusionary suggestions for future directions.

Chapter 2 Literature Review

The purpose of this literature review is first to provide a brief background on the anatomy of the brain's vasculature, and the history of assessing cerebrovascular function at SL and HA. Additionally, the following sections will outline the primary mechanisms, methodology, and significance associated with CBF regulation at SL and HA. The overall purpose of this thesis is to better understand the mechanisms associated with cerebrovascular stiffness and the effects of pharmacological intervention (i.e., INDO, DOB) on CBF in SL and HA conditions. The mechanisms of CBF regulation will be discussed further investigating the role of blood gases (i.e., oxygen and carbon dioxide), changes in blood pressure, cerebral metabolism of oxygen, and the autonomic nervous system, all while considering the differential impact at HA. Then mechanisms of vascular stiffness and compliance will be summarized followed by the implications for DFi. Finally, pharmacological cerebrovascular responses to DOB+ACZ and INDO will be outlined.

2.1. Cerebrovascular Anatomy

The brain contains a vast network of vessels which supplies nutrients through two major vascular sources: 1) the internal carotid arteries (ICA); and 2) the vertebral arteries (Byoun & Hwang., 2020; Duvernoy et al., 1981; Turgay., 2015). The common carotid arteries, found on either side of the neck, carry blood towards the brain originating from the aortic arch of the heart (left) and the brachiocephalic artery (right) then bifurcating at the C4 vertebral body into the internal (ICA) and external (ECA) carotid arteries (Byoun & Hwang., 2020). The ICA delivers ~80% of the blood to the brain and supplies the forebrain (Byoun & Hwang., 2020; Carr et al., 2021; Zarrinkoob et al., 2015). The ICA splits into the anterior cerebral artery, the middle cerebral artery (MCA), and the posterior communicating artery supplying the frontal, temporal, and parietal lobes, plus the diencephalon and internal capsule (Chandra et al., 2017). The vertebral arteries deliver ~20% of the brains blood and supply the posterior , originating most commonly from the supraposterior aspect of the subclavian artery supplying the occipital lobe, much of the brainstem, and the cerebellum (Cloud, G. C., & Markus, H. S., 2003; Zarrinkoob et al., 2015). The vertebral arteries merge into the basilar artery along which the bilateral anterior inferior cerebellar arteries, pontine perforating branches, and the superior cerebellar arteries originate (Krishnaswamy et al., 2010). Flow for the left and right hemisphere are connected through The Circle of Willis, as is the anterior and posterior flow (Krishnaswamy et al., 2010). The Circle of Willis is a structure within the base of the brain (**Figure 1**) comprised of the anterior cerebral artery, anterior communicating artery, ICA, posterior cerebral artery, posterior communicating artery, and the basilar artery (Chandra et al., 2017; Hoiland et al., 2019). Traveling towards the surface of the brain, arteries branch into smaller vessels arriving at the subarachnoid space where they are referred to as pial vessels (Hoiland et al., 2019). Pial vessels give rise to smaller arteries

that penetrate the brain tissue where they become parenchymal arterioles. While a majority of this thesis will focus on the functional regulation of cerebrovascular hemodynamic stress, the anatomical structures also play a crucial role in hemodynamic regulation. For instance, bifurcations provide important hemodynamic buffering. Further, the circle of Willis has multiple bifurcations, and the primary shape results in a perpendicular wall against the vertical stress from extracranial blood flows. Ultimately, this anatomical buffering is assumed as constant in longitudinal study designs as the structure is not expected to change**.**

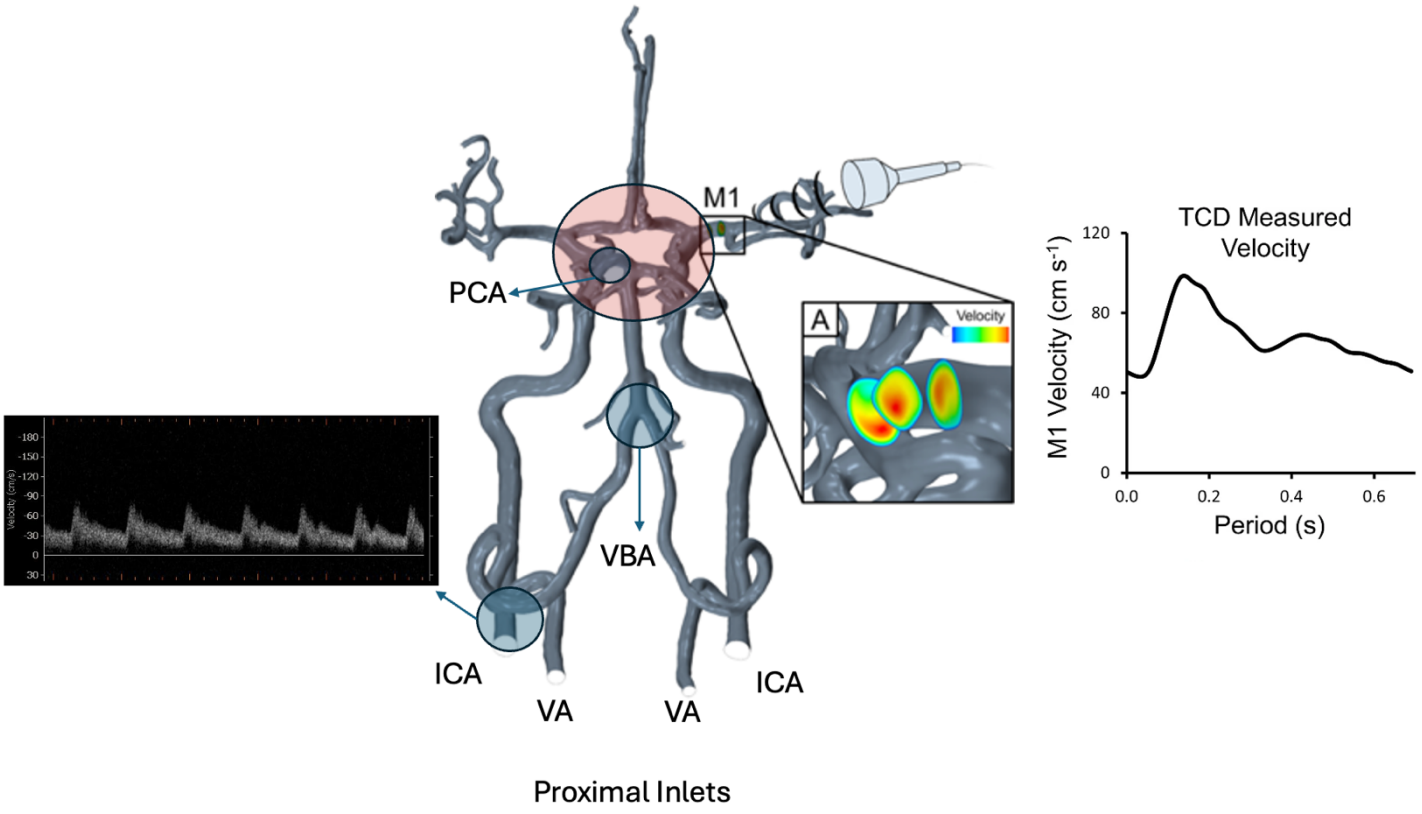

Figure 1. Computational rendering of the arterial inflows to the Circle of Willis (posterior view) and the primary arteries that branch from it. M1 velocity profile of the middle cerebral artery derived using transcranial doppler ultrasound. Inlay (A) of the M1 middle cerebral artery segment showing computationally derived circumferential velocity patterns. On the left pulse wave velocity of the internal carotid artery collected using Duplex ultrasound. Adapted with permission from Caddy et al., (2023).

2.2. Cerebral Blood Flow Regulation

This section will discuss the historical review of CBF assessment and focus on the primary regulators of CBF: section 2.2.2: partial pressure of carbon dioxide (P_aCO_2) and oxygen (P_aO_2); section 2.2.3: mean arterial pressure (MAP); section 2.2.4: cerebral metabolism; and section 2.2.5: the autonomic nervous system (ANS) (Willie et el., 2014).

2.2.1 Historical Review

Angelo Mosso, an Italian physiologist, first documented measures of CBF in humans in his study entitled "Sulla circolazione del sangue nel cervello dell'uomo" or "On the circulation of blood in the human brain" (1880) by observing pulsations in patients with skull defects using plethysmography (1846–1910) (Ainslie & Subudhi., 2014; Willie et al., 2014; Tymko et al., 2018). A decade later (1890) Charles Roy and Charles Sherrington observed changes in the brain pulsations of animals in response to stimuli such as asphyxia and demonstrated the relationship between CBF, pH, blood pressure, and neural activation (Hoiland et al., 2019; Roy & Sherrington.,1890). The next breakthrough was in 1945, Seymour Kety and Carl Schmidt developed a new technique that diverged from the reliance of skull abnormalities. The Kety-Schmidt technique uses nitrous oxide inhalation as a tracer to calculate the difference in appearance and clearance between arterial and jugular venous sampling across the brain. Mathematical interpolation of the rate of appearance and clearance using the Kety-Schmidt technique provided reliable and valid assessment of CBF in humans for the first time. While the Kety-Schmidt technique provides an accurate and valid assessment of CBF (i.e., strong spatial resolution), it does not provide sufficient temporal resolution to measure cerebrovascular function during dynamic stimulation. Regardless, thanks to these early works it was later determined that resting CBF is approximately 45-55 ml/100 g tissue/min (Lassen., 1985), and that the brain is highly sensitive to arterial blood gases and changes in metabolism (Kety &

Schmidt., 1947; Kety & Schmidt., 1948). In high altitude research Angelo Mosso was again a pioneer of CBF measures using barometric chambers to observe the physiological effects of hypobaria. In the 1980's, a century from Mosso's landmark measures, the transcranial doppler (TCD) became recognized as a viable, non-invasive method to measure the velocity of blood in cerebral arteries largely thanks to Rune Aaslid and colleagues who developed transcranial Doppler techniques still used today (Aaslid., 1986; Barlinn et al., 2022; Hoiland et al., 2019). The introduction of TCD in research was appealing for its portability, affordability, and non-invasive nature though it is not without its drawback which will be discussed in later section (i.e., section 3.1.2. *validity of TCD)*.

Today, studies such as Lefferts et al., (2020) use TCD in concert with vascular Duplex ultrasound to assess extra-intracranial changes in PI as a means of measuring hemodynamic forces (Lefferts et al., 2020). However, TCD does not provide a measure of diameter only velocity. Recently, it has been demonstrated that vascular Duplex ultrasound (VDu) can image diameter and velocity simultaneously in extracranial arteries due to the higher frequency (~7MHz) used for imaging superficial vessels (i.e., carotids). Combining TCD and VDu provides a more robust understanding of cerebrovascular hemodynamics, making it possible to image CBF as it enters the brain (VDu) and how it is distributed following its arrival in the Circle of Willis. Another promising tool is 7T MRI which has a high spatial resolution and can image flow in smaller vessels as demonstrated by Kerkhof et al., (2023). Kerkhof et al., (2023) identified an association between impaired cerebrovascular damping and size of the perivascular spaces visible to MRI. They suggested that the larger perivascular spaces were likely the product of higher pulsatile transmission from larger cerebral arteries to the microvasculature. Although MRI is a useful tool in controlled clinical settings, it has limited capacity on field expeditions.

Similarly, positron emission tomography (PET), another method that provides accurate regional measures of hemodynamic flow and metabolism is difficult to use in the field considering the required radioactive labelling. Further, despite it providing accurate regional measures of hemodynamic flow and metabolism it is expensive to use and necessitates extensive technical training similar to MRI (Berridge et al., 1991).

Thanks to previous work using high resolution and high temporal imaging, it is accepted that the brain is uniquely sensitive to changes in arterial blood gases particularly carbon dioxide (CO_2) (Carr et al., 2022; Gibbs & Lennox., 1940; Hoiland et al., 2019). Additionally, our understanding of CBF autoregulation (i.e., perfusion pressure kinetics) is shifting away from a pressure-resistive model (i.e., limited change in CBF following blood pressure challenges) to a more dynamic pressure passive model (i.e., parallel CBF and blood pressure responses) (Brassard et al., 2021; Willie et al., 2014). This pressure model takes into consideration the role of microvessels and conduit arteries as it aims to derive the impact of blood pressure changes as a product of macro and microvascular compliance (i.e., the ability of the vasculature to buffer pressure hemodynamics) (Aaslid et al., 1989; Tzeng & Ainslie., 2014). Over the past centuries the understanding of CBF has grown from Mosso's landmark measures (1880) to the development of the widely use Kety-Schmidt technique (1945) which was overtaken by the popularization of higher temporal resolution devices such as TCD (Aaslid, 1980) and VDu (Thomas et al., 2015). Today, the accumulation of years of scientific work has led to multimodal CBF measures with higher resolutions (i.e., TCD, VDu, MRI, PET) making it possible to image the relationship that structure and function plays in determining a healthy cerebral vasculature.

The following sections will outline the mechanisms of CBF and the impact of hemodynamic stress on cerebral arteries vascular stiffness and compliance. Throughout each section the effect

of HA on the respective mechanisms will be discussed, and lastly pharmacological cerebrovascular responses (i.e., DOB+ACZ, INDO) will be summarized.

2.2.2. The Influence of Arterial Blood Gases on Cerebral Blood Flow

Partial pressure of arterial carbon dioxide

The cerebral vasculature is uniquely sensitive to changes in arterial CO_2 more so than the periphery (Carr et al., 2022; Hoiland et al., 2019). As previously discussed, the brain requires constant flow to sustain normal function and its CO_2 sensitivity helps to maintain homeostasis and regulate central pH (Ainslie & Duffin., 2009; Willie et al., 2012). The brain has an extensive network of blood vessels, and the capillaries separating the brain from the extracellular fluid have unique properties (e.g., tight junctions) which tightly regulate the passage of nutrients from the blood into the brain (i.e., blood-brain barrier) (Daneman & Prat et al., 205; Fris et al., 1980). Although the blood-brain barrier is highly selective, P_aCO_2 easily diffuses from cerebral tissues to capillaries along a pressure gradient between the blood and brain tissue (Caldwell et al., 2021b; Fris et al., 1980). An increase in the partial pressure of arterial P_aCO_2 (i.e., hypercapnia) causes cerebral vasodilation, which decreases cerebrovascular resistance (CVR), ultimately increasing CBF (**Figure 2**). Conversely, a decrease of P_aCO_2 (hypocapnia) causes cerebral vasoconstriction, which increases cerebrovascular resistance (CVR), reducing CBF (**Figure 2**) (Ainslie & Duffin., 2009; Hoiland et al., 2019; Willie et al., 2012). Although change in CO_2 is one of the most important factors in regulating CBF, the brain is also sensitive to P_aO_2 (Cohen et al., 1967; Lucas et al., 2011; Willie et al., 2014).

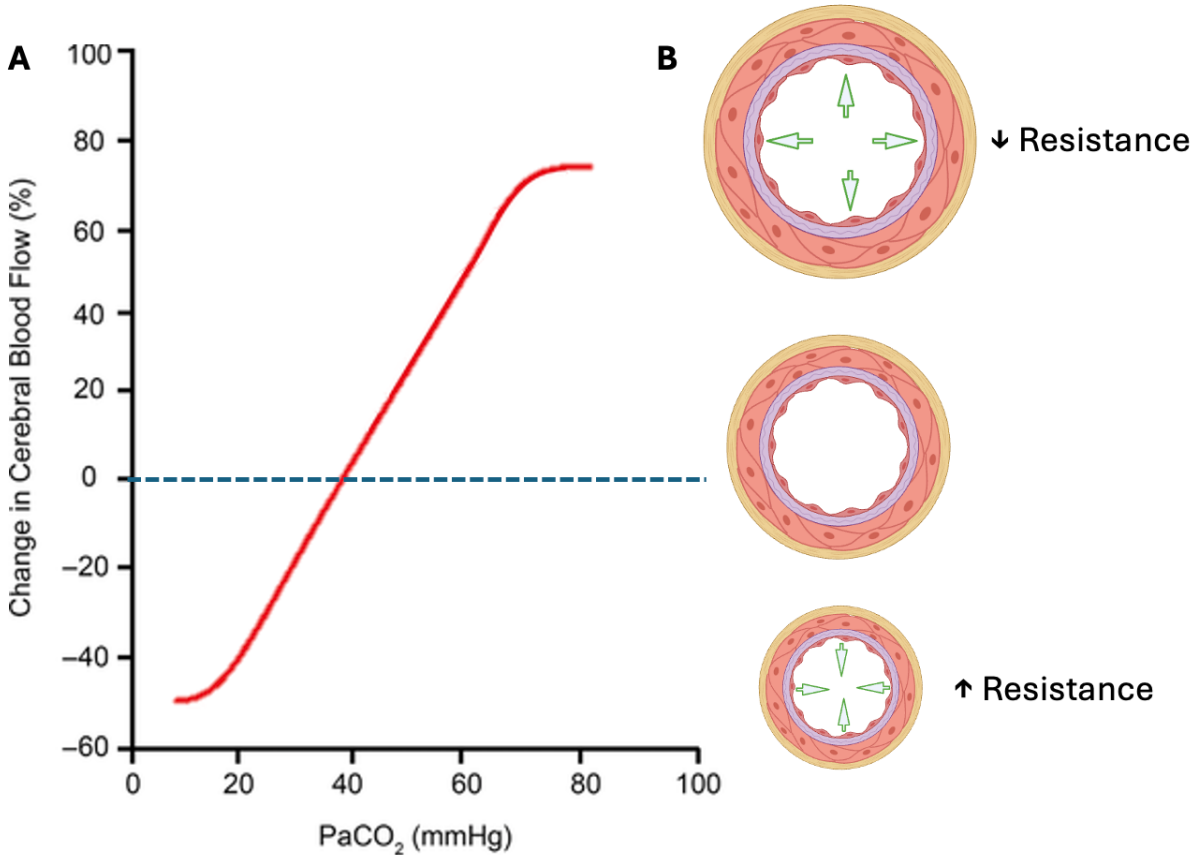

Figure 2. (A) The percent change in cerebral blood flow (CBF) plotted against changes in arterial partial pressure of carbon dioxide (P_aCO_2). The dashed blue line indicates a zero percent change in blood pressure. The red line indicates the percent change in cerebral blood flow in relation to changes in the partial pressure of arterial carbon dioxide (P_aCO_2). The red and blue line intersect at 40mmHg P_aCO_2 indicating rest. This is the threshold in which deviations above or below result in a similar change in cerebral blood flow. (B) Illustrative response of vessel diameter in relation to changes in P_aCO_2 and CBF. Hypercapnic P_aCO_2 provokes a vasodilatory response and reduced resistance. Conversely hypocapnic P_aCO_2 provokes vasoconstriction and increases resistance. (A) Adapted with permission from Willie et al., (2014). Integrative regulation of human brain blood flow. *The Journal of physiology*, 592(5), 841-859.

Partial pressure of arterial oxygen

Hypoxia: At HA the brain is challenged by reduced B_p, as atmospheric pressure and inspired O_2 pressure fall almost linearly with ascent to altitude. At 5500m atmospheric pressure is roughly 50% of SL (Peacock., 1998). The decrease in inspired O_2 leads to a reduced drive for gas

exchange in the lungs inducing an oxygen cascade effect (**Figure 3**) (Peacock., 1998). The reduced P_aO_2 greatly impacts C_aO_2 by: 1) lowering the saturation of oxygen bound to hemoglobin, resulting in desaturation (Severinghaus., 1979); and by 2) reducing the concentration of dissolved O_2 in the blood. The current cerebrovascular literature regarding P_aO_2 sensitivities frequently presents cerebrovascular hypoxic reactivity in relation to falling P_aO_2, saturation (S_aO_2), or C_aO_2 (Carr et al., 2021; Willie et al., 2013). Although this thesis does not report reactivity, these variables, and their relationships to the CBF response to hypoxia are important. The specific response pattern for hypoxic CBF reactivity is dependent on which variable is used. For example, when charting P_aO_2 in relation to change in CBF the relationship is exponential, as CBF response to changes in P_aO_2 is relatively stable until a drop below ~50mmHg (Carr et al., 2021; Hoiland et al., 2016). Conversely, S_aO_2 and C_aO_2 demonstrate a linear relationship (Hoiland et al., 2016). The kinetics associated with the oxygen dissociation curve largely explain the difference between this response, however regardless of the slope and variable used to describe hypoxic CBF reactivity, all relationships support a hypoxic/hypoxemia induced increase in CBF, and each providing details on how this hypoxic cerebrovascular vasodilation is served to maintain O_2 delivery to the brain.

Considering the exponential relationship between CBF and P_aO_2, it makes sense that small reductions in P_aO_2 have little effect on CBF, whereas greater reductions (i.e., - 40mmHg) from resting influences C_aO_2, provoke cerebral vasodilation (Cohen et al., 1967; Lucas et al., 2011; Willie et al., 2014). The vasodilation provides compensatory increases in CBF to maintain adequate substrate and O_2 delivery to the brain. At about 3475m above sea-level CBF is expected to increase ~24% when observed using P_aO_2 as the measurement variable (Jensen et al., 1990;

Severinghaus et al., 1966). Continuing to altitudes greater than 5000m 40-70% increases in CBF have been observed (Ainslie & Subudhi., 2014; Lucas et al., 2011; Willie et al., 2014). Thus, ascent to HA CBF response is dependent on the degree of altitude ascension, the rate of ascension, and the severity of the hypoxic stimulus (see section 2.4.) (Hoiland et al., 2018; Willie et al., 2014). Additionally, depending on the severity of hypoxia and the duration of HA acclimatization the vasodilatory effect of hypoxia may be counterbalanced balanced by integrative hyperventilation induced hypocapnic vasoconstrictions (Lucas et al., 2011; Willie et al., 2014). With regards to the experimental outcomes and interpretations, it is understood that HA produces systemic responses that can lead to changes in cerebrovascular function. These changes play an important role in the integrative regulation of CBF at HA and are important to consider in the context of how the brain buffers hemodynamic stress while maintaining adequate O_2 delivery.

Integrative influence of arterial oxygen and carbon dioxide

The balance of arterial gases upon ascent to HA presents an interesting paradox between hypoxic-induced vasodilation and hypoxic-hyperventilation induced hypocapnic vasoconstriction (Lafave at al., 2019). Hypoxia (reduced P_aO_2) initially results in cerebral vasodilation accompanied by compensatory physiological responses of the upstream (e.g., increased heart rate) vasculature. As discussed above, stimulated hypoxic chemoreceptors increase ventilation resulting in hypocapnia, and consequently cerebral vasoconstriction, increased cerebrovascular resistance (CVR) (Ainslie & Duffin., 2009; Lucas et al., 2011). This balance of blood gases is tightly linked to ventilatory sensitivity which can vary person to person and may be altered throughout acclimatization to HA (Lucas et al., 2011). At ~4000m altitude it appears a

"threshold phenomenon" occurs in which the hypoxic stimulus overtakes the hypocapnic stimulus and CBF substantially increases to address hypoxemic reductions in CaO_2 (Lafave et al., 2019).

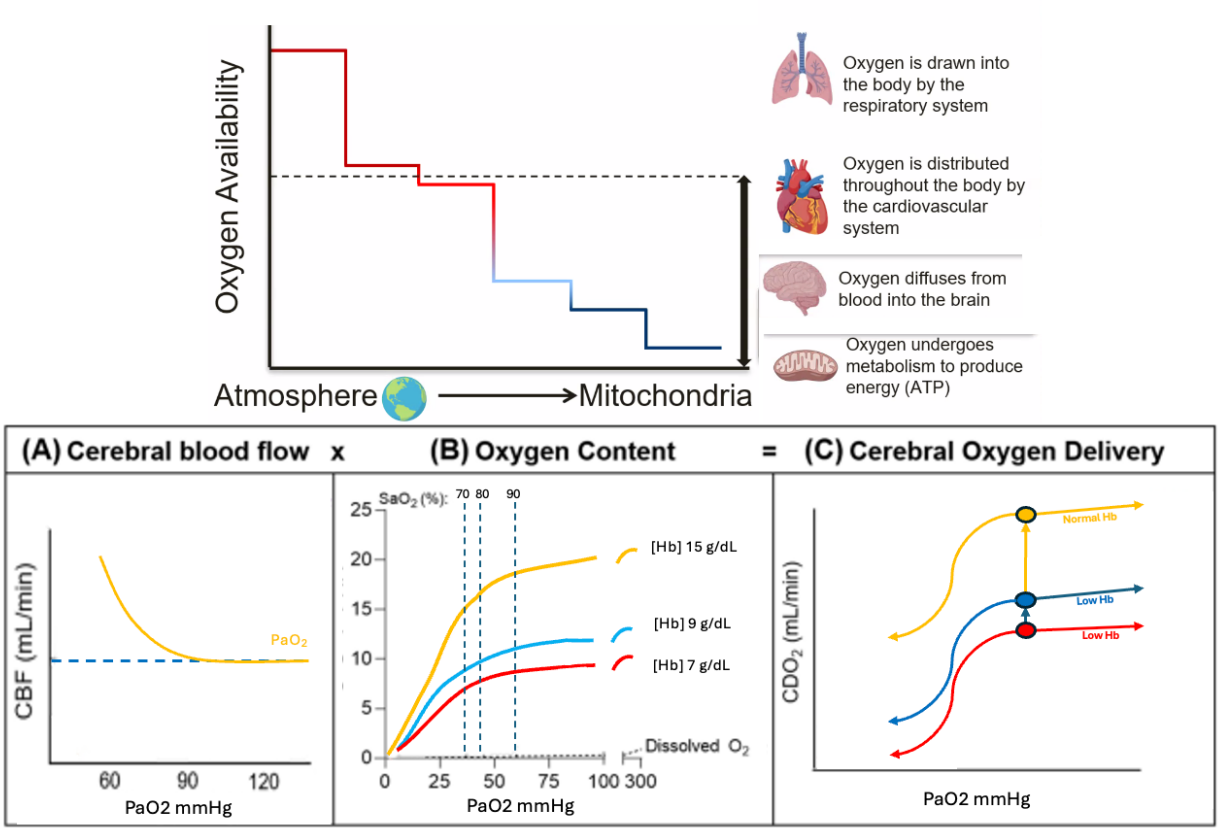

Figure 3. The top image depicts the oxygen cascade from the atmosphere as it is drawn into the lungs, distributed throughout the body, diffused from the blood into the brain, and metabolised at the mitochondria. Graph A: Cerebral blood flow plotted against the arterial partial pressure of oxygen (mmHg). Graph B: Arterial oxygen content (mL/dL) in relation to arterial partial pressure of oxygen (mmHg). Graph C: Cerebral oxygen delivery (mL/min) in relation to changes of arterial partial pressure of oxygen (mmHg) and hemoglobin. Modified with permission from Hoiland et al., (2023) Clinical targeting of the cerebral oxygen cascade to improve brain oxygenation in patients with hypoxic–ischaemic brain injury after cardiac arrest. Intensive Care Med 49, 1062–1078 (2023).

Acclimatization: Balance of oxygen and carbon dioxide

The initial days at HA there is a low P_aO_2 to P_aCO_2 ratio and a greater hypoxic vasodilation for a given hypocapnic vasoconstriction. Acclimation to HA following prolonged exposure is related

in part to the balance of CO_2 and ventilation. Because of acute reductions in CaO_2 initially at HA hypoxic vasodilation appears to override hypocapnic vasoconstrictions during the first few days (Lucas et al., 2011). Days 7-9 at altitude CBF starts to trend towards sea level values as metabolic and hematological acclimatory responses improved hypoxic ventilatory stability and CaO_2. Hypoxic-induced increases in ventilation help to stabilize cerebrovascular PaCO2 reactivity at 12-15 days (Lucas et al., 2011). Additionally, ascent to altitude increases sympathetic nerve activity steadily peaking around day 6 (Mazzeo et al., 1998). Sympathetic nerve activity impacts the sympathoadrenal system leading to changes in heart rate, stroke volume, vascular resistance, and blood pressure. Following acclimation to HA, blood pressure typically returns to normal, however heart rate will remain elevated (Naeije., 2010). In fact, permanent residents at HA can see a decrease in resting BP (Naeije., 2010). The impact of blood pressure and autonomic nervous system regulation on CBF is described in more detail below. The data in this thesis is following a total of two weeks acclimation to altitude, including 8 days trekking (**Figure 4**).

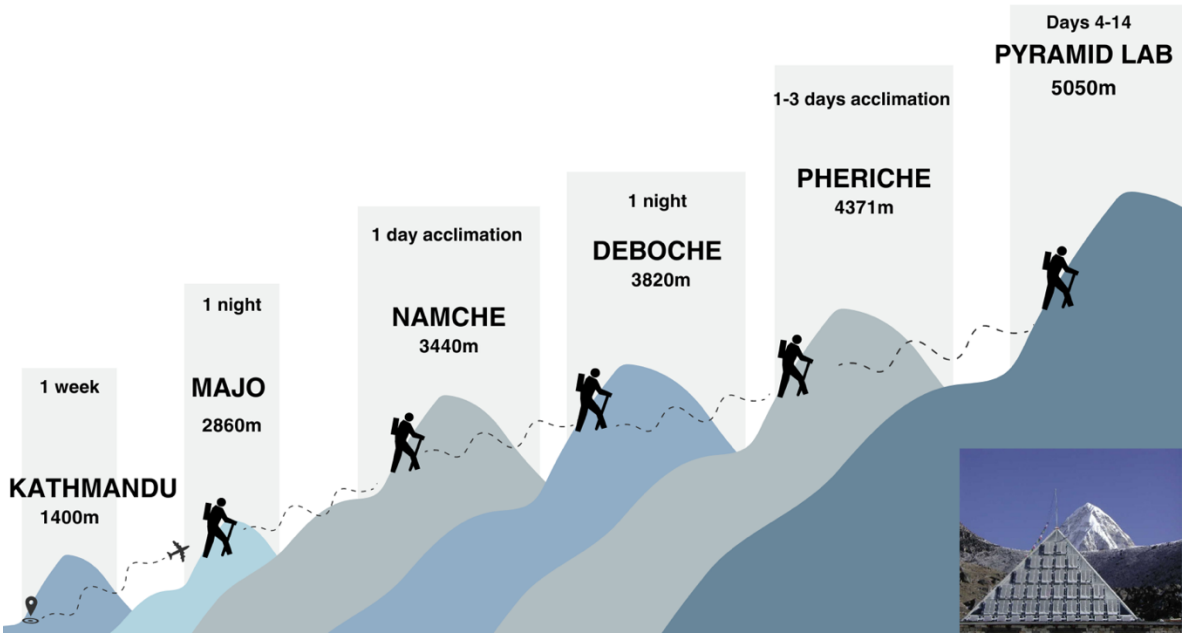

Figure 4. Ascent from Kathmandu to 5050m Pyramid lab. The team flew into Kathmandu where they stayed for 1 week before flying to Lukla (1400m) and starting the trek to Namche (3440m). One day was spent in Namche before trekking to Debuche (3860m) where another day of acclimation occurred. The team then trekked to Periche (4371m) where 1-3 days was spent acclimating before the final trek to the Pyramid lab (5050m). During the first 6-7 days trekking to 5050m, acetazolamide was given in low doses (125mg orally, twice a day) as an acute mountain sickness prophylactic. Acetazolamide was discontinued on day 8 of the trek at 4371m to allow for washout before the first data collection session. The half-life of acetazolamide is ~10 hours, so greater than 24 hours is sufficient. Pyramid image sourced from Associazione Riconosciuta Ev-K2-CNR: https://www.evk2cnr.org/cms/en/evk2cnr_committee/pyramid/story

2.2.3. Blood pressure: Autoregulation of Cerebral Blood Flow

In order for blood flow to enter the brain input perfusion pressure needs to be large enough to bypass intracranial impedances imposed by the skull, internal pressures (i.e., CSF), and outflow factors that regulate intracranial pressure (Claassen et al., 2021; Lawley et al., 2016). This means that the mean arterial pressure (MAP) needs to be greater than intracranial pressure (ICP). Thus, cerebral perfusion pressure (CPP: pressure required for maintaining CBF) is defined as MAP minus ICP (Claassen et al., 2021; Lawley et al., 2016). At SL, ICP is stable, and while at HA it may increase marginally (Lawley et al., 2016). Therefore, the maintenance of appropriate CPP in the face of changing arterial blood pressures serves to maintain a stable CBF (i.e., cerebral

autoregulation) (Aaslid et al., 1984; Strandgaard & Paulson., 1984), has been a major focus for researchers investigating individuals sojourning to HA. As stated previously, the cerebral circulation is tightly regulated by overlapping mechanisms which allow for near constant substrate delivery to meet its high metabolic demands. Initially, it was believed CPP remained constant over a large MAP range (i.e.,50-150mmHg) (Aaslid et al., 1984; Lassen et al., 1959). Lassen et al., (1959) erroneously summarized that prolonged fluctuations in MAP were countered by opposing fluctuations in cerebral vascular resistance (CVR), keeping CBF stable. This concept has since been associated with the term static autoregulation, which is the regulation CBF in response to slow and gradual changes in CPP like those that occur naturally at rest (Numan et al., 2014; Panerai et al., 1998) or over time with pathological aging (Smirl., 2015). The classical view of static cerebral autoregulation is that most of CPP regulation occurs as a product of the cerebral microvasculature, which can augment blood flow by increasing or decreasing resistance (Fog., 1938; Lassen., 1959; Willie et al., 2014). However, animal studies have demonstrated that the larger conduit arteries play a greater role in CBF autoregulation, likely through local resistive and conductive hemodynamic regulation, than previously believed (Faraci et al., 1978; Heistad et al., 1978; Kontos et al., 1978).

These studies provide an important understanding of cerebral autoregulation, for static autoregulation does not account for rapid changes in blood pressure such as those occurring with changes in posture, during exercise, and other dynamic physiological or environmental conditions. What has been observed by these studies is that the rate and severity of blood pressure adjustments to any stimulus provokes hypo and hypertensive decreases and increases in CBF, respectively. This dynamic CPP relationship is often referred to as dynamic autoregulation (Claassen et al., 2021; Lucas et al., 2010; Tzeng & Ainslie., 2013), and is an important

contributor to healthy cerebrovascular aging. Hemodynamic determinants of organ perfusion are typically understood using Poiseuille's law (Eq 1). In context of the cerebral vasculature, resistance is an important regulator of perfusion, especially considering that the cerebrovasculature has more tortuous sections than the periphery which creates turbulent flow, increasing the resistance for a given lumen diameter (Panerai et al., 1998). The balance and ability for the cerebral vasculature to manage changes in flow (i.e., dampen) is an important indicator of brain health.

Eq. 1

$$Q = \frac{\Delta P}{R}$$

In the cerebral circulation P= cerebral perfusion pressure, or the difference between MAP and downstream pressure. R= resistance. Resistance is a product of diameter, viscosity, and length. Viscosity and length are considered constant, making resistance the primary determinant of resistance and flow.

The mechanisms behind cerebral autoregulation are difficult to distinguish as changes in ventilation can alter the partial pressure of CO_2, which alters CBF (Tzeng & Ainslie., 2013). There is some debate on whether the mechanism of regulation is pressure related or more so governed by metabolism and neurovascular responses (Aaslid et al., 1984; Fog., 1930; Fog., 1938). The initial works by Fog (1930) investigating cerebral regulation in cats observed a pial vasomotor response independent of neurogenic stimuli. Additionally, Fog's later works (1938) demonstrated that a decrease in vessel diameter in response to increased blood pressure prevents a rise in capillary pressure, protecting against cerebral edema. Thus, upon increases or decreases in CPP, the myogenic reflex will result in vasoconstriction or vasodilation, respectively (Strandgaard & Paulson., 1984). Myogenic tone classically refers to the partial vasoconstriction

of isolated vessels when maintained at a constant pressure, although reductions in blood pressure may impact myogenic tone. However, this has not been investigated in vivo in human cerebral arteries (Aaslid et al., 1984; Bayliss 1901; Claassen et al., 2021). It may be that myogenic tone is a response to changes in transmural wall tension versus changes in blood pressure (Claassen et al., 2021; Cipolla., 2009). Currently, there is debate of Lassen's original curve stating that CBF is likely more pressure-passive than previously believed (Heistad & Kontos, 1983; Lucas et al., 2010). Historically, the brain was assumed to autoregulate and changes in blood pressure would result in similar changes in CBF (**Figure 5**) (Bayliss et al., 1895; Roy & Sherrington, 1890), however findings like those of Fog (1938) suggested the brain does have the presence of an arterial pressure range wherein autoregulation seemed effective (Brassard et al., 2021). Further, the old debate states regulation is static and mostly resulting from the microvasculature, but as discussed in section 2.4.2 the conduit arteries likely play a larger role than initially thought.

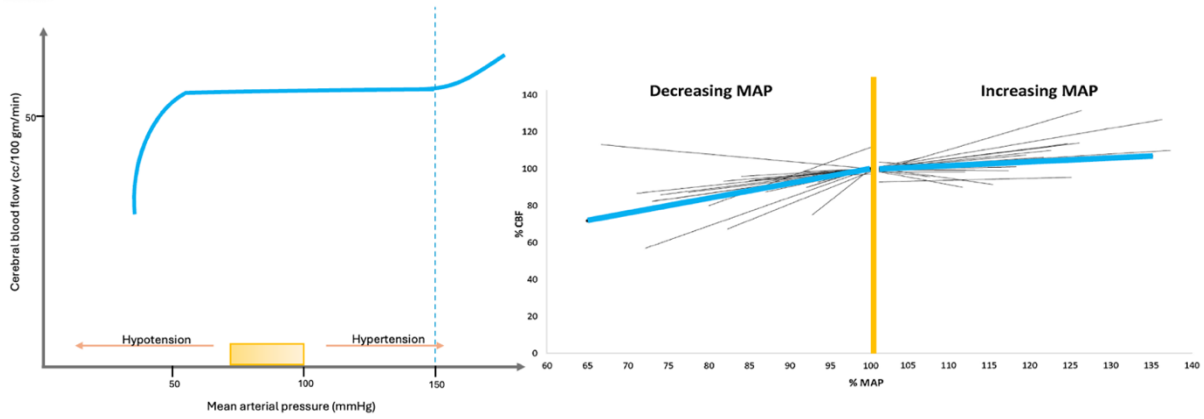

Figure 5. Comparing Lassen's original autoregulation curve to recent studies. Left= Lassen's original autoregulation curve plotting cerebral blood flow and mean arterial pressure. The data plotted includes 11 groups of subjects reported in seven studies. The data from Lassen's original curve has been disputed over the past years, and research is shifting away from its use (Brassard et al., 2021). Right= Review by Numan et al., (2014). The review included 49 studies, 41 of which used transcranial Doppler. Each black line on the graph indicates an individual experiment, the length of the line indicates the range of mean arterial pressure measured. The blue line is emphasizing the average slope for the decrease and increased mean arterial pressure and cerebral blood flow. Numan's figure demonstrates the contemporary understand of changes in how changes in mean arterial pressure impact cerebral blood flow. It is interesting to note that

recued mean arterial pressure appears to impact cerebral blood flow more dramatically, indicated by the steeper average slope, than increasing mean arterial pressure. Adapted with permission from Lassen (1959) and Numan et al., (2014).

2.2.4. Cerebral Metabolism and Regulation of Cerebral Blood Flow

Cerebral metabolic rate of oxygen

Stated above; the brain has an incredibly high energy demand, and this energy demand is primarily met by oxidative metabolic activity (Kety & Schmidt., 1948 as review by Smith & Ainslie., 2017). The average resting CBF, assuming the average brain mass of 1.4kg for a typical 60-100kg person, is 54 $ml.100g^{-1}min^{-1}$ (~750 $ml.min^{-1}$). Combing CBF with arterial and jugular venous differences of oxygen, it has been determined that the average cerebral metabolic rate of oxygen ($CMRO_2$) is ~$3.3ml.100g^{-1}.min^{-1}$. It is important to understand that the $CMRO_2$ is being used to oxidize glucose at a ratio of 6:1 (O_2: Glucose). The cerebral oxidative glucose index at rest has been observed to be relatively stable, and thus $CMRO_2$ provides an important index of how well the brain is fueling itself, and thus CBF measures provide an important assessment of how well CBF is meeting changes in brain metabolism. During acute hypoxia (Willie et al., 2015), progressive hypoxia (Ainslie et al., 2014) and following three weeks acclimation to HA (Møller et al., 2022) no change in cerebral metabolic rate of glucose was observed. However, hypoxia does appear to increase glucose uptake (Cohen et al., 1967) and glycolysis (Hamburger & Hydén., 1963). Kety & Schmidt (1947) found that $CMRO_2$ remained stable over a range of hypoxic and hyperoxic fractions of inspired O_2 (i.e.,10-100%), as well as hypercapnic ranges (i.e., + 5% & 7% CO_2). However, Xu et al., (2011) observed reduction in $CMRO_2$ of 13% from normocapnia to hypercapnia, which is inconsistent with Kety & Schmidt's findings, but aligns with animal studies by Kogure et al., (1975), Sicard and Duong (2005), and Barzilay et al (1985). Differences in the method of measurement and subject conditions (i.e., dogs vs. humans,

anaesthesia) may account for this variation. Further, during progressive hypoxia $CMRO_2$ remained stable despite changes in CBF (Ainslie et al., 2014).

It makes sense that CBF is a mechanism that supports the brains demand for O_2, although it is unclear exactly how much $CMRO_2$ changes over various conditions. Ainslie et al., (2014) found that $CMRO_2$ was held stable during hypoxic increases in CBF. Xu et al., (2012) observed an increase in CBF with hypoxia by inhalation of 14% O_2 and an increase of $CMRO_2$, but no significant changes in CBF were seen with hyperoxia although $CMRO_2$ did decrease. Cerebral metabolic rate of oxygen appears constant during severe hypoxia (P_aO_2 ~35mmHg) and acute moderate hypoxia at SL (Ainslie et al., 2014). Also, following three weeks acclimation to HA (5,260m, PaO_2 ~35mmHg) $CMRO_2$ appeared unchanged (Møller et al., 2002). In contrast Smith et al., (2014) found CBF and $CMRO_2$ was elevated at HA following four days of acclimatization to 5050m. Cohen et al., (1967) saw an increase in CBF during hypoxia and a 17% increase in O_2 delivery to the brain, though no consistent changes in $CMRO_2$ were observed. For the majority of response, changes in CBF seem to parallel $CMRO_2$ as expected. Thus, assessing the hemodynamic responses to pharmacological increases and decreases in CBF will provide further details pertaining to the hemodynamic forces associated with maintaining $CMRO_2$ through CBF mediated mechanisms.

2.2.5. Autonomic Nervous System Regulation of Cerebral Blood Flow

The entire cerebrovasculature is innervated by adrenergic and cholinergic fibres (Bleys et al., 1996). There is debate on the presence and degree of sympathetic regulation of CBF (Levine & Zhang., 2008). Although CBF sees greater impact from autoregulation and CO_2 reactivity,

animal studies have shown increased SNA directed to cerebral vessels with acute hypertension (Cassaglia et al., 2008). This was not observed with hypotension, meaning this may be a protective mechanism of the microvasculature (Ainslie & Duffin., 2009; Cassaglia et al., 2008). D'Alecy et al., (1979) conducted a study on dogs that sympathetically electrically stimulated cerebral vessels and found a decrease in CBF, even during hypercapnic vasodilation. Overall, they saw an 18% decrease in CBF with sympathetic stimulation. Jordan et al., (2000), using TCD during head up tilt and complete ganglionic blockade, found that changes in sympathetic tone have a limited effect on CBF at a normal P_aCO_2 but seems to attenuate CO_2 induced increases in CBF. Further, the sympathetic nervous system tends to increase ventilation meaning it can indirectly increase cerebrovascular tone through hyperventilation induced changes in P_aCO_2 (Jordan et al., 2000). Sympathetic activity can influence CBF reactivity to P_aCO_2, given the increased changes of P_aCO_2 observed upon ascent to HA it can be expected there will be changes in sympathetic nerve activity in some capacity (Ainslie & Duffin., 2009; Willie et al., 2014). Acute hypoxia is a potent activator of sympathetic nervous system activity and has been shown to increase the sympathoadrenal system in animal studies resulting in an increased release of catecholamines, increased heart rate, and regional vasoconstriction (Bernardie et al., 1998; Hainsworth et al., 2007). However, cerebral sympathetic nerve activity appears to act opposite of the peripheral circulation and is mediated by changes in ICP and cerebral blood volume. Elevations in cerebral SNA could be to prevent hyperperfusion injury in humans (Koepp et al., 2022), necessitating the consideration of environmental and pharmacological interventions that might impact autonomic activity. The mechanisms by which this increased hemodynamic burden is managed is of particular interest for this thesis, as changes in PI from the ICA to the MCA provide a measure of cerebrovascular damping. We are interested in how beta-adrenergic

stimulation, as well as the influence of HA autonomic excitation on cerebrovascular hemodynamics.

2.3. Cerebral blood flow during ascent to high altitude

At HA the prevalence of AMS can vary from 40-90% depending on the specific altitude, the rate of ascent, individual sensitivity, and degree of preacclimation (Hackett & Roach., 2001; Luks et al., 2017). Acute mountain sickness is popularly characterized using the Lake Louise AMS Score and commonly manifests as a headache and the presence of 1 or more of the following symptoms: gastrointestinal symptoms, insomnia, dizziness, and fatigue (Roach et. al., 1991). Less often, the critical end stage of AMS is high altitude cerebral edema, which can lead to brain damage that presents as drowsiness, confusion, ataxia and, without the proper treatment, death (Hackett & Roach., 2001). Ascent profile greatly affects one's response when ascending to HA, as too rapid an ascent increases the possibility of high altitude pulmonary edema, high altitude cerebral edema, and AMS (Paralikar., 2012; Zhang & Zhang, 2022). To support ascent to HA ACZ can be taken (250 mg, 2 doses taken 8 hours apart) for prevention of AMS. The impact of AMS on cerebrovascular responses (e.g., CBF) remains unclear (Swanson et al., 2016).

Willie et al., (2014) was one of the first studies to volumetrically quantify CBF during ascent to HA, and throughout a stay at altitude. This study showed CBF peaked after ~60 hours at 5050m dropping down to 20% above SL values after 2 weeks acclimatization. Willie et al., highlight the variability between subjects in the CBF increase with ascent, and CBF decrease with acclimatization. Further, dilation of the MCA was observed despite no observable dilation of the neck arteries (Wilson et a., 2011). This was interpreted as the intracranial arteries may have greater relative hypoxic sensitivity and play a more prevalent role in CBF regulation during HA

ascent. The ascent profile was gradual which is represented in **Figure 3**. Hoiland et al., (2018) extensively reviewed cerebrovascular regulation at HA, highlighting that CBF changes throughout ascent to HA and during acclimation (**Figure 6**). Upon ascent to HA the reduction in C_aO_2 is mirrored by the compensatory increase in CBF. As previously discussed, ventilation is a major mechanism of the change in CBF at HA, as the body compensates to maintain O_2 delivery and acid/base balance (Hoiland et al., 2018). It remains to be seen if ascent to HA influences the hemodynamic forces while aiming to maintain delivery to metabolism.

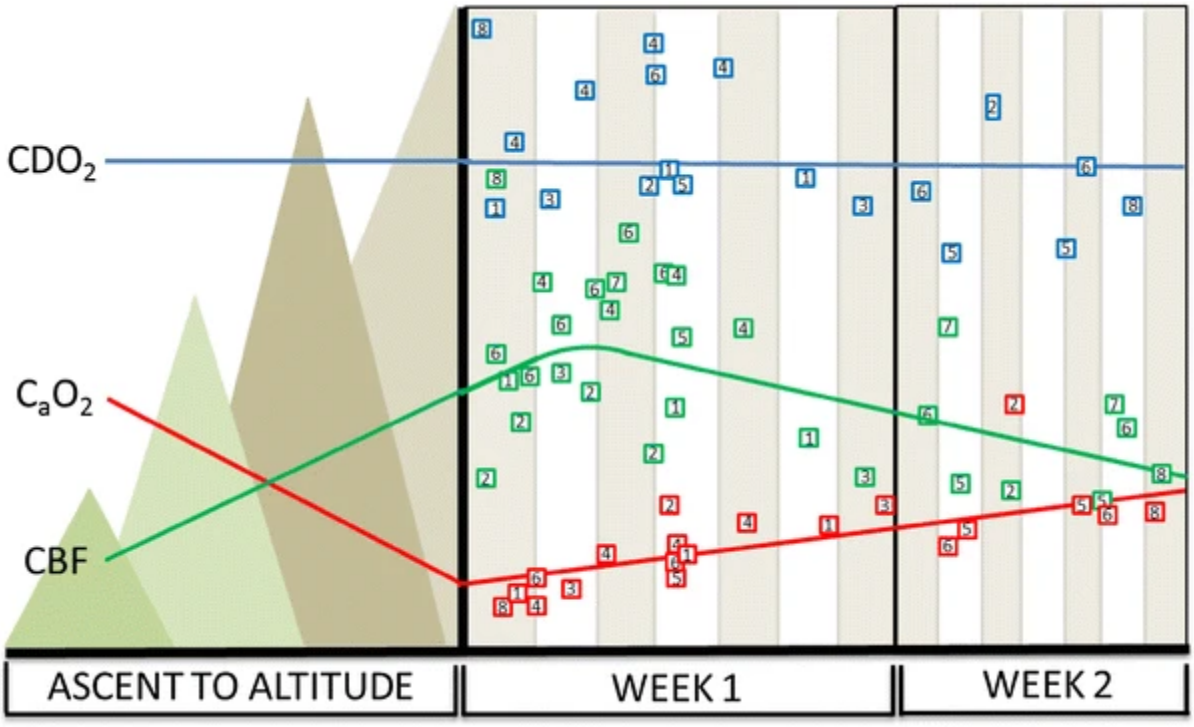

Figure 6. Changes in cerebral blood flow upon ascent to altitude in relation to arterial oxygen content, and cerebral oxygen delivery plotted over two weeks acclimation. Extensively review by Hoiland et al., (2018), figure included with no adaptations. The red line shows the reduction of arterial oxygen content upon ascent to altitude and over the following two weeks. The green line shows the compensatory increase in cerebral blood flow which serves to maintain constant cerebral oxygen delivery, shown with the blue line. Hoiland et al., plotted the studies using the following numerical assignments: 1=Severinghaus et al., (1966), 2=Huang et al., (1987), 3= Jensen et al., (1990), 4= Baumgartner et al., (1994), 5=Lucas et al., (2011), 6 & 7 = Willie et al., (2014), 8= Subudhi et al., (2014).

2.4. Mechanisms of Cerebral Hemodynamic Buffering

Healthy cerebral arteries are compliant vessels capable of mitigating the energy transmission of pulsatile forces prior to their arrival in microvasculature (Kerkhof et al., 2023; Zieman et al., 2015; Zarrinkoob et al., 2016). This section will first review basic vessel anatomy and introduce where and how stiffness can occur. Next, methods of measuring vascular stiffness will be summarized followed by the structural and cellular components. Finally damping, the measure of interest for this thesis, will be discussed with perspective on the effect of HA.

2.4.1. Arterial Stiffness and Compliance

As discussed, healthy cerebral arteries are compliant and able to manage changes in pulsitility (Kerkhof et al., 2023; Zieman et al., 2015; Zarrinkoob et al., 2016). This compliance is achieved through several structural (i.e., tortuosity, circle of Willis) and functional components that can increase and decrease vascular resistance (Muskat et al., 2021; Shirwany & Zou., 2010; Vrselja et al., 2015; Zieman et al., 2005). Arterial stiffening is observed with age, however, is often viewed as a pathological change in the structural component of blood vessels (Kohn et al., 2015). This stiffening with age is also correlated with disease states such as diabetes and hypertension (Climie et al., 2019; Shirwany & Zou., 2010). Given the limitations related to imaging cerebrovascular function, it is not surprising that most research focuses on aortic and peripheral stiffness measures rather than cerebrovascular stiffness and is often performed in individuals with significant signs of vascular aging. This section will first review basic vessel anatomy and introduce where and how stiffness can occur. Following this I will review methods of measuring vascular stiffness, which will be preceded by a summary of the structural and cellular components assessed in these measures. The structural components of arteries (i.e., layers) will

be discussed as they relate to arterial stiffening, as will the relevant cellular mechanisms important to vascular function (e.g., endothelial dysfunction). Finally, this section will conclude with a discussion on vascular damping and its importance as a measure of interest for this thesis, will be discussed with perspective on the effect of HA on cerebrovascular damping.

2.4.2. Arterial Stiffness

Arteries are primarily composed of three layers: the intima, media, and adventitia. The intima (i.e., inner most layer) includes a thin layer of endothelial cells along a basement membrane (Kohn et al., 2015). A primary function of endothelial cells is the release of vasoactive factors that affect vascular smooth muscle tone such as nitric oxide, an endothelium-dependent vasodilator (Sandoo et al., 2010). The media (i.e., middle layer) contains smooth muscle and elastic lamina which allows for contraction and dilation of the artery, while also providing support for the vessel to withstand changes in flow and pulsitility (Kohn et al., 2015; Mercadante & Raja., 2023). The adventitia (i.e., outermost layer) connects the artery to the rest of the tissues in the body, provides structure, and may also play a role in reactive oxygen species production to modulate the activity of smooth muscle cells residing in tunica media (Kohn et al., 2015; Mercadante & Raja., 2023). Increased mitochondrial oxidative stress can induce an accelerated vascular aging characterized by increased pulse wave velocity and vascular smooth muscle cell stiffening, in part through altered nitric-oxide bioavailability (Lacolley et al., 2020). The exquisite balance of structure and compliance allows arteries to manage fluctuations in pressure that occur with daily life. All vascular cells work to maintain an optimal mechanical state and disruption of this homeostasis is related to vascular diseases, cardiac disorders (e.g., heart failure), and can adversely affect brain function (Humphrey & Tellides., 2019). Arterial

stiffening occurs largely at the tunica media, with the tunica media being influenced by the endothelial layer. Arterial stiffening is a disruption of the homeostasis resulting from structural and cellular mechanisms which directly impacts vascular compliance. Structural arterial stiffening tends to occur following chronic inflammatory stimulation and/or nutrient depletion over longer time periods (months, years) than the duration of the experiments conducted in this thesis (Shirwany & Zou., 2010; Townsend et al., 2015). Details pertaining to the structural and cellular components involved are discussed in the following two sections.

Structural components of arterial compliance and stiffness

The scaffolding of arteries is made of collagen, which provides strength and maintains structure despite high pressure, and elastin, which allows reversible extensibility making the vessel compliant to changes in pressure and pulsitility (Shirwany & Zou., 2010; Wagenseil & Mecham., 2012). Typically, the collagen and elastin undergo balanced cycles of building and degradation however inflammatory changes and increased luminal pressure (e.g., hypertension) can cause over and underproduction respectively resulting in a less compliant vessel (Shirwany & Zou., 2010; Zieman et al., 2005). Matrix metalloproteases (MMP's) regulate collagen and elastin and degrade the extracellular membrane by creating less effective collagen and broken elastin molecules which can result in arterial stiffening. Further, advanced glycation end products (AGE), which result from nonenzymatic protein glycation, forms irreversible cross-links. Collagen linked with AGE is stiffer and resists regulatory turnover resulting in accumulation of structurally compromised collagen molecules (Shirwany & Zou., 2010; Zieman et al., 2005). The structural mechanisms of vascular stiffening overlap with cellular influences, compounding and further impacting vascular compliance.

Cellular components of arterial compliance and stiffness

Endothelial cell signalling and vascular smooth muscle tone are the major cellular mechanisms that acutely impact vascular stiffness (Zieman et al., 2015). The endothelium is a single layer of cells lining the blood vessels, and a major player in regulation of vascular tone (Donato et al., 2018; Félétou, 2011). Endothelial dysfunction can be characterized by an impaired vasodilatory response to acetylcholine, as acetylcholine causes endothelium-dependent vasodilation through muscarinic receptor activation. Endothelial dysfunction is likely a result of an imbalance between NO, endothelium-derived hyperpolarizing factor, vasoconstricting hormones and oxygenases (Matz et al., 2000; Shirwany & Zou., 2010; van Bussel et al., 2001; Zieman et al., 2005). Additionally, in vitro evidence has demonstrated that increased matrix stiffness may impair flow-induced dilation by reducing the ability of the endothelium to affect a response to shear stress (Donato et al., 2018; Kohn et al., 2014). Thus, impaired endothelial function may contribute to arterial stiffening by increasing the active tone in arteries, a result of reduced NO availability, increased activity of vasoconstrictors (e.g., endothelin 1), and changes in extracellular matrix composition (Donato et al., 2018; van Bussel et al., 2001). Impaired endothelial function in cerebral arteries has been observed in pathological aging (Xu et al., 2017).

While assessing the impact of chronic structural remodelling directly requires invasive methods where vascular segments and structures are either excised completely, or biopsies of interested the vascular structures are taken. This provides great biochemical understanding of the factors that lead to long term negative structural remodelling. However, it is difficult, expensive, and ethically impossible to perform biopsies on alive, apparently healthy humans without significant

vascular dysfunction. In contrast, assessing pulsatile hemodynamics including measures of velocity and cross-sectional area (i.e., vascular sonography) allows for an indirect assessment of how structural disruptions influence arterial function. The approaches currently used in the literature will be discussed in the following sections.

2.4.3. Assessing vascular stiffness

Techniques to assess vascular stiffness include measures of pulse-wave velocity, wave intensity, beta stiffness, distensibility, compliance and damping. These measures will be briefly summarized below with greater detail given to damping. The main discussion on damping will focus on its use as a comprehensive measure of hemodynamic buffering in this thesis. Specifically, it ability to provides a quantifiable metric of hemodynamic forces altered by upstream and downstream and local factors that impact functional stiffness and compliance.

Pulse-wave Velocity

Pulse-wave velocity is the measure of time taken for a forward pressure wave to travel between two measured points. The speed of transmission indicates local stiffness but does not necessarily relate to systemic vasculature. Further, this method is more effective in large, superficial arteries and less suited to central arteries (Mackenzie., 2002). Pulse wave velocity is commonly measured from the aorta to vascular tree or the carotid-femoral artery (Mackenzie., 2002; Millasseau., 2005), but recently there have been measures from the common carotid artery to the ICA using MRI (Jung et al., 2021; Rivera-Rivera et al., 2020).

Wave Intensity

Wave intensity is a hemodynamic index of stiffness that can be defined at any site throughout the body but is easiest in superficial vessels. Wave intensity is the product of pressure and velocity measures taken over constant short time intervals (Chiesa et al., 2019; Sugawara et al., 2009). Using colour Doppler, studies have measured within the common carotid artery and found wave intensity to be predictive of cognitive decline (Chiesa et al., 2019). However, wave intensity is commonly applied to the peripheral vasculature and the need for simultaneous blood pressure measurement (via tonometry) limits the application to the cerebral vasculature, as measures of peripheral pressure are not necessarily indicative of CPP. Further, although the tonometer provides an excellent measure of pressure, it is prone to movement artifacts (e.g., from breathing) and the pressure applied by the technician needs to be consistent.

Beta Stiffness

Another method used to assess the stiffness of large arteries is beta (ß) stiffness. ß-stiffness can be calculated using the log-transformed ratio of systolic/diastolic blood pressure to the relative change of arterial diameter during cardiac cycle as first proposed by Hayashi et al., (1980) (Morioka et al., 2021). Studies have used carotid ß-beta stiffness as an indicator of reduced cognitive function and atherosclerosis, and it can be impacted by age, sex, and lifestyle (DuBose et al., 2017; Morioka et al., 2021). ß-stiffness is also associated with cardiovascular risk factors such as smoking, insufficient physical activity, hypertension, obesity, metabolic syndrome, insulin resistance, and type 2 diabetes (Morioka et al., 2021). However, a revised version of the ß-stiffness equation called the cardio-ankle vascular index (CAVI) can be calculated using blood pressure and PWV measures. CAVI requires blood pressure cuffs placed on both arms and

ankles, and a microphone on the chest. When tested against carotid-femoral pulse wave velocity measures it showed a decrease effect of heart rate and blood pressure on stiffness (Wohlfahrt et al., 2013).

Distensibility

Distensibility is calculated from ultrasound images of superficial vascular walls (e.g., carotid, femoral) as they are easier to image. Edge detection software is used to obtain the maximum and minimum areas of the vessel, if blood pressure is also recorded distensibility can be calculated as $\Delta V/\Delta P.V$ (change in volume/ change in pressure x volume) (McKenzie et al., 2002). The primary drawback of this method is the user dependence of ultrasound. Compliance is calculated as the change in volume/ the change in pressure. A lower carotid distensibility has been associated with an increased risk of developing hypertension (McKenzie et al., 2002). Despite potential external carotid artery shunting, common carotid distensibility in response pulsatile pressure fluctuations provide an index of cerebral artery stiffness similar to ß-stiffness, however no measure has been determined distal to the common carotid artery (i.e., ICA).

Damping as an indicator of vascular stiffness

Damping is calculated as the difference in PI along a known section of artery. By assessing changes in pulsatile amplitude in a proximal to distal direction in an arterial segment with minimum contamination from major bifurcations, damping can provide important information about that segment's capacity to buffer hemodynamic forces. Measures of PI can be collected using vDu, TCD, and MRI all of which have their benefits and limitations (Lefferts et al., 2020; Lefferts & Smith., 2021; Zarrinkoob et al., 2016). Pulsitility is the product of dividing the

amplitude of pulsatile velocity (peak velocity- velocity at the onset of the systolic upstroke) by mean velocity in a single pulse. In the cerebral vasculature damping can be measured from the carotids (e.g., common carotid, ICA) to the MCA if using TCD, or as far as the microvasculature if using MRI (Kerkhof et al., 2023; Lefferts et al., 2021). Damping values of 1 indicated that no hemodynamic transmission or blunting has taken place, at least within that arterial segment. A reduction from 1 is indicative of transmission, interpreted as a vascular stiffening, while an increase above 1 indicate a buffering of the hemodynamic pulsations, interpreted as compliant. Damping has been shown to decrease with age and may lead to microvascular damage associated with dementia (Mitchell et al., 2011). Damping as a marker of cerebrovascular compliance will be discussed further in the following section. At HA, while volumetric oxygen delivery following acclimation has been investigated, important hemodynamic markers of stress have yet to be analyzed. The mechanisms responsible for the increases in CBF at HA, also have been observed to influence markers of vascular stiffness (e.g., increased heart rate, increased ventilation). Further, pharmacological interventions (e.g., DOB+ACZ, INDO) may differentially impact damping at HA, the mechanisms of which will be discussed in further detail in the following section (2.5). Additionally, sympathetic nervous system activity (SNA) is excited considerably at HA. Increases in sympathetic vasomotor activity (Simpson et al., 2020) are defined by an elevated muscle sympathetic nerve activity. Elevated SNA provides a functional response that alters vascular tone (i.e., vasoconstriction), and serves as a modulator of vascular control in the face of multiple systemic changes caused by HA (e.g., blood volume, hyperventilation, acid base regulation, etc.) Thus, at HA, sympathetic excitation may serve to improve vascular control as a means of maintaining O_2 delivery but may have a negative impact on vascular factors responsible for hemodynamic buffering (i.e., functional stiffening).

2.4.4. Hemodynamic Buffering

Cerebrovascular hemodynamics are impacted by the anatomy of vessels, and changes in microvasculature resistance all of which serve to manage pulsatile blood flow and ensure smooth delivery to the microvessels. The capacitance of this system to manage pulsatile blood flow is best defined as compliance, which describe the ability of this system to store blood and reduce the pressure required to maintain perfusion to the micro vessels. Capacitance can be viewed each cardiac cycle by assessing the distension of large blood vessels. This distension is impacted by upstream and downstream hemodynamic forces, thus assessing pulsitility in proximal and distal segments provides information on the compliance of the cerebral vasculature (Arts et a., 2022; Gosling et al., 1974).

A decrease in compliance can be a result of altered arterial and blood pressures due to increases in wall thickening, collagen deposition, or elastin fragmentation (Zieman et al., 2005). Pulsitility is related to cerebral vascular resistance in the arterioles but also a contribution of larger cerebral arteries (Zarrinkoob et al., 2016). Damping of flow pulsations is known to be associated with arterial compliance as the ability of elastic vessels to stretch, recoil, and absorb pulsatile energy protects the cerebral vasculature (Arts et al., 2022; Mitchell et al., 2011). The cerebral vasculature has other mechanisms to further mitigate pulsatile waveforms and ensure smooth flow for the microvasculature including the anatomy of vessels, arterial compliance, and microvascular resistance.

Anatomical hemodynamic buffering

When observing the circulation as a pump (i.e., heart) and a series of tubes (i.e., vessels), principles of fluid dynamics can be applied to understand blood flow through vessels. When

blood leaves the heart, it encounters the aortic arch and travels to the carotid arteries, which then bifurcate into the ICA and ECA. Conduit arteries such as the carotids have several important features of buffering pulsitility such as bifurcations and tortuosities. Schubert et al., (2011) observed reductions in ICA PI from distal to proximal of the carotid siphon, likely related to the contorted, tortuous shape of the distal ICA. A vessel with curves in contrast to a straight vessel generates a centrifugal force, leading to an energy transfer from the blood flow to the vessel wall. These principles also apply to the Circle of Willis which can reduce PI due to multiple bifurcations, and the primary shape is the result of tortuosity which anatomically serves as a perpendicular wall against the vertical forces travelling up extracranial vessels (Vrselja et al., 2014). Bifurcations ensure a significant decrease in blood velocity, larger transfer of kinetic energy and larger increases in hydrostatic pressure (Vrselja et al., 2014). Ultimately, this anatomical buffering is assumed as constant in acute and longitudinal study designs where the vascular structure is not expected to change. In addition to anatomical buffering, healthy vessels are complaint and have elastic properties that can further manage PI through what is referred to herein as the Windkessel effect.

The Windkessel effect: Vascular compliance

The large extracranial arteries (i.e., carotid arteries) convert high pulsatile flow by absorbing energy laterally. This hemodynamic buffering continues through the Circle of Willis and to the large intracranial vessels into smaller vessels converting pulsatile flow to continuous non-pulsatile flow by the time it arrives at the capillaries (**Figure 7**) (Lefferts et al., 2020). Arteries absorb energy by way of the "The Windkessel Effect" in which the elastic vascular walls act as a reservoir for pressure temporarily, over a single cardiac cycle, storing blood during systole and releasing it during diastole to create continuous flow (Belz., 1995; Westerhof et al., 2009). Chan

et al., (2011) found using a two element Windkessel model an average 80-90% of MCA_v response to hypertension and hypotension could be explained by constant gain Windkessel buffering. Thus, suggesting that a Windkessel model is effective in explaining a substantial part of the cerebrovascular hemodynamic regulation across varying blood pressure conditions. Modelling the Windkessel effect requires continuous sampling of blood pressure at a steady state for several minutes making it difficult to assess following dynamic tasks. Aortic to Carotid Doppler decay was observed by Nagai et al., (1999) to be a suitable indicator of Windkessel function in extracranial cranial vessels. Thus, it is reasonable to include the Windkessel function as playing an important role in the hemodynamic regulation assess using the proposed DFi in this thesis. Research has demonstrated the Windkessel effect should be regarded as an important element of dynamic CBF modulation, especially as cerebral vessel changes in steady state resistance can influence the speed of CBF response to changes in blood pressure (i.e., phase) and the amplitude CBF changes (i.e., gain) with different effects depending on compliance (Chan et al., 2011; Zhang et al., 2009). The Windkessel effect, compliance, and damping collectively contribute to the ability of cerebral vessels to regulate blood flow, ensuring a stable and adaptive response to hemodynamic changes (Bateman et al., 2008; Egnor et al., 2002; Greitz., 1993). Measurement of extra to intracranial damping provides an assessment that incorporates all of these contributions to how hemodynamic forces enter the brain and are managed prior to the microvasculature. Using an experimental design that alters perfusion pressure proximal to the intracranial segment or alters the resistance distal to the intracranial segments may provide a unique methodological intervention to investigate how hemodynamic stress is dealt with in the cerebrovasculature. Additionally, altering vascular smooth muscle function can also provide a

unique methodology to assess the influence of structural and functional responses to pulsatile hemodynamic stress.

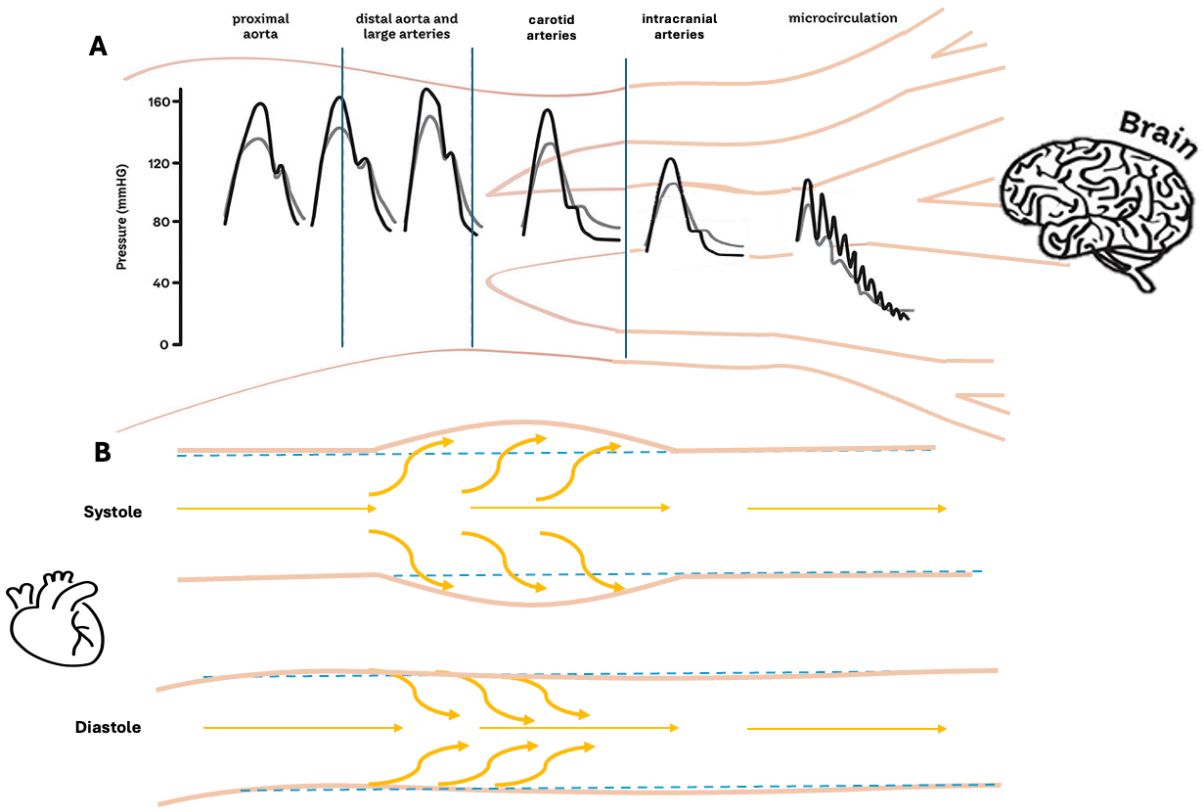

Figure 7. Panel (A) depicts damping (mmHg) of a pulsatile waveform as it moves from the proximal vessels (i.e., aorta) to the distal arteries (i.e., carotids) to the intracranial arteries (i.e., middle cerebral artery) into the microvasculature (i.e., arterioles, pial arteries, capillaries) of the brain. Adapted with permission from Climie et al., (2019). Panel (B) is a rendering of the vascular Windkessel. First depicting how a healthy vessel will stretch to accommodate a pulsatile waveform during systole as the vessel walls act as a reservoir. Then depicting the blood returning into flow during diastole as the pressure reduces, and the elastic vessels returns to baseline tone. The yellow arrows= direction of flow. The blue dashed line indicates the baseline vessel diameter during diastole and provides reference for change during systole.

Measuring cerebrovascular damping

Peripheral hemodynamics, like pulsitility, pulse wave velocity and damping are measured by observing the kinetics and temporal hemodynamics associated with PI as it travels from the

femoral to the carotid artery (Townsend et al., 2015). The benefit of this approach is that it is a long and consistently straight section of vasculature. By measuring the temporal aspects along a known carotid to femoral length – it has been demonstrated that the speed (pulse wave velocity; PWV) and the PI at which a pulse pressure travels is positively related to the level of arterial stiffening (Townsend et al., 2015). However, the cerebral vasculature is more tortuous than the carotid to femoral section, making accurate measures of length and consequently PWV difficult but, PI and damping measures can be performed. Considering the multifaceted regulation of the cerebral vasculature, dynamic measurements of vascular hemodynamic damping, including changes in damping during increases and decreases of CBF, specific to the brain are required. In the past, PI measures have been taken from the carotid artery to the MCA (Lefferts et al., 2021). However, the carotid artery bifurcates into the ECA and ICA, and while this bifurcation provides damping to the brain, ECA interference is not expected to influence extra-intracranial damping. Thus, by measuring changes in PI from the ICA to the MCA, a more direct representation of pulsatile buffering in the brain is achievable.

In summary, our use of DFi as a measure of change in cerebrovascular hemodynamics encompasses 1) the role of Windkessel, and the necessity of a complaint vessel to maximise the smoothing of a pulsatile flow 2) Reduces confounding from ECA by measuring above the bifurcation at the ICA. To further understand these regulatory mechanisms pharmacological interventions were used to observe the cerebral vascular hemodynamic responses to increases and decrease in CBF at SL and HA.

2.5. Pharmacological Cerebrovascular Responses

The brain is sensitive to multiple types of pharmacological interventions despite being protected by the blood-brain barrier. The following section will outline the mechanisms of action of DOB, ACZ, and INDO including the expected impact on CBF at SL and HA. First, a summary will outline the rational of the initial study by Burgess et al., (2018) that provided the data analyzed in this thesis.

The study by Burgess et al., (2018) investigated central sleep apnea at HA. The pharmacological interventions DOB+ACZ were used to increase CBF. Acetazolamide increases tissue pH and helps to optimize CO_2 washout by increasing the sensitivity of the microvessels to CO_2 while DOB increases cardiac output which increases CBF. It has been observed that during sleep CBF falls, largely due to hyperventilation induced hypocapnia, and the fall in CBF is greater in those with central sleep apnea. Thus, increasing CBF using DOB+ACZ was hypothesized as a treatment to mitigate the onset of central sleep apnea. Conversely, INDO was given to reduce CBF as a means of observing the if reducing CBF would exacerbate central sleep apnea severity at HA. Burgess et al., (2018) found that DOB+ACZ increased CBF at HA and resulted in a reduction of central sleep apnea. Following administration of INDO, CBF decreased and although P_aCO_2 did not change metabolic acidosis was still observed. Further, hypoxic ventilatory response did not significantly change following INDO, which is likely linked to the unchanged P_aCO_2. There was no significant change in central sleep apnea following administration of INDO at HA.

Dobutamine

Dobutamine is a synthetic catecholamine and selective beta-1 adrenergic receptor agonist commonly used for treatment of conditions such as heart failure and to conduct echocardiogram

stress tests (Ashkar et al., 2023; Leier & Unverferth., 1983; Overgaard & Dzavík., 2008; Tuttle & Mills., 1975; Secknus & Marwick., 1997). Dobutamine has an inotropic and chronotropic effect that specifically targets the heart and augments myocardial contractility consequently increasing cardiac output and stroke volume (Ashkar et al., 2023; Leier & Unverferth., 1983; Overgaard & Dzavík., 2008; Tuttle & Mills., 1975). Dobutamine is shown to increase cardiac output by binding and activating beta-1 receptors, there is also beta-2 receptor activity to a lesser extent which reduces systemic vascular resistance (Ashkar et al., 2023; Overgaard & Dzavík., 2008). It is typically infused intravenously in doses ranging from 2.5 mcg/kg/min- 15 mcg/kg/min (Ashkar et al., 2023; Overgaard & Dzavík., 2008; Tacon et al., 2012). The risks associated with DOB are largely related to the presence of pre-existing conditions as it is used with high-risk populations (e.g. cardiac decompensation, heart failure). Following infusion most experience an increase of systolic blood pressure and heart rate; this is a greater risk for those with pre-existing hypertension. Contraindications to DOB include having a previous allergic reaction to it or any sulfite use, patients with acute myocardial infarction, unstable angina, left main stem disease, severe hypertension, arrhythmias, acute myocarditis, acute pericarditis, hypokalemia, and idiopathic hypertrophic sub-aortic stenosis (Ashkar et al., 2023). Following administration of DOB, Ogoh et al., (2017) saw and increase in cardiac contractility, cardiac output, and arterial pressure, however ICA blood flow and conductance decreased slightly from resting. Further, ECA blood flow and conductance increased, which is interpreted as a protective effect from cerebral over perfusion. Zhang et al., (2023) found DOB decreased CBF in the anterior circulation, mainly in the frontal lobe. At HA (5050m) Burgess et al., (2018) demonstrated a significant increase of CBF following DOB+ACZ administration.

Acetazolamide

Acetazolamide is a carbonic anhydrase inhibitor that mitigates pH buffering, which re-establishes acid base regulation across the blood-brain barrier, resulting in blunted vasoconstriction and increased CBF (Caldwell et al., 2021). Acetazolamide is commonly used to ameliorate AMS and it accelerates acclimation to HA through increased ventilation and renal extraction of HCO_3^- (Caldwell et al., 2021b; Leaf & Goldfarb., 2007; Teppema et al., 2007). Other common uses include treatment of glaucoma, idiopathic intracranial hypertension, congestive heart failure, altitude sickness, periodic paralysis, epilepsy, and it has been investigated for treatment of sleep apnea (Burgess et al., 2018; Farzam & Abdullah., 2023). The typical dose ranges from 250 mg/day to 1,000 mg/day (Farzam & Abdullah., 2023; Leaf & Goldfarb., 2007). The most common side effect of ACZ is diuresis, but can also include fatigue, nausea, vomiting, abdominal pain, and diarrhea (Farzam & Abdullah., 2023; Hultgren., 1997). Contraindications for ACZ include those with impaired liver function, hyperchloremic acidosis, and taking salicylates, bicarbonates, or anti-folates (Farzam & Abdullah., 2023).

Acetazolamide increases ventilation and arterial oxygen saturation through maintenance of acid-base balance (e.g., enhanced renal excretion of bicarbonate) (Cain & Dunn., 1966; Leaf & Goldfarb., 2007; Teppema et al., 2007). At SL ACZ has a modest effect, prompting small increases in CBF through the maintenance of acid-base balance and promoting ventilation (Ehrenreich et al., 1961; Hauge et al., 1983; Okazawa et al., 2001). During hypoxia ACZ causes vasodilation of the cerebral arterioles which reduces distal cerebrovascular resistance (Okazawa et al., 2001; Teppema et al., 2007). Dobutamine and ACZ when administered together act to

increase cardiac output through upstream macrovasculature and decrease downstream resistance at the cerebral microvascular, overall resulting in an increase of CBF.

Indomethacin

Indomethacin is a non-steroidal anti-inflammatory drug (NSAID) and non-selective cyclooxygenase (COX) inhibitor used for treatment of many conditions including arthritis, fever, headache syndromes, and dysmenorrhea (Lucas., 2016; Suleyman et al., 2010; Summ & Evers., 2013). The inhibition of COX (1&2) results in blocked prostaglandin synthesis (**Figure 8**) (Lucas., 2016; Suleyman et al., 2010; Summ & Evers., 2013). Prostaglandins are lipids with hormone-like functions, critical modulators of vascular tone and generally induce vasodilation (Davidge., 2001; Rosehart et al., 2021). Animal studies have shown, and largely been confirmed in humans, that INDO decreases CBF at normocapnia from 18-40%, and attenuates the cerebrovascular reactivity to hypercapnia with vasocontraction occurring homogenously across the brain (Rasmussen., 2005). Small, low resistance vessels see the primary effect and because the brain is a high filter, low resistance organ so it makes sense that its more sensitive to INDO (Rasmussen., 2005). Cerebral vasoconstriction leads to decreased CBF and thus, reduced intracranial pressure (Jensen et al., 1991; Rasmussen., 2005). Adverse effects with INDO are largely dose related and commonly include headache, dizziness, dyspepsia, and nausea (Lucas., 2016; Munjal & Allam., 2023). A typical dose ranges from 25-150 mg depending on dosage strength and purpose (Lucas., 2016; Mayo Clinic., 2023). While the inhibition of COX-2 enzyme is thought to be responsible for its anti-inflammatory effects the concurrent inhibition of COX-1 can result in gastrointestinal side effects (e.g., indigestion, nausea, gastric ulcers) (Munjal & Allam., 2023; Suleyman et al., 2010). Use of INDO is contraindicated for those with a history of

NSAID or salicylate-induced hypersensitivity and atopic reactions after taking NSAIDs, a previous history of coronary artery bypass graft surgery and pregnant women starting the third trimester of pregnancy (Munjal & Allam., 2023).

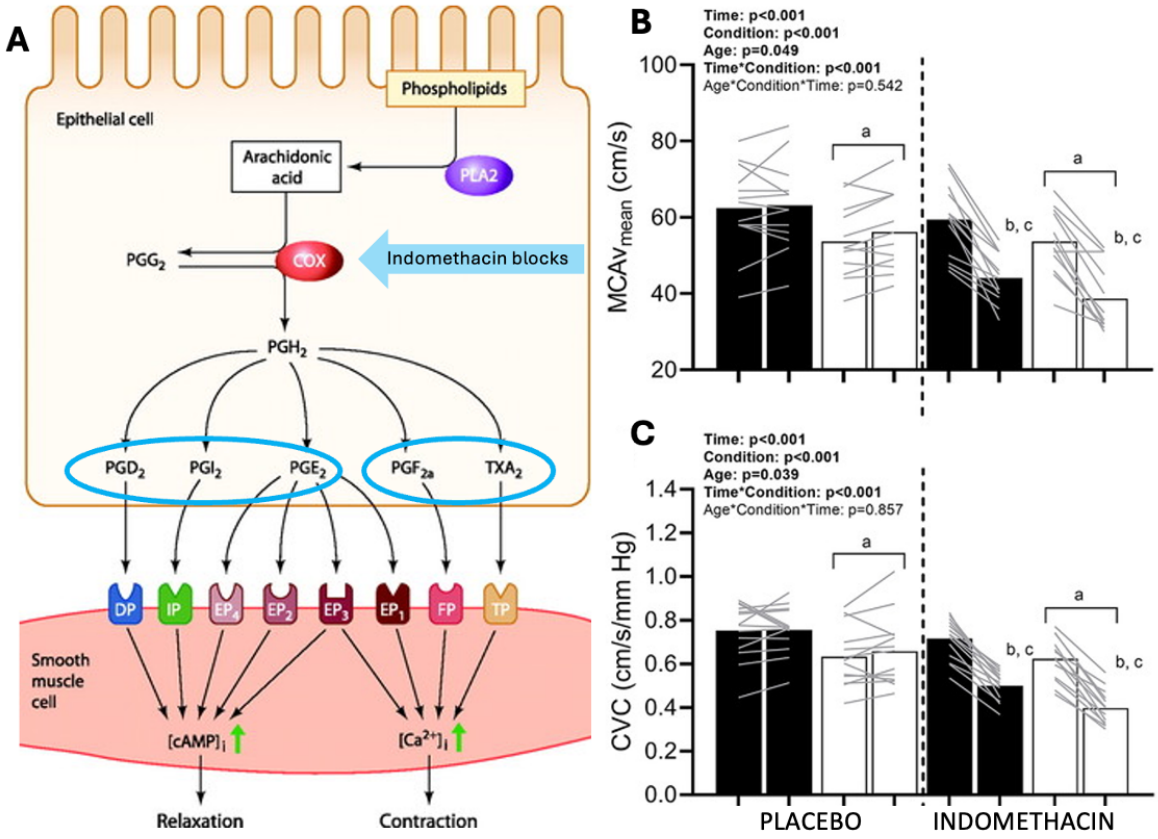

Figure 8. (A) The cyclooxygenase (COX) pathway from the epithelial cell to smooth muscle. Indomethacin acts by blocking COX (indicated by blue arrow) resulting in inhibited prostaglandin synthesis, impairing smooth muscle relaxation, and inducing vasoconstriction. Adapted with permission from Ruan et al., (2011). (B & C) Black bars=young adults, white bars=older adults. The data to the left of the dashed line is placebo, to the right is the indomethacin intervention. Each horizontal line within the bars indicates one participant. (B) $MCAV_{mean}$ = Mean middle cerebral artery velocity (cm/s). Middle cerebral artery velocity was measured pre and post indomethacin or placebo. Following indomethacin, the mean middle cerebral artery velocity was significantly decreased. (C) CVC= Cerebrovascular conductance (cm/s/mm Hg). Following administration of indomethacin CVC, or the ease with which blood can flow through the vessel, was reduced. Adapted with permission from Shoemaker et al., (2021).

2.6. Purpose and Hypothesis

In the literature review above, the anatomy and principles of cerebral blood flow regulation at SL and HA were discussed in detail. This discussion included historical findings, as well as contemporary views on cerebrovascular regulation derived from research. This has been presented in such a way to reveal that further investigation is needed to discern how cerebrovascular structure and function influences hemodynamic forces at sea-level and high altitude. Specifically, the importance of arterial blood gases, with a focus on P_aCO_2 CBF regulation, as well as the integrative cerebrovascular balance between P_aO_2 and P_aCO_2 responses. This discussion is provided to illustrate the impact of upstream and downstream vasodilatory and vasoconstrictive responses on cerebrovascular hemodynamic buffering. Traditional and contemporary perspectives of cerebrovascular autoregulation have also been provided and suggest that despite dogmatic views suggesting that the brains microvasculature solely provides resistance to CBF fluctuations, a more dynamic pressure passive cerebral autoregulatory response governed throughout the entire vascular tree is more probabilistic. Thus, further investigation is required to quantify the degree to which extra and intracranial vessels influence hemodynamic buffering in the brain. Research aiming to assess hemodynamic forces throughout the cerebrovascular tree, not just in the microvasculature should consider this contemporary pressure passive approach to help understand how the brain may be impacted by conditions where pulsatile stressors are altered.

These details discussed in the literature search above have been provided as rationalization of research question central to this thesis, as well as providing details on hemodynamic regulation during environmental and pharmacological interventions pertinent to the cerebral vasculature.

2.6.1. Thesis research question

This thesis aimed to investigate how DOB at SL, and DOB+ACZ at HA influence pulsatile cerebrovascular hemodynamics when CBF is pharmacologically increased through upstream cardiac contractility (DOB) and downstream reductions in microvascular resistance (ACZ). We further sought to understand and quantify the effects of CBF reduction following INDO administration at SL and HA on pulsatile hemodynamic damping in large cerebral arteries.

2.6.2. Purpose

The purpose of this investigation is to provide details that help further the understanding of how pharmacological interventions at SL and HA that increase and decrease CBF provide an experimental opportunity to assess the mechanisms involved in buffering cerebrovascular hemodynamic stress. This series of experiments seeks to quantify changes in vascular compliance using DFi. We aimed to characterize pulsatile cerebrovascular hemodynamic DFi, as an index of cerebral hemodynamic buffering, by observing PI in ICA and MCA following pharmacological increases (experiment 1) and decreases (experiment 2) in CBF at SL and following acclimation to HA.

2.6.3. Hypothesis

Our hypothesis was that DOB administration at SL would trigger an increase CBF and cerebrovascular PI, which would result in compensatory downstream vascular resistances (i.e., increased DFi). Further, we hypothesized that reducing CBF at SL and at HA using INDO would result in a reduced DFi, caused by an increased extra to intracranial hemodynamic transmission which we interpreted as an impaired cerebrovascular compliance. At HA, we hypothesized that

because DOB+ACZ administration would lower cerebrovascular resistance, that cerebrovascular DFi would increase despite the HA acclimatization response.

Chapter 3 Methods

In the original study by Burgess et al., (2018), where this data was sourced from, 12 healthy volunteers where included (8M, 4F; 31 ± 7 yr, body mass index 25.6 ± 3.6 kg/m2) in a randomized placebo-controlled single-blind study at 5,050 m in Nepal. The study had approval from the University of Victoria, the University of British Columbia Ethics Committee, the Nepal Health Medical Research Council, and conformed to the standards set by the Declaration of Helsinki. Written informed consent was obtained. Other experiments were conducted on the same expedition before and after these experiments however, there was no overlap with the sleep experiments or any confounding pharmacological manipulation or exercise. Participants were non-smokers and were not taking medications besides acetazolamide throughout ascent. They were instructed to abstain from caffeine and alcohol 24 hours prior to measurements. Eleven health volunteers were included in this secondary analysis which has approval from the University of Victoria 23-0629. While a discussion of the ascent profile is included here the experimental design is discussed in detail in chapter 4 (i.e., experimental section).

3.1 Instrumentation

The equipment and tools used for data collection in experiments 1 and 2 outlined within will be discussed in detail. This will include details pertaining to all cardiorespiratory assessments, as well as TCD and VDu.

3.1.1 The Principles of Ultrasound

Ian Donald is credited with the popularization of ultrasound imaging (1958) and decades later it is a widely used tool in clinical and research settings (Ian Donald et al., 1958). Sound is waves of mechanical energy that travel parallel to the direction of propagation (Olusanya., 2023). The

human ear hears in the range of 20-20,000Hz, sound frequencies greater than 20,000Hz are called ultrasound (Olusanya., 2023). An ultrasound wave is transmitted through a handheld probe containing piezoelectric crystals. In response to electrical current the crystals vibrate and create ultrasound waves which are transmitted through tissues (e.g., skin, bone, brain, walls) and reflect off the moving red blood cells back to the transducer (Aaslid et al., 1982). The velocity of the moving cells is proportional to the Doppler-shift (Eq 2) (Aaslid., 1986; Olusanya., 2023; Purkayastha & Sorond, 2012). Because flow within vessels is not uniform across the width of the vessel multiple velocity signals are acquired and meaningful velocity values can be extracted through calculation of the maximum or mean velocity using approximately 5 second sections (Willie et al., 2011). The fast Fourier transformation assists in taking the blood velocity shifts and expressing them as a time domain function (Willie et al., 2011).

Eq. 2

$$Doppler\ Shift\ (f_d) = \frac{2f_o v \cos\theta}{c}$$

f_o =emitting frequency

v = propagation velocity

θ = Doppler angle

c = sound propagation speed

Where f_o is the transmitted frequency (i.e., 2MHz); v is the propagation speed; cosθ is the correction factor based on the angle of insonation; and c is the speed of sound in the blood (1540 $m.s^{-1}$) (Uppal & Mogra., 2010).

Pulsed-wave Doppler

Pulse-wave Doppler emits short pulses into the tissue and waits for them to return, only measuring the frequency shift of the returning pulses. Range gating is used to facilitate signal

analysis from a small area at a specified depth from the transducer. A benefit of pulse-wave Doppler is the depth acuity as the sample gate can be moved along the Doppler line. However, at high frequencies pulse wave-Doppler experiences signal aliasing, whereas continuous-wave Doppler has no signal aliasing but does not have depth ambiguity (Reeder et al., 1986). Further, because pulse-wave Doppler is emitting pulses at a high frequency and waiting for the returning signal, there is a maximum velocity that can be accurately measure (i.e., maximum Doppler shift).

3.1.2 Transcranial Doppler Ultrasound

First used and popularized by Aaslid (1982), TCD is a non-invasive cerebrovascular imaging modality that utilizes a 1-2 MHz ultrasonic beam to penetrate the skull (Aaslid et al., 1982; Barlinn & Alexandrov., 2022; Willie et al., 2011; Moppett & Mahajan., 2004; Naqvi et al.,2013). It should be noted that TCD can be used to measure velocity of blood but not the volumetric flow or total blood volume as it does not measure diameter (Aaslid et al., 1982; Barlinn & Alexandrov., 2022; Willie et al., 2011; Moppett & Mahajan., 2004; Naqvi et al.,2013). Thin boney sections of the skull located using facial and head landmarks (i.e., zygomatic arch, ear, lateral edge of the orbital bone) known as acoustic windows allow for insonation of the large primary arterial branches of The Circle of Willis. There are four main windows the transtemporal, suboccipital, transorbital, and submandibular (Moppett & Mahajan., 2004; Naqvi et al., 2013; Willie et al., 2011). The data provided in this thesis utilized the transtemporal window (**Figure 9**). Further, there are three windows within the transtemporal approach the anterior window, the middle window, and the posterior window, all are located above the zygomatic arch (Purkayastha & Sorond, 2012; Willie et al., 2011). Due to the skulls varying

thickness the temporal region is the preferred section to insonate for imaging of the MCA as the bone is thinner and the location allows for attachment of a headpiece (Willie et al., 2011).

Insonation angles

The angle of insonation is the angle between the emitted wave relative to the direction of flow in the vessel and it is vital to optimize this as it directly impacts accuracy (**Figure 9**). For example, an insonation angle of zero means the wave is parallel to the vessel the cosine of 0 is 1 thus this is the most accurate. A larger angle results in a larger cosine and greater potential for error, an angle of <30° is ideal yielding and error of <15% (Purkayastha & Sorond, 2012).

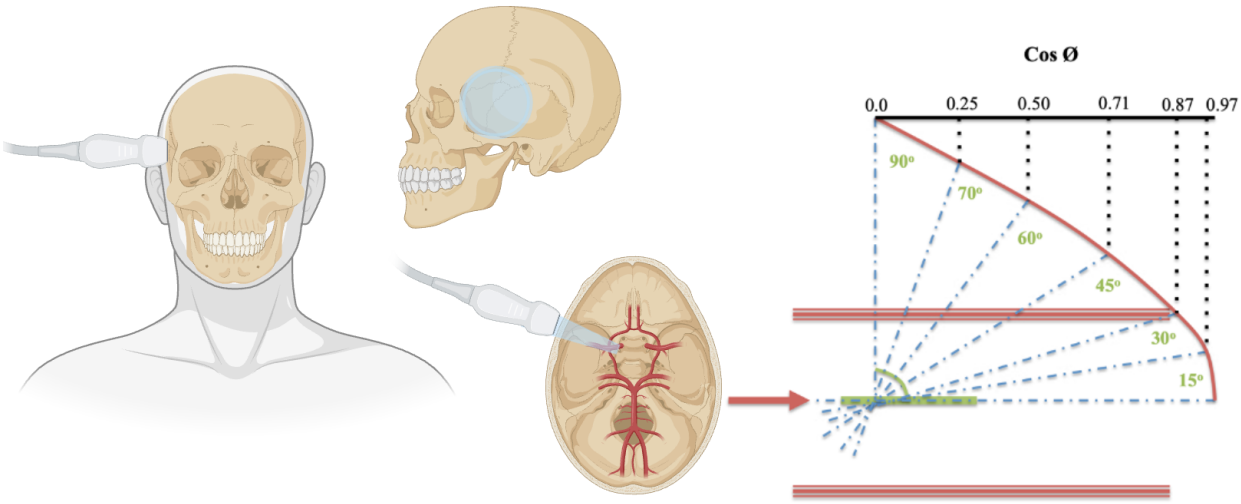

Figure 9. The left image depicts insonation of the middle cerebral artery using the transtemporal window, located on the thinner area of the skull above the zygomatic arch and in line with the eye. The image on the right demonstrates the relationship between angle of insonation and cosine of the angle (Cos θ). As the angle of insonation increases towards 90° the percentage of the reflected signal reduces, when entirely perpendicular to the vessel no signal will be recorded. The red stripped lines = vessel walls, red arrow = direction of blood flow, blue dashed lines= ultrasound beam, green bar = angle cursor, black dashed lines = percentage of the reflected ultrasound signal that is received by the receiver.

Assessment of intracranial velocity using transcranial Doppler ultrasound

The steps for measuring velocity on cerebral arteries such as the MCA are described in detail in the following steps. 1) Because ultrasound will dissipate through air, a generous amount of ultrasound gel is required to provide an acoustic medium between the ultrasound probe and the skin. This gel medium increases the probes surface area in contact with the skin. 2) TCD ultrasound probes are transfixed to the head and held in place using a specialized head band (Mark 600, Spencer Technologies LTD, USA) placed on the participants head, sitting just above the eyebrows and the base of the occipital bone (back section of skull). The headpiece greatly reduces between testing error as it positions the TCD probes in a position that is easily repeatable by accounting for anatomical landmarks, head piece size, and using pictures to ensure that probe position is similar between measures once the scanner finds the optimal acoustic window. The appropriate window is determined after the probe is loosely transfixed to the probe holder. Several windows in the temporal acoustic window will be assessed using large macro adjustments before securing the probe in place. Confirmation techniques allow accurate identification of the intended vessel. First, consider the depth and direction of blood flow relative to the probe (Willie et al., 2011). This thesis observes the MCA, which is commonly found through the transtemporal window at a depth of ~5cm (50mm) with flow coming towards the probe (Aaslid et al., 1982; Barlinn & Alexandrov., 2022; Moppett & Mahajan., 2004). As expected, the MCA depth in this data set ranged from 45-55 mm. To further confirm, carotid compression will result in a reduction of the ipsilateral MCA with a compensatory increase of the PCA (Moppett & Mahajan., 2004; Willie et al., 2011). 4.) Once the preferred acoustic window is established, micro adjustments (tilt or rotate) are made to ensure the maximum velocity trace is obtained, this also minimizes the angle of insonation which is assumed to be zero.

Validity of transcranial Doppler

Since its popularization as a measure of CBF by Aaslid et al., in 1982 TCD has been used as a surrogate of CBF. As outlined in the VDu section, blood flow is calculated as the product of velocity times cross-sectional area. Studies have explored the validity of TCD (Serrador et al., 2000) and whether the MCA changes diameter during cerebrovascular stimulation. The findings by Coverdale (2015) and Verbree (2014) demonstrated that the Serrador paper was likely incorrect, showing that cerebral vessels do vasodilate during changes in $PaCO_2$. During open craniotomy Giller et al., (1993) did report changes in MCA diameter of <4% but saw changes as high as 29% at the more distal segments (i.e., M2) and arterioles. Thus, TCD may closely reflect blood flow through the insonated artery. At HA Wilson et al., (2011) indicated that the MCA vasodilates above 5,300m but seems consistent at lower altitudes. Similarly, Willie et al., (2014) showed a sustained MCA dilation for the duration of exposure to 5050m although diameter was not assessed after the ascent which is a limitation of the findings. On its own, TCD does not seem to provide and precise representation of flow especially following cerebrovascular stimulus (e.g., hypoxia) however, pulsatile hemodynamic buffering is not necessarily dictated by diameter but by the difference between proximal to distal systolic and diastolic pressures (i.e., pulsitility). The distention during the cardiac cycle likely impacts DFi but outside of PET which requires radioactive tracers, the current technology is not sufficient for capturing large cerebral vascular vasodilation's.

3.1.3. Vascular Duplex Ultrasound

This section summarizes comprehensive guidelines for extracranial vascular ultrasound imaging (Thomas et al., 2015). Vascular duplex ultrasound is a non-invasive method of assessment for extracranial arteries that provides both velocity and diameter measures in real time. Although the

principles of vascular Duplex are similar to TCD there are some distinctions. First, a higher frequency (7MHz or greater) probe is used with VDu and provides high temporal and spatial resolutions to quantify velocity and cross-sectional area contemporaneously. The waves are transmitted into the skin and reflected off tissue and moving blood cells. The returning ultrasound waves are computed to reveal the anatomical structures beneath the transducer. Images consist of 2D gray scale images (brightness mode; *B*-mode) (**Figure 10**). *B*-mode allows for differentiating and measuring artery structures during VDu examinations (e.g., wall thickness). Imaging using these guidelines provides a standardized imaging methodology, improving the accuracy of extracranial cerebrovascular measures (Thomas et al., 2015).

Duplex ultrasound assessment techniques

In the interest of accuracy, reliability and validity when assessing extracranial blood flow at rest a systematic and standardized approach is needed. The following section outlines this approach.

Identification of the internal carotid artery

The initial steps to identify the internal carotid artery are as follows. 1) Start by insonating the carotid artery cross-sectionally. The carotid artery can be distinguished by applying light pressure, veins will collapse, and the artery will maintain its shape. Follow the carotid towards the jaw until it bifurcates (splits into two smaller vessels i.e., ICA and ECA). Some people have higher bifurcations in which case insonating from a slight posterior angle can provide a better image. Pivot the probe to long section in the area of the bifurcation, if needed slide the probe down away from the jaw to reorient on the carotid artery then follow it back up. The ICA is typically found posteriorly-laterally to the carotid artery. Depending on the angle of approach, the ICA and the ECA may be visible in the same plane. If the ICA and ECA are not visible in the

same plane, a slight sweep of the transducer will visualize each vessel, and distinguishing which vessel is insonated using the same criteria: 2.) Distinguish the ICA by its diameter, which is ~4-6 mm. 3.) Further, the ICA has no extracranial branches compared to the external carotid artery which does. Colour doppler can be used to better determine the presence of branches. 4.) The characteristics of the waveform can help distinguish between the ICA and the ECA. The ICA waveform is lower resistance with a gradual upstroke and broader systolic peak. The flow is continuous and tapering with a higher end diastolic velocity. The ECA waveform has a higher resistance waveform with a lower end-diastolic peak. 5.) Finally, the vessel can be confirmed using a temporal tap. A firm tap is delivered in the area of the superficial temporal artery and will produce a distortion on the spectral Doppler if imaging the ECA. Perform this for both the assumed ECA and ICA to help distinguish between them, however if the distortion is present for both vessels skip this step.

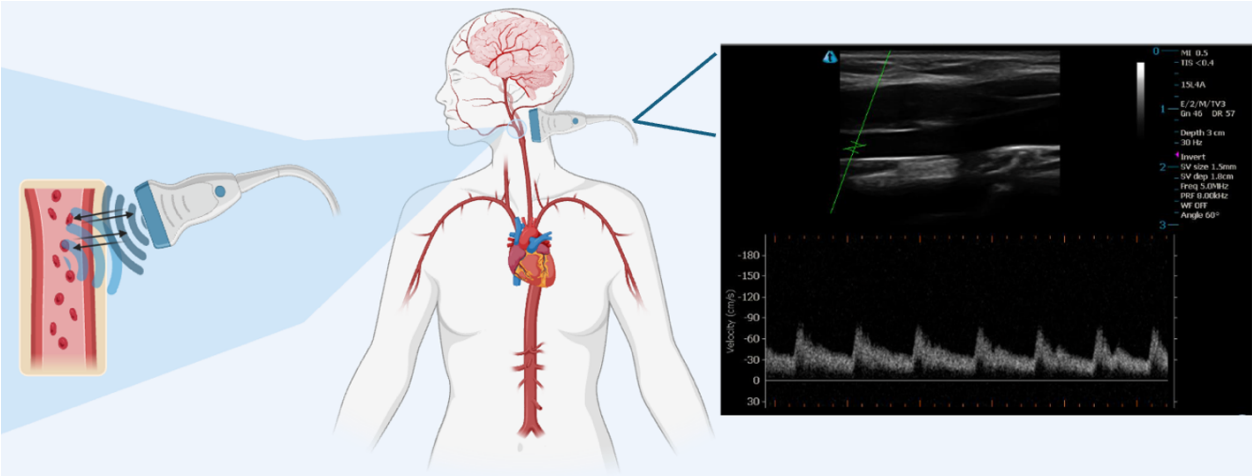

Figure 10. Vascular Duplex in the ICA. A depiction of insonating the internal carotid artery using vascular Duplex ultrasound. The far-left shows ultrasound pulse waves being transmitted from the transducer, encountering the moving red blood cells, and transmitting back to the transducer. On the far right is a *B*-mode image of the internal carotid artery where the green line=steering angle, dark are in the middle of the vessel= lumen, bring white outline of the lumen=vessel walls. Beneath the image of the vessel is the velocity trace (cm/s).

Optimizing vascular duplex B-Mode image

Once the sonographer is confident in the identification of the vessel, the image can be optimized using the settings described below.

Brightness mode

Brightness mode also known as *B*-mode is the first adjust made when imaging extra-cranial vessels. It is a grey scale representation of the structures underlying the transducer. To ensure accuracy of the image it can be optimized using depth, focus, and gain which is explained in further detail below.

Depth

To optimize depth the vessel will ideally take up 2/3 of the display, although depending on vessel depth this is not always possible. This reduces wasting of Doppler propagation ensuring higher frame rates and keeps the vessel on the screen in the event of movement. Ideally, the ultrasound beam is 90° to the tissue interface this ensures the best reflectivity of the vessel walls (i.e., clearer walls). The "heel toe" technique or rocking the transducer from end to end will improve the alignment.

Focus

The focus points can be adjusted to provide better lateral resolution. Shifting the focus points to the area of the vessel walls will make them clearer.

Gain

Optimizing the *B*-mode image is especially important if using edge-detection software. This can be done by adjusting overall gain, time gain compensation, and dynamic range. First, reducing overall gain will increase the contrast between black and white. This will reduce artifacts within the lumen and increase echogenic contrast. Next, at the region of interest time gain compensation

can be adjusted to increase local contrast between the vessel and surrounding tissue and further decrease contrast in the lumen. Finally, dynamic range will increase the contrast of the entire *B*-mode image and increase noise rejection helping to eliminate noise and weak echoes in the lumen.

Pulsed-wave Doppler

Pulsed-wave Doppler adjustments are used to optimize the velocity trace based on the received Doppler shift. Overall, this will further optimize the extra-cranial vascular assessment. Pulsed-wave Doppler is outlined in greater detail in the TCD instrumentation section, however VDu differs because of the ability to measure diameter. The angle of approach, placement of sample volume, angle correction, baseline, scale and gain can all be adjusted to provide a more accurate velocity trace.

Angle of approach (Doppler angle)

The angle of approach, or Doppler angle, refers to the angle between the beam and the direction of travel of the moving reflector. To reduce measurement error the beam steer can be adjusted to an angle of 30°-60°. The angle should never be larger than 60°, as even a small error in angle alignment will result in large errors in the velocity calculation due to the rapidly changing cosine function.

Sample volume placement

The sample volume indicates the depth along the beam axis where information is being obtained. It should be placed in the area with the fastest flow with the width encompassing the entire region of interest. Ideally the sample gate will cover 80% of the lumen, this will ensure consistent sampling even in the event of movement. Often, and in this thesis, the calculation of flow uses the time-averaged maximum velocity derived from the peak velocity envelope.

Angle correction

The sample volume should reflect the Doppler angle and align with the direction of flow. Typically, found within the sample volume the angle between the cursor and the central axis of the beam is used to calculate velocity and thus, must be correct to obtain and accurate tracing.

Doppler baseline

The Doppler baseline is a horizontal line that indicates 0 cm/s. This line should be set low on the screen to allow the full velocity trace to be within the display. If the baseline is too high, it will cause the systolic peak to wrap around and overlap with the diastolic measures. Additionally, if the baseline is too low it may cut-off retrograde velocity. Further, if the velocity trace appears upside down (due to probe orientation) it can be flipped using the invert button.

Doppler scale

The Doppler scale is represented by the y-axis on the spectral display. It must be set to accommodate fluctuations in velocity, ensuring all measures stay within the display. Typically, setting the scale so the trace takes up 2/3 or 60% of the screen is appropriate.

Doppler gain

Similar to the *B*-mode gain, optimizing the velocity trace is especially important if using edge detection software. Thus, gain must be adjusted to reduce noise in the spectral window (e.g., "speckle") while still ensuring a clear, crisp image. Dynamic range can be adjusted to further improve the contrast of the trace (white) with the background (black).

Trade-off between B-mode and pulse wave display

Duplex mode allows for data collection from *B*-mode (diameter) and Doppler (velocity) simultaneously which allows for measures of beat-to-beat flow and other hemodynamic variables

(e.g., stiffness). However, as previously discussed to optimize the *B*-mode image the vessel will be horizontal but for an ideal velocity trace the angle of between the beam and flow should be 0°-60°. This necessitates a compromise using beam steering and the heel-toe technique to achieve and optimal angle of insonation (≤60°).

Edge detection: Assessment of diameter

The use of edge detection software allows for a more objective calculation of diameter and velocity (Woodman et al., 2001). To collect extracranial diameter a computerized edge detection system was used that automatically tracts the artery wall (**Figure 11**). A screen recording was taken using Camtasia, which allows for frame-by-frame reference following data collection. Simultaneously collecting velocity and diameter data provides greater accuracy for the calculation of flow.

Coefficient of variation

A limitation of duplex ultrasound is the user dependence, as the sonographer must be highly skilled to consistently acquire an optimal image. The lower the coefficient of variation the lower the potential for measurement error. To mitigate this risk extensive practice, observation from a qualified sonographer, practice analyzing data, and determination of each scanners coefficient of variation is required (Smith et al., 2014; Willie et al., 2014).

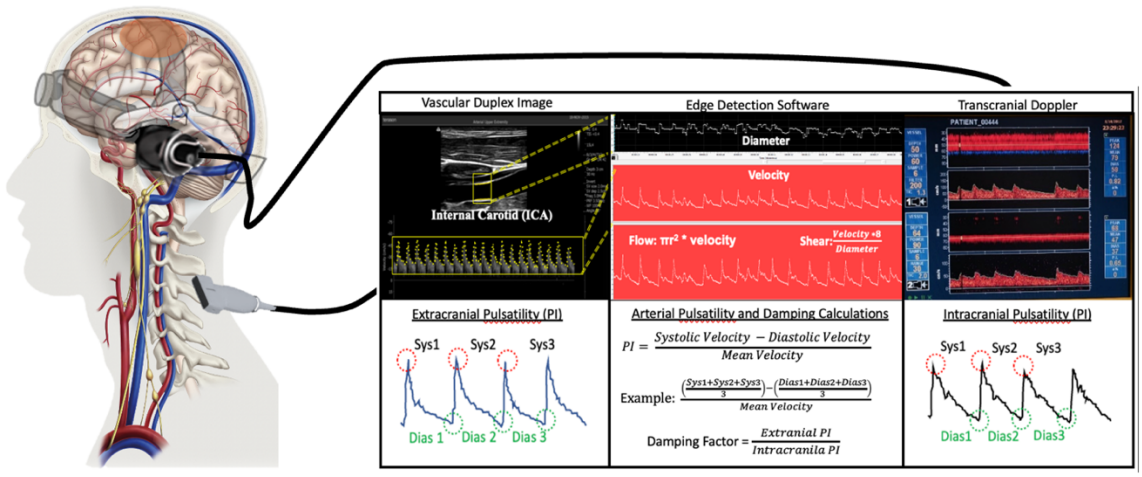

Figure 11. The left is a stylised imager of the brain and the insonated vessels Willie et al., (2014) adapted to include a transcranial Doppler ultrasound headpiece that supports the Doppler probe insonating the M1 segment of the middle cerebral artery accompanied by the velocity trace. The vascular Duplex ultrasound probe is insonating the internal carotid artery, accompanied by the *B*-mode image of the vessel (top portion) and the pulse wave trace (lower image). Using edge detection software continuous velocity and diameter of the ICA vascular walls help to reduce user bias when assessing the vessel. Both transcranial and vascular duplex ultrasound are able to measure pulsitility in the middle cerebral (PI_{MCA}) and internal carotid artery (PI_{ICA}) by dividing the systolic minus diastolic velocities by the mean velocities. Extra to intracranial damping factor is then calculated as the ratio of PI_{ICA}:PI_{MCA}.

3.1.4. Cardio-respiratory Instrumentation and Assessment

To better understand the mechanisms impacting changes in CBF, the following section outlines the steps taken to accurately assess cardio-respiratory responses known to be associated with CBF regulation to assess the integrative impact that pharmacological interventions might have on CBF at SL and HA.

Data acquisition

All cardiorespiratory signals were collected using an analog-to-digital converter device and were connected to a continuous data acquisition device (Powerlab/16SP ML 880; ADInstruments, Colorado, US). These signals were cardiovascular (heart rate and arterial blood pressure) and

respiratory (ventilation and partial pressure of end-tidal carbon dioxide) measures and were assessed at 1000 Hz. All digital data acquired was transmitted and organized in a digital computer charting software (LabChart7; ADInstruments, Colorado, US) which is used to time align all cardiorespiratory signals with TCD measures.

Assessment of heart rate

A 3-lead electrocardiography (ECG) transducer was used to collect heart rate data and was connected to an acquisition device (Powerlab/16SP ML 880; ADInstruments, Colorado, US). The leads were placed using a triangle pattern (i.e., Einthoven's triangle) (Barold et al., 2003) around the heart, monitoring the direction and magnitude of electrical rhythms. The electrical rhythms of the heart are a product of neuromuscular electrical signals which contract (depolarize) and relax (repolarize) the cardiac tissue. The ECG tracing creates 5 distinct shapes and waveforms that display different cardiac cycle stages. 1.) P wave – Atrial depolarization represented by a small deflection wave. 2.) PR interval – Time between the first deflection of the P wave and the first deflection of the QRS complex. 3.) QRS complex – Three waves representing ventricular depolarization. The Q represents depolarization of the interventricular septum, the R wave reflects depolarization of the main mass of ventricles, and the S wave represents the final depolarization of the ventricles at the base of the heart. 4.) Lastly, the T wave reflects the ventricular repolarization. The R wave is the largest and typically yields the greatest increase in healthy individuals, making it a useful landmark to measure beat-to-beat heart rate. The heart rate data was collected using R to R wave detection on the ECG (leadII, Dual Bio Amp, ADInstruments) connected to the data acquisition device (Ashley & Niebauer., 2004).

Blood pressure assessment using photoplethysmography

Photoplethysmography (Finometer Pro, Finapres Medical Systems, Amsterdam, Neth) is a non-invasive measure of beat-to-beat systolic and diastolic blood pressure. Worn at the fingertip it detects changes in blood volume of the microvascular bed using infrared light (Subasi., 2019). The light illuminates red blood cells and quantifies the amount of light absorbed (Nijboer et al., 1981). The microvessels do not change in diameter, thus allowing for a continuous measure of diameter and volume of red blood cells moving through the vessel. The data collected from the finger is filtered and reconstructed to an estiamte of brachial artery pressure (Guelen et al., 2003). The pulse wave shape differences between brachial and finger arterial pressure are typical waveform distortions that can be expressed as a transfer function. An inverse transfer function can be applied to finger pulse pressure to reconstruct brachial pressure. Additionally, level correction strongly reduces the differences between the finger arterial pressure and the brachial pressure and reduces the variability of these differences. To further reduce the standard deviations of the differences a return-to-flow systolic pressure can be used to calibrate the waveform (Guelen et al., 2003).

Assessment of ventilation and gas exchange

A two-way pneumotach (Series 3813, Hans Rudolph, Shawnee, KS) connected to the data acquisition device (Powerlab/16SP ML 880; ADInstruments, Colorado, US) was used to measure breathing frequency, tidal volume, and ventilation. The pneumotach was calibrated against a 3L syringe to standardize the oscillatory (inspiration and expiration) pressure changes received by the spirometer pod during breathing. The total dead space of the breathing set up was set at less <250ml. The spirometer pod was then attached to the data acquisition device

(Powerlab/16SP ML 880; ADInstruments, Colorado, US) to calculate continuous tidal volume, breathing frequency and V_E. ADInstruments gas analyzer (model ML 206, ADInstruments, Colorado, US) connected to the data acquisition device was used to sample $P_{ET}O_2$ and $P_{ET}CO_2$. A thin plastic sample tube connected to a pump at the mouth was used to draw gas samples into the transducer for analysis, extracting the expired fractions of O_2 (F_eO_2) and CO_2 (F_eCO_2) each breath. The simplified alveolar gas equation was used to calculate end-tidal gases each breath (Eq 3).

Eq. 3

$$P_{ET}O_2 \; and \; P_{ET}CO_2 \; (mmHg) = (F_{ET}O_2 \; or \; F_{ET}CO_2) \times \; (Pb - 47mmHg)$$

Simplified alveolar equation where $P_{ET}O_2$ = partial pressure of end-tidal oxygen (mmHg), $P_{ET}CO_2$ = end-tidal carbon dioxide (mmHg), $F_{ET}O_2$ = fractional end-tidal oxygen, $F_{ET}CO_2$ = fractional end tidal carbon dioxide, Pb = atmospheric pressure (~760 mmHg at sea-level, ~400 mmHg at HA), 47mmHg = vapour pressure.

The gas analyzer quantifies O_2 fluctuations using absorption spectroscopy. A laser diode emits a band of light through the sample and a detector quantifies the amount of light absorbed by the O_2 using laser absorption spectroscopy (~760 nm). The more light that is absorbed the greater amount of O_2 and the less light will be reflected to the transducer. Conversely, the more O_2 present the less light absorbed, thus more light is reflected to the transducer. Quantification of CO_2 fluctuations is obtained following the assessment of O_2 in the gas analyzer. An infrared lamp is projected through the gas sample and infrared-red wavelength is absorbed by the gas molecules with similar spectral properties as the infrared light (i.e., CO_2). Then the absorbed infrared light is filtered using an optical filter in the sampling tube which absorbs all the wavelengths of non-CO_2 derived light. The difference of light filtered, and light absorbed is

compared at the end of the sampling tube and is proportional to the percentage of CO_2 in each breath-by-breath sample.

3.2. Study Design

Baseline measurements were collected in Kelowna (344m) and repeated 2,8, and 14 days following arrival to 5050m (the Ev-K2-CNR Pyramid Laboratory; B_p 413 ± 1 mmHg).

Participants

A total of 30 participants embarked to Kathmandu, but 12 (4 female, 8 male) with a mean age of 31±7 years and a body mass index of 25.6 kg/m^2 were included in the initial testing after providing written informed consent and making the trek to 5050m. Out of the 12 participants, 8 participants completed experiments one and two at SL. However, different combinations of these 8 participants completed experiments 1 (n=6) and 2 (n=6) at HA. Reasons for not completing certain aspects of each test include quality of ultrasound scans (n=3), altitude related illness (n=1), or other medical emergencies (n=1). All participants were typical residents of sea-level altitude, with two having experienced high altitude prior to this. The last previous high-altitude exposure was >4 yrs. For the duration of the study subjects abstained from caffeine and alcohol but were permitted acetaminophen if needed. Before each measurement session subjects rested in a prewarmed sleeping bag for a minimum of 10 minutes as part of the effort to ensure they were warm and calm. When evening measurements were taken (17:00-22:00) it was at least 1 hour after eating. Morning measurements (04:00-08:00) were collected before eating. Baseline measurements were collected in Kelowna (344m) and repeated 2,8, and 14-days following arrival to 5050m (the Ev-K2-CNR Pyramid Laboratory; barometric pressure 413 ± 1 mmHg).

Protocol

Experiments 1 and 2 were performed in a randomized order, with no less than 48 hours occurring between each experiment to allow for adequate pharmacological washout.

Experiment 1 (pharmacological increase of CBF): Approximately 24 hours after completing polysomnography, cardiovascular, and cerebrovascular screening, participants visited the sea-level laboratory (344m) to have their resting cerebrovascular function measured prior to completing several respiratory and cerebral reactivity tests (hyperoxic rebreathe; hypoxic reactivity; squat stands). Following an initial instrumentation period, participants were instructed to rest silently in a supine position for 10-minutes. Cerebral and cardiorespiratory baseline measures were taken over a 5-minute resting period after the initial 10-minutes of rest. Following the baseline measures, several reactivity tests (previously published data by Willie et al., 2015) were completed over approximately 30-minutes. Intravenous administration of DOB using an infusion pump at a rate of 2-5 μg/kg/min for 30-minutes was used to increase CBF at sea-level. Participants rested quietly during this period. Cerebral and cardiorespiratory measures were collected over a 5-minute resting period following drug infusion similarly to the pre drug infusion protocol. Drug infusion rate was maintained during resting measures. An identical protocol was followed at high-altitude testing, except drug infusion consisted of DOB +ACZ (2-5 μg/kg/min; 10 mg/kg). The addition of ACZ was used to counter the potential high altitude related hypocapnic vasoconstriction. Inhibition of carbonic anhydrase via ACZ infusion was intended to increase acidosis, and thus counter the impact of high altitude related hypocapnia expected to trigger a reduction in CBF and increase in vascular resistance.

Experiment 2 (Pharmacological reduction in cerebral blood flow): Experiment two was conducted in a similar fashion to experiment 1. Following a 20-minute instrumentation period, a 10-minute supine resting period preceded the 5-minute baseline cerebral and cardiorespiratory assessment period. The same tests were performed over a 30-minute period, prior to participants ingesting INDO (100 mg). The INDO dosage was used to reduce CBF over a 90-minute window. Participants were free to move about the laboratory initially following ingestion (60 minutes) but were asked to lie supine for re-instrumentation and rest for 30 minutes prior to post INDO ingestion measures. Post INDO cerebral and cardiorespiratory measures were collected during a 5-minute resting period similar to pre-INDO and DOB protocols.

Cardiorespiratory function

Heart rate, blood pressure, end-tidal pressure of oxygen and carbon dioxide, and arterial oxygen saturation were assessed using electrocardiography (ECG bio amp, ADInstruments, Colorado Springs, CO, USA), photoplethysmography (Finameter Pro, Finapres Medical Systems, Amsterdam, The Netherland), respiratory gas analysis (ML206, ADInstruments, Colorado Springs, CO, USA), and pulse oximetry (ML320 Oximeter Pod, ADInstruments, Colorado Springs, CO, USA0, respectively. All data were time aligned using acquisition device (Power lab/16SPML795; ADInstruments, Colorado Springs, CO, USA). Respiratory gases were sampled from a mouthpiece connected to the gas analyzer via nafion tubing and desiccant.

3.2.1. Analysis of Ultrasound Acquired Hemodynamics

As mentioned above, VDu allows for collection of diameter and velocity data simultaneously which allows for investigation of vascular hemodynamics such as compliance and stiffness. To

gain a measure of cerebral vascular stiffness extracranial and intracranial data are required. The best practice for measurement of the MCA using TCD is outlined in section 3.1.2 and VDu is outline in section 3.1.3. The following section will outline the process of extracting and analysing the data starting with the analysis of the MCA data followed by the ICA data.

Analysis of the MCA data

All TCD signals were recorded through a data acquisition system (Power lab/16SPML795; ADInstruments, Colorado Springs, CO, USA) and analyzed post hoc using a commercially available computational software (LabChart 9, ADInstruments, Colorado Springs, CO, USA). Then the data is sent to Labchart (1,000Hz) and displays and envelope of MCA velocity. The pre-set macro is applied to ensure data pad and channels are using the desired settings (e.g., pulsitility calculation).

Analysis of the ICA data

The data obtained from the ICA (i.e., extracranial measures) includes a screen recording of both the pulse-wave velocity and vessel (i.e., measure of diameter). All ICA hemodynamic data was stored in an audio video interleave (.avi) file format for post hoc offline edge detection analysis (Woodman et al., 2001). Following edge detection analysis, data was transferred at 30Hz into the same computational software as the TCD values (i.e., Labchart9, ADInstruments, Colorado Springs, CO, USA). All extracranial and intracranial values were then time aligned to ensure that post-hoc calculations were performed during the same period.

Edge detection

Computerized offline edge-detection software (**Figure 11**) allows for more accurate and reproducible measures and minimizes inter rater bias, providing sufficient resolution to assess a

0.2 mm change in diameter with a coefficient of variation of 5% using VDu (Woodman et al., 2001). Standardizing region of interests (ROI) in the vessel segments using edge detection software requires landmarking and adjusting settings necessary to ensure that reproduction of ICA scans is achieved using edge-detection software that is performed post-hoc. There are several ROI used in the edge detection software: the first ROI is selected to scale for the diameter in the *B*-mode image and is used to determine how many pixels represents a known measure of distance (i.e., 1 – 3 cm). The second ROI is selected by drawing a box around the desired segment of the ICA in the *B*-Mode image. Edge-detection tracks the intraluminal vessel walls through a contrast recognition software that can discriminate between vessel walls (white) and intraluminal space (black). The diameter is automatically determined based on this contrast discrimination and is visualized by a yellow line imposed one the ROI has been chosen. At this stage it is important to watch the entire duration of video where the measurement will be pulled to ensure the tracking does not pick up on other sections outside of the vessel wall. Once the section is determined to be satisfactory ROI's for the velocity trace must be calibrated. The third ROI requires a similar pixel calibration in relation to the velocity (i.e., 30-50 cm/s). The final ROI is used to capture the velocity trace (White) can be selected and is traced against the black backing in the velocity window using a contrast discrimination technique. Once wall tracking and velocity edge detection has been performed the software will automatically calculate velocity, blood flow, and other hemodynamic factors that are not discussed in this thesis (i.e., shear rate).

Calculations

Post hoc calculations for intra and extracranial cerebral and cardiorespiratory values were collected during the supine resting pre and post drug period offline using edge detection as well

as using LabChart. Considering that even during steady state rest fluctuations in continuous signals occurs special care was taken to time align extra and intracranial hemodynamics over a range of five to ten stable cardiac cycles. Stability was defined as signals that had no more than a 2-unit change in any cardiac cycle in both intra and extracranial signals. All cardiorespiratory average values were selected based off this range.

Eq. 4

$$Q_{ICA}(ml.min^{-1}) = CSA\ x\ Velocity$$

Calculation of internal carotid artery blood flow. Where CSA = cross-sectional area, calculated as CS$A = \pi r^2$, where r = radius of the ICA, and velocity is the mean velocity of each cardiac cycle selected.

Eq. 5

$$PI_{ICA\ or\ MCA}\ (a.u) = \frac{Sys-Dias}{Velocity}$$

Calculation of pulsitility index for both the ICA and MCA. Where Sys is the systolic (maximum) and Dias is the diastolic (minimum) average velocities calculated for each cardiac cycle during the stable range selected. Velocity was the mean velocity over the entire stable range selected in arbitrary units (a.u).

Eq. 6

$$DFi\ (a.u) = \frac{PI_{ICA}}{PI_{MCA}}$$

Calculation for damping factor index (DFi). Where PI_{ICA} is the pulsitility index of the ICA and the PI_{MCA} is the pulsitility index of the MCA in arbitrary units.

Eq. 7

$$CVRi\ \left(\frac{cm.s^{-1}}{mmHg}\right) = \frac{MCAv}{MAP}$$

Calculation of cerebrovascular resistant index (CVR_i). Where MCA_v is the mean velocity for the middle cerebral artery and MAP was the mean arterial pressure calculated over the cardiac cycle range.

Eq. 8

$$CVCi\ \left(\frac{mmHg}{cm.s^{-1}}\right) = \frac{MAP}{MCAv}$$

Calculation of cerebrovascular conductance index (CVC_i), the reciprocal of resistance. Where MCA_v is the mean velocity for the middle cerebral artery and MAP was the mean arterial pressure calculated over the cardiac cycle range.

Eq. 9

$$CVR_{ICA}\left(\frac{ml.min^{-1}}{mmHg}\right) = \frac{Q_{ICA}}{MAP}$$

Calculation of cerebrovascular resistance (CVR_{ICA}). Where Q_{ICA} is internal carotid artery blood flow, and MAP was the mean arterial pressure calculated over the cardiac cycle range.

Eq. 10

$$CVC_{ICA}\left(\frac{mmHg}{ml.min^{-1}}\right) = \frac{MAP}{Q_{ICA}}$$

Cerebrovascular conductance (CVC_{ICA}), the reciprocal of resistance. Where Q_{ICA} is internal carotid artery blood flow, and MAP was the mean arterial pressure calculated over the cardiac cycle range.

Statistical Analysis

All pre-post within group data were analyzed using paired T-tests conducted through R studio (see appendix). Because, of the loss of subjects at HA, pre SL and pre HA comparisons were ran using unpaired t-tests. The exception to this was if the data was not normally distributed. Normal

distribution was assessed using a Shapiro-Wilks Test. If the data was not normally distributed a Mann Whitney U/Wilcoxon Signed rank test was used instead. In comparisons with tied ranks – tied ranks were averaged prior to determining the sum of ranks.

Chapter 4 Altering Cerebral Hemodynamics at Altitude

Mechanisms of cerebral artery compliance at sea-level and following acclimation to high altitude. Underwood Destiny R[1], Craig Tabitha V[1], Smith, Brianne D[1], Day Trevor[2], Willie Chris K[3], Lucas Samuel JE[4], Burgess Keith R. [5,6], Ainslie Philip N[2], Smith Kurt J[1]. I was responsible for all data analysis and interpretation, written presentation of results, and the conceptualization of the secondary analysis and manuscript preparation for submission to the Journal of Experimental Physiology in 2024.

4.1. Purpose and Background

Adequate cerebral blood flow (CBF) regulation is a requirement to healthy brain aging. While it is crucial that continuous nutrient delivery matches the high metabolic activity of the brain, the regulation of consequent hemodynamic forces through the cerebral vasculature is also important. For instance, compliant cerebral vessels are required to attenuate the energy generated each cardiac cycle (Belz., 1995). The attenuation of this energy, as the pressure pulsation travels in a proximal (heart) to distal (microcirculation) vascular direction is referred to as damping (Gosling., 1974). In vessels that may have impaired compliance, the delivery of essential nutrients to the neurovascular unit, may have a costly hemodynamic burden (i.e., poor damping) (Gosling., 1974). This hemodynamic burden can be assessed using several ultrasound and pressure tonometry techniques.

Recently, Chiesa et al., (2017), demonstrated that increased carotid wave intensities (CWI) were associated with greater age-related cognitive declines in older adults over a 10-year period. Central artery stiffness in several populations with cardiovascular pathologies is associated with

CWI, and thus has recently been used to index the stiffness and/or compliance of the cerebral vasculature. Damping factor index (DFi) is another method positively associated with CWI, and assesses changes in the blood velocity pulsitility as it propagates distally from extra (internal carotid artery; ICA) to intracranial (middle cerebral artery; MCA) cerebral vessels. Lower DFi's have been observed in older compared to younger individuals with higher central artery stiffness and CWI's. What is currently unknown, is if environmental and pharmacological interventions known to alter cerebral blood flow via upstream (cardiac output) and downstream (microvascular resistance) mechanisms influence cerebrovascular damping. Additionally, it was of interest to investigate if adaptation to prolonged environmental stress (i.e., high altitude) alters the pharmacological sensitivity of the brain to dampen cerebrovascular pulsitility.

Hypoxia is a prominent environmental factor known to alter CBF regulation via upstream and downstream mechanisms. Exposure to high altitude reduces the partial pressure of oxygen and arterial oxygen content, resulting in prolonged hypoxemia and leading to increased CBF due to cerebral vasodilation. Additionally, high-altitude hypoxemia triggers a cascade of systemic physiological responses (e.g., hypocapnia, hypertension, and increased heart rate) that can influence both upstream and downstream cerebrovascular hemodynamics (Ainslie & Subudhi., 2014; Severinghaus., 1966). For instance, hypoxemia can cause vasodilatory compensation to ensure adequate delivery, but consequent hyperventilation induced hypocapnia may counter this vasodilatory action as a result of the cerebrovascular sensitivity to carbon dioxide. More specifically, where hypoxic vasodilation's reduces downstream vascular resistance (increase DFi), hypocapnic vasoconstriction increases downstream resistance (reduce DFi). Thus,

cerebrovascular DFi caused by high altitude hypoxemia is dependent on the magnitude and direction of the downstream changes in vascular resistances.

Hypertension caused by increased sympathetic activity during high-altitude hypoxemia (Ainslie et al., 2012), should increase perfusion pressure. Furthermore, high altitude exposure also triggers increases in central artery stiffness (Salvi et al., 2022). For cerebral vasculature to maintain DFi at sea-level ranges while acclimatizing to high altitude induced hypertension and central artery stiffening an increase in cerebrovascular resistance would be required. Currently, it is unknown if the upstream and downstream hemodynamic interactions caused by high-altitude exposure provide synergistic protection to the brain by maintaining cerebrovascular damping, or if maintaining oxygen delivery comes at a price that attenuates this important hemodynamic protection. Further comparisons are needed to understand the impact of high altitude acclimatization on cerebrovascular DFi.

Considering that cerebrovascular damping has emerged as a marker of cerebral artery stiffness and compliance in healthy and pathological conditions (Kerkhof et al., 2023; Lefferts et al., 2020), we aimed to identifying the potential impact of upstream and downstream cerebrovascular modulation on DFi during high altitude acclimation. To do this, we conducted a secondary analysis of previously published work (Burgess et al., 2018) that focused on increasing (dobutamine; DOB) and reducing (indomethacin; INDO) CBF at sea-level and following acclimation to high altitude using a pharmacological intervention (i.e., DOB, DOB+ACZ, and INDO, respectively). The secondary analysis included two differential pharmacological experiments to alter CBF at sea-level and high altitude.

In experiment 1 DOB was used to increase CBF at sea-level and high altitude. Additionally, at high altitude, to counter respiratory alkalosis and acute mountain, acetazolamide (ACZ) was given in conjunction with DOB. Thus, we aimed to characterize differences between high altitude and sea level cerebrovascular damping with and without pharmacological increases in upstream hemodynamic pulsatile forces (i.e., cardiac output). We hypothesized that DOB administration at sea-level would trigger an increase CBF and cerebrovascular pulsitility, which would result in DFi being supported by compensatory downstream vascular resistances (i.e., increased DFi). At HA, we hypothesized that DOB+ACZ administration would cause a reduced cerebrovascular DFi as downstream reductions in resistance would cause an increase in the transmittance of hemodynamic forces through extra to intracranial vessels.

In experiment 2 indomethacin (INDO) was used to reduce CBF at SL and HA through blockage of cyclooxygenase. We hypothesized that reducing CBF at sea-level and at high-altitude using INDO would result in a reduce DFi, caused by an increase extra to intracranial hemodynamic transmission which we interpreted as an impaired cerebrovascular compliance.

4.2. Methods

Participants

A total of 12 participants (4 female, 8 male) with a mean age of 31±7 yr and a body mass of 25.6 kg/m^2 were included in the initial testing after providing written informed consent. The study was approved by the University of British Columbia Ethics Committee and the Nepal Health and Medical Research Council and conformed to the standards set by the Declaration of Helsinki. Out of the 12 participants, 8 participants completed experiments one (DOB) and two (INDO) at

sea-level. However, different combinations of these 8 participants completed experiments 1 (n=6) and 2 (n=6) at high-altitude. Reasons for incomplete data include quality of ultrasound scans (n=3), altitude related illness (n=1), or other medical emergencies (i.e., appendicitis; n=1). All participants were typical residents of sea-level altitude, with two having experienced high altitude prior to this. The last previous high-altitude exposure was >4 yrs.

Inclusion/exclusion: Participants were non-smokers and underwent polysomnography screening to assess cardiovascular & cerebrovascular health at sea-level prior to participating in the research study. Pulmonary function was also screened. All known cardiovascular disease, cerebrovascular disease, and pulmonary or respiratory disorders were contraindications to participation.

Experimental Design: Experiments 1 (DOB) and 2 (INDO) were performed in a randomized order, with no less than 48 hours occurring between each experiment to allow for adequate pharmacological washout. Participants were instructed to avoid caffeine and alcohol 12 hours prior to measures and fasted 4 hours prior to each visit. All data was collected as part of the 2012 Ev-K2-CNR Pyramid expedition with baseline testing occurring in February and May of 2012 at sea-level (334 m above sea-level, Kelowna, BC, Canada) following 8 days of travel to 5050 m (Lobuche, Nepal), and during the second week of acclimation. Testing was approved by the Clinical Research Ethical Review Board of the University of British Columbia and the Nepal Medical Research Council.

Experiment 1 (pharmacological increase of cerebral blood flow): Approximately 24 hours after completing polysomnography, cardiovascular, and cerebrovascular screening, participants visited the sea-level laboratory to have their resting cerebrovascular function measured prior to completing several respiratory and cerebral reactivity tests (hyperoxic rebreathe; hypoxic reactivity; squat stands). Following an initial instrumentation period, participants were instructed to rest silently in a supine position for 10-minutes. Cerebral and cardiorespiratory baseline measures were over a 5-minute resting period after the initial 10-minutes of rest. Following the baseline measures, several reactivity tests (previously published data Willie et al., 2015) were completed over approximately 30-minutes. Intravenous administration of DOB using an infusion pump at a rate of 2-5 μg/kg/min for 30-minutes was used to increase CBF at sea-level (post drug). Participants rested quietly during this period. Cerebral and cardiorespiratory measures were collected over a 5-minute resting period following drug infusion in similarly to the pre drug infusion protocol. Drug infusion rate was maintained during resting measures. An identical protocol was followed at high-altitude testing, except drug infusion consisted of DOB +ACZ (2-5 μg/kg/min; 10 mg/kg).

The addition of ACZ was used to counter the potential high altitude related hypocapnic vasoconstriction and AMS. Inhibition of carbonic anhydrase via ACZ infusion was intended to increase acidosis, and thus counter the impact of high altitude related hypocapnia expected to trigger a reduction in CBF and vascular resistance. Previously it has been observed that ACZ by itself can provoke an increase in CBF (Fan et al., 2012; Lassen et al., 1987), however pilot data from our lab during sea-level testing did not show any increase in CBF during ACZ infusion.

Experiment 2 (INDO)(Pharmacological reduction in cerebral blood flow): Experiment two was conducting in a similar fashion to experiment 1. Following a 20-minute instrumentation period, a 10-minute supine resting period preceded the 5-minute baseline cerebral and cardiorespiratory assessment period. The same reactivity tests were performed over a 30-minute period, prior to participants ingesting INDO (100 mg). The INDO dosage was used to reduce CBF over a 90-minute window. Participants were free to move about the laboratory initially following ingestion (60 minutes) but were asked to lie supine for re-instrumentation and rest for 30 minutes prior to post INDO ingestion measures. Post INDO cerebral and cardiorespiratory measures were collected during a 5-minute resting period similar to pre-INDO and DOB protocols.

Experimental Procedures:

Cardiorespiratory function

Heart rate, blood pressure, end-tidal pressure of oxygen and carbon dioxide, and arterial oxygen saturation were assessed using electrocardiography (ECG bio amp, ADInstruments, Colorado Springs, CO, USA), photoplethysmography (Finameter Pro, Finapres Medical Systems, Amsterdam, The Netherland), respiratory gas analysis (ML206, ADInstruments, Colorado Springs, CO, USA), and pulse oximetry (ML320 Oximeter Pod, ADInstruments, Colorado Springs, CO, USA0, respectively. All data was time aligned using acquisition device (Power lab/16SPML795; ADInstruments, Colorado Springs, CO, USA). Respiratory gases were sampled from a mouthpiece connected to the gas analyzer via nafion tubing and desiccant.

Intracranial Hemodynamics

Middle cerebral artery (MCA) hemodynamics were continuously measured using a transcranial Doppler ultrasound (TCD) system (Spencer Technologies, Seattle, WA, USA). The intracranial

cerebral artery is a primary terminal branch of the circle of Willis and can be imaged using standardized TCD procedures (Willie et al., 2011). All TCD signals were recorded through a data acquisition system (Power lab/16SPML795; ADInstruments, Colorado Springs, CO, USA) and analyzed post hoc using a commercially available computational software (LabChart 9, ADInstruments, Colorado Springs, CO, USA). The 2MHz TCD ultrasound probe was transfixed and held in place via a headband fixation device (Mark600, Spencer Technologies, Seattle, WA, USA).

Extracranial Hemodynamics

Continuous extracranial hemodynamics, including velocity, diameter, flow, and pulsatility were assessed in the ICA using a high-resolution duplex ultrasound machine (Terason 3000, Teratech, Burlington, MA, USA) for the final minute of the 5-minute resting period. All ICA measures were obtained as least 2 cm from the carotid bifurcation, with sample volume positioned in the centre of each vessel, adjusted to ensure an insonation angle of 60 deg was achieved as previously reported by our group (Burgess et al., 2018; Smith et al., 2014) which follows standardized procedures (Thomas et al., 2015).

All ICA hemodynamic data was stored in an audio video interleave (.avi) file format for post hoc offline edge detection analysis (Woodman et al., 2001). Following edge detection analysis data was transferred at 30 Hz into the same computational software as the TCD values. All extracranial and intracranial values were then time aligned to ensure that post-hoc calculations were performed during the same period.

Calculations:

Post hoc calculations for intra and extracranial cardiorespiratory values were collected during the supine resting pre and post drug period offline using LabChart. Considering that even during steady state rest fluctuations in continuous signals occurs special care was taken to time align extra and intracranial hemodynamics over a range of five to ten stable cardiac cycles. Stability was defined as signals that had no more than a 2-unit change in any cardiac cycle in both intra and extracranial signals. All cardiorespiratory average values were selected based off this range.

Internal carotid artery blood flow was calculated as:

$$Q_{ICA}\left(ml.min^{-1}\right) = CSA\ x\ Velocity$$

Where CSA = cross-sectional area, calculated as CS$A = \pi r^2$, where r = radius of the ICA, and velocity is the mean velocity of each cardiac cycle selected.

Pulsitility Index (PI) was calculated for both the ICA and MCA as:

$$PI_{ICA\ or\ MCA}\,(a.u) = \frac{Sys - Dias}{Velocity}$$

Where Sys is the systolic (maximum) and Dias is the diastolic (minimum) average velocities calculated for each cardiac cycle during the stable range selected. Velocity was the mean velocity over the entire stable range selected in arbitrary units (a.u)

Damping Factor index (DFi) was calculated as:

$$DFi\,(a.u) = \frac{PI_{ICA}}{PI_{MCA}}$$

Where PI_{ICA} is the pulsitility index of the ICA and the PI_{MCA} is the pulsitility index of the MCA in arbitrary units.

Cerebrovascular Resistance index (CVR_i) was calculated as:

$$CVRi\left(\frac{cm.s^{-1}}{mmHg}\right) = \frac{MCAv}{MAP}$$

Where MCA_v is the mean velocity for the middle cerebral artery and MAP was the mean arterial pressure calculated over the cardiac cycle range.

Cerebrovascular Conductance index (CVC_i), the reciprocal of resistance was calculated as:

$$CVCi\left(\frac{mmHg}{cm.s^{-1}}\right) = \frac{MAP}{MCAv}$$

Where MCA_v is the mean velocity for the middle cerebral artery and MAP was the mean arterial pressure calculated over the cardiac cycle range.

Cerebrovascular Resistance (CVR_{ICA}) was calculated as:

$$CVR_{ICA}\left(\frac{ml.min^{-1}}{mmHg}\right) = \frac{Q_{ICA}}{MAP}$$

Where Q_{ICA} is internal carotid artery blood flow, and MAP was the mean arterial pressure calculated over the cardiac cycle range.

Cerebrovascular Conductance (CVC_{ICA}), the reciprocal of resistance was calculated as:

$$CVC_{ICA}\left(\frac{mmHg}{ml.min^{-1}}\right) = \frac{MAP}{Q_{ICA}}$$

Where Q_{ICA} is internal carotid artery blood flow, and MAP was the mean arterial pressure calculated over the cardiac cycle range.

Statistical Analysis

All pre-post within group data were analyzed using paired T-tests conducted through R studio. Because, of the loss of subjects at HA, pre SL and pre HA comparisons were ran using unpaired t-tests. The exception to this was if the data was not normally distributed. Normal distribution was assessed using a Shapiro-Wilks Test. If the data was not normally distributed a Mann Whitney U/Wilcoxon Signed rank test was used instead. In comparisons with tied ranks – tied ranks were averaged prior to determining the sum of ranks.

4.3. Results

All experiment 1 and 2 cardiorespiratory, intracranial, and extracranial hemodynamics can be found in tables 1 and 2, respectively.

Experiment 1(Table 1) - Six individuals participated in experiment one. Two males and two females completed all SL and HA tests (n=4), with one male and female completing only the SL tests, and one male and female only completing the HA tests. This occurred because of an unforeseen medical emergency at high altitude, which resulted in a male and female participant having to be airlifted to sea-level. SL and HA statistical comparisons were performed with only 4 individuals, while pre and post drug comparisons include 6 participants.

Cardiorespiratory Hemodynamics

At sea level administration of DOB did not result in a different HR, MAP, S_aO_2, and $P_{ET}O_2$ prior to (62 ± 17; 97 ± 11mmHg; 93 ± 11%; 100 ± 4 mmHg, respectively) or during DOB infusion (59 ± 15; 110 ± 9 mmHg; 92 ± 11 %; 100 ± 6 mmHg respectively). $P_{ET}CO_2$ at sea level decreased pre (43 ± 3mmHg) to post (40 ± 3mmHg) DOB (p=0.01).

Observations at HA did not reveal any significant ($p<0.05$) pre (MAP: 89 ± 9 mmHg; S_aO_2: 78 ± 5 %; $P_{ET}O_2$: 45 ± 5 mmHg) or post (MAP: 98 ± 11 mmHg; S_aO_2:78 ± 7 %; $P_{ET}O_2$: 46 ± 4 %) differences following DOB+ACZ administration. No significant change was observed in $P_{ET}CO_2$ at HA pre (29 ± 3 mmHg) – post (31 ± 11 mmHg) DOB+ACZ administration. DOB+ACZ administration increased HR (83 ± 14 bpm) compared to pre-DOB+ACZ administration (78 ± 14 bpm) (p=0.04).

Table 1. Cardiorespiratory and cerebrovascular hemodynamics at sea-level and high altitude pre and post dobutamine.

Variable	Condition	Pre	Post	Δ	Pre vs Post	SL vs HA pre post Δ
HR	SL	62 ± 17	59 ± 15	- 3	0.2	0.02**

(BPM)	HA	78 ± 14	83 ± 14	5	0.04*	
MAP	SL	97 ± 11	110 ± 9	13	0.08	0.52
(MMHG)	HA	89 ± 9	98 ± 11	9	0.07	
S_aO_2	SL	93 ± 11	92 ± 11	-1	0.9	0.59
(%)	HA	78 ± 5	78 ± 7	0	0.8	
$P_{ET}O_2$	SL	100 ± 4	100 ± 6	0	0.9	0.67
(mmHg)	HA	45 ± 5	46 ± 4	1	0.4	
$P_{ET}CO_2$	SL	43 ± 3	40 ± 3	-3	0.01*	0.18
(mmHg)	HA	29 ± 3	31 ± 11	2	0.6	
MCA_v	SL	67 ± 14	67 ± 14	0	0.9	0.01**
($cm.s^{-1}$)	HA	74 ± 15	91 ± 17	17	0.01*	
PI_{MCA}	SL	0.78 ± 0.1	1.2 ± 0.1	0.42	0.004*	-0.42
(a.u)	HA	0.67 ± 0.07	0.79 ± 0.1	0.12	0.09	
ICA_{Diam}	SL	5.0 ± 0.02	5.4 ± 0.1	0	0.3	0.39
(mm)	HA	5.0 ± 0.04	5.3 ± 0.03	0	0.04*	
ICAv	SL	50 ± 13	44 ± 11	-6	0.2	0.04**
($cm.s^{-1}$)	HA	45 ± 15	55 ± 4	10	0.1	
Q_{ICA}	SL	297 ± 92	304 ± 111	7	0.7	0.15
($ml.min^{-1}$)	HA	319 ± 69	360 ± 68	41	0.01*	
PI_{ICA}	SL	0.97 ± 0.15	1.4 ± 0.12	0.4	0.005*	0.03**
(a.u)	HA	1.0 ± 0.28	1.2 ± 0.29	0.2	0.02*	
DF_i	SL	1.3 ± 0.1	1.2 ± 0.1	-0.1	0.02*	0.59
(a.u)	HA	1.5 ± 0.4	1.5 ± 0.4	0	0.9	
CVR_{MCA}	SL	1.5 ± 0.3	1.6 ± 0.3	0.1	0.09	0.02**
($mmhg.cm.s^{-1}$)	HA	1.2 ± 0.3	1.1 ± 0.3	-0.1	0.04*	
CVR_{ICA}	SL	0.35 ± 0.1	0.41 ± 0.18	0.06	0.2	
($mmhg.ml.min^{-1}$)	HA	0.29 ± 0.06	0.27 ± 0.04	-0.02	0.3	0.15
CVC_{MCA}	SL	0.70 ± 0.1	0.60 ± 0.1	-0.1	0.06	0.008**
($cm.s.\ mmhg^{-1}$)	HA	0.80 ± 0.2	0.96 ± 0.3	0.2	0.06	
CVC_{ICA}	SL	3.1 ± 0.9	2.8 ± 1.1	-0.3	0.4	
($ml.min.mmhg^{-1}$)	HA	3.6 ± 0.8	3.7 ± 0.6	0.1	0.4	0.31

HR: HEART RATE; MAP: MEAN ARTERIAL PRESSURE; $P_{ET}O_2$: PARTIAL PRESSURE OF END-TIDAL OXYGEN; $P_{ET}CO_2$: PARTIAL PRESSURE OF END-TIDAL CARBON DIOXIDE; MCAV: MIDDLE CEREBRAL ARTERY; $PI_{MCA\ \&\ ICA}$: MIDDLE CEREBRAL AND INTERNAL CAROTID ARTERY PULSATILITY INDEX; ICA_{DIAM}; INTERNAL CAROTID DIAMETER; ICAV; INTERNAL CAROTID ARTERY VELOCITY; Q_{ICA}; INTERNAL CAROTID ARTERY FLOW; DF_I; DAMPING FACTOR INDEX; $CVR_{MCA\ \&\ ICA}$; CEREBROVASCULAR RESISTANCE IN THE MIDDLE CEREBRAL AND INTERNAL CAROTID ARTERIES; $CVC_{MCA\ \&\ ICA}$; CEREBROVASCULAR RESISTANCE IN THE MIDDLE CEREBRAL AND INTERNAL CAROTID ARTERIES * INDICATES SIGNIFICANCE PRE AND POST DRUG, $P<0.05$ N=6; ** INDICATES SIGNIFICANCE BETWEEN THE PRE AND POST CHANGES AT SL AND HA, $P < 0.05$, N = 4.

Intracranial Hemodynamics

At SL MCA_v did not change pre (67 ± 14 $cm.s^{-1}$) to post (67 ± 14 $cm.s^{-1}$) DOB (**Figure 12**). PI_{MCA} increased (p=0.004) pre (0.78 ± 0.1 a.u) to post (1.2 ± 0.1 a.u) DOB administration. CVR_{MCA} and CVC_{MCA} did not change significantly (p = 0.09; p =0.06) pre (1.5 ± 0.3 $mmHg.cm^{-1}.s^{-1}$; 0.7 ± 0.1 $cm.s.mmHg^{-1}$) to post (1.6 ± 0.3 $mmHg.cm^{-1}.s^{-1}$; 0.6 ± 0.1 $cm.s.mmHg^{-1}$), DOB respectively.

At HA, MCA_v pre (74 ± 15 $cm.s^{-1}$) DOB+ACZ was lower compared to post (91 ± 17 $cm.s^{-1}$) DOB infusion (p=0.01) (**Figure 12**). In contrast, PI_{MCA} pre (0.67 ± 0.07 a.u) and post (0.79 ± 0.1 a.u) DOB+ACZ were not significantly different at HA (p= 0.09). Additionally, CVR_{MCA} at high altitude decreased from pre (1.2 ± 0.3 $cm.s^{-1}.mmHg^{-1}$) to post (1.1 ± 0.3 $cm.s^{-1}.mmHg^{-1}$) DOB+ACZ administration (p=0.04). Similarly, CVC_{MCA} at HA did not significantly change pre (0.8 ± 0.2 $mmHg.cm^{-1}.s^{-1}$) to post (0.96 ± 0.3 $mmHg.cm^{-1}.s^{-1}$) DOB+ACZ.

Pre and post MCA_v changes (p=0.01) following DOB and DOB+ACZ administration were different at SL (Δ 0.04 ± 5.7 $cm.s^{-1}$) compared to HA (Δ +17 ± 10.86 $cm.s^{-1}$), respectively. Further, when comparing the CVR_{MCA} change scores at SL (Δ0.1±0.27 $mmHg.cm^{-1}.s^{-1}$) to HA (Δ-0.1 ±0.12 $mmHg.cm^{-1}.s^{-1}$) directional changes pre and post DOB+ACZ infusion were significantly different (p=0.02). Additionally, the directionality of SL (Δ-0.1 ± 0.08 $mmHg.cm^{-1}.s^{-1}$) and HA (Δ0.2 ± 0.12 $mmHg.cm^{-1}.s^{-1}$) changes to CVC_{MCA} pre and post DOB+ACZ administration was significant (p=0.008).

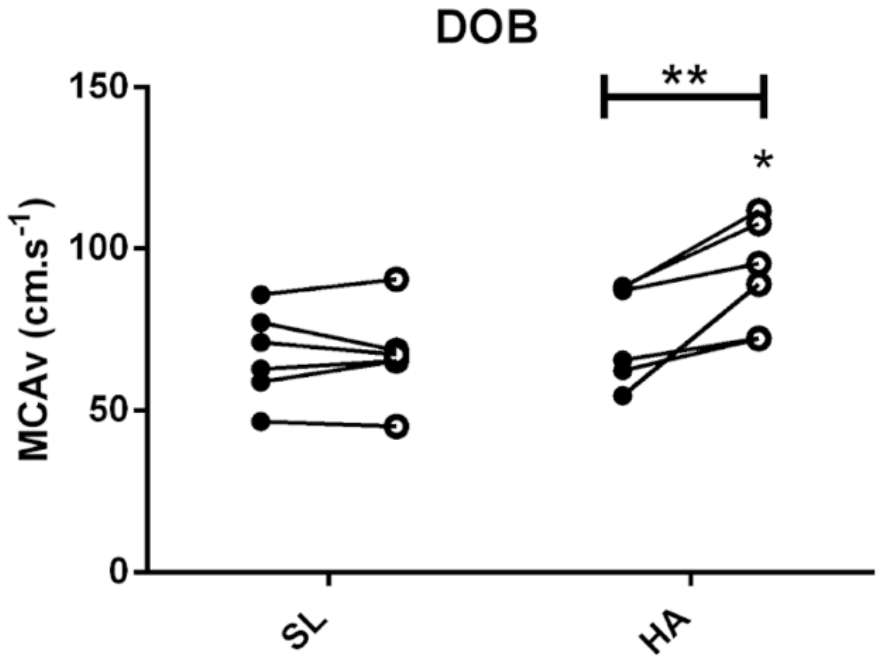

Figure 12. The middle cerebral artery velocity (MCA_v $cm.s^{-1}$) at sea level (SL) and high altitude (HA; 5050 m above SL) pre (closed circles) and post (open circles) dobutamine (DOB).
* Illustrates a difference post drug compared to pre drug ($p<0.05$): ** Illustrates that the change score between pre to post drug was different between SL and HA, $p<0.05$.

Extracranial Hemodynamics

The change in ICA_{diam} (mm) at SL post DOB administration (5.4 ± 0.1 mm) was not observed to be significant (p=0.3) compared to pre DOB administration (5.0± 0.02 mm) (**Figure 13**). At SL, ICA_V did not change pre (50 ± 13 $cm.s^{-1}$) compared to post (44 ± 11 $cm.s^{-1}$) DOB administration (p = 0.2). Post administration of DOB Q_{ICA} (304 ± 111 $ml.min^{-1}$) $_{was}$ not altered compared Pre (297 ± 92 $ml.min^{-1}$) administration of DOB at SL (**Figure 13**). However, SL PI_{ICA} pre (0.97 ± 0.15 a.u) DOB administration was observed to be increased post (1.4 ± 0.12 a.u) administration (p=0.005). At SL, both CVR_{ICA} (p = 0.2) and CVC_{ICA} (p = 0.4) were not observed to be different pre (0.35 ± 0.1 $mmHg.ml^{-1}.min^{-1}$; 3.1 ± 0.9 $ml.min^{-1}.mmHg^{-1}$) compared to post (0.41 ± 0.18 $mmHg.ml.min^{-1}$; 2.8 ± 1.1 $ml.min^{-1}.mmHg^{-1}$) DOB administration, respectively.

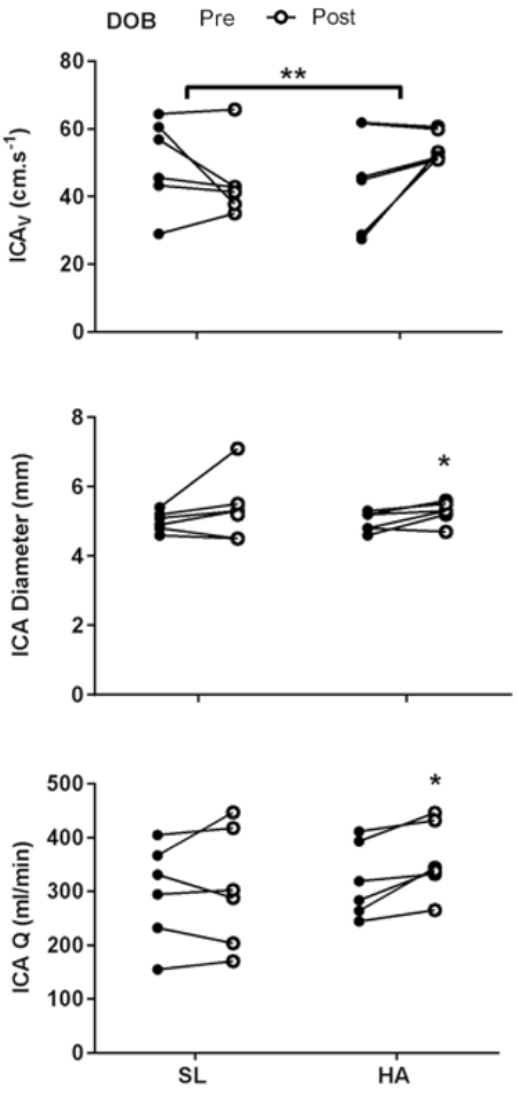

Figure 13. Extracranial artery velocity (ICA_v cm.s^{-1}), diameter (ICA_{diam} mm), and flow (Q_{ICA} ml.min^{-1}) pre/post dobutamine (DOB). ICAv (cm.s^{-1}), ICA_{diam} (mm) and Q_{ICA} (ml.min^{-1}) at sea level (SL) and high altitude (HA; 5050m above SL) pre (closed circles) and post (open circles) DOB. *Illustrates a difference post drug compared to pre drug ($p<0.05$): ** Illustrates that the change score between pre to post drug was different between SL and HA, $p<0.05$.

At HA, DOB administration revealed a greater ICA_{diam} post (5.3 ± 0.04 mm) compared to pre (5.0 ± 0.03mm) DOB+ACZ administration ($p=0.04$). Similar to SL, HA ICA_V did not change pre (45 ± 15 cm.s^{-1}) compared to post (55 ± 4 cm.s^{-1}) DOB+ACZ administration ($p = 0.1$). However, Q_{ICA} post DOB+ACZ administration (360 ± 68 ml.min^{-1}) was greater compared to pre (319 ± 69

$ml.min^{-1}$) DOB+ACZ administration at HA (p=0.01). Similarly, HA PI_{ICA} was greater post (1.2 ± 0.3 a.u) compared to pre (1 ± 0.3 a.u) DOB+ACZ administration (p=0.02). Both pre (0.29 ± 0.06 $mmHg.ml.min^{-1}$; 3.6 ± 0.8 $ml.min^{-1}.mmHg^{-1}$) and post (0.27 ± 0.04 $mmHg.ml.min^{-1}$; 3.7 ± 0.6 $ml.min^{-1}.mmHg^{-1}$) CVR_{ICA} (p = 0.3) and CVC_{ICA} (p = 0.4) were not altered following DOB+ACZ administration at HA.

Comparing pre and post ICA_V changes at SL (Δ-6 ± 12.01 $cm.s^{-1}$) and HA (Δ+10 ± 9.79 $cm.s^{-1}$) revealed directional differences following DOB+ACZ administration (p=0.04). A greater PI_{ICA} (p = 0.03) response to DOB+ACZ administration was observed at SL (Δ 0.4 ± 0.25 a.u.) compared to HA (Δ 0.2 ± 0.27 a.u.). No other differences between SL and HA ICA responses were observed.

Proximal to Distal Hemodynamics

At SL, DFi (a.u) was higher pre (1.3 ± 0.1 a.u) compared to post (1.2 ± 0.1 a.u) DOB infusion (p=0.02). In contrast, DFi did not differ between pre (1.5 ± 0.4 a.u) and post (1.5 ± 0.4 a.u) DOB +ACZ administration at HA (p=0.9). DOB and DOB+ACZ administration was not found to significantly impact SL and HA DFi (p =0 .59), respectively (**Figure 14**).

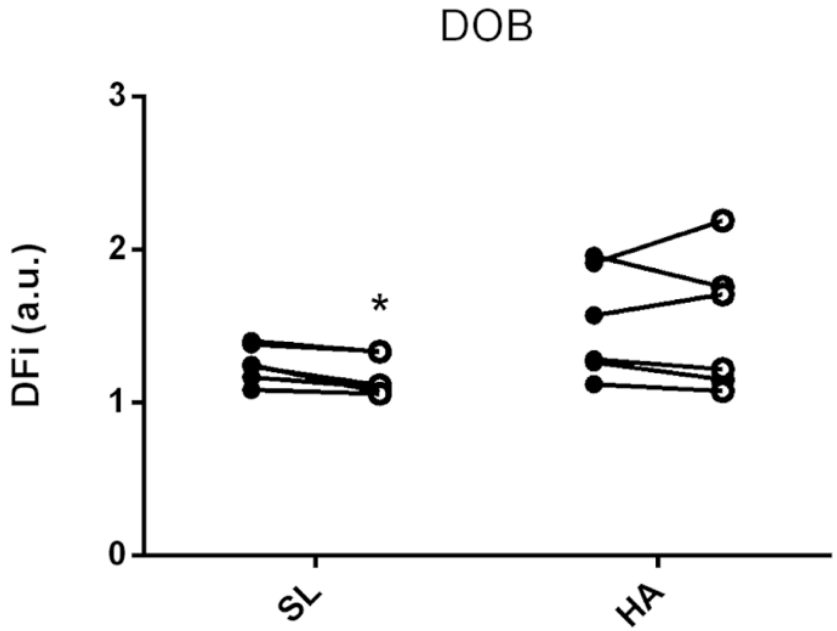

Figure 14. Damping factor index (DFi) (a.u) pre-post pharmacological intervention at sea-level (SL) and high altitude (HA; 5050m above SL) pre (closed circles) and post (open circle) dobutamine (DOB). * Illustrates a difference post drug compared to pre drug ($p<0.05$). DFi (a.u) was not significantly changed post DOB at HA. DFi (a.u) significantly decreased at SL post DOB.

Experiment 2 (Table 2) – 10 individuals participated in experiment two. Sea level and high altitude statistical comparisons were performed with only 4 individuals (2 male, 2 female). High altitude logistics resulted in different individuals completing experiment experiments 1 and 2. This occurred, in part, because of an unforeseen medical emergency at high altitude, which resulted in a male and female participant having to be airlifted to sea level. Sea level and high altitude statistical comparisons were performed with only 4 individuals, while pre and post drug comparisons include 6 participants.

Table 2. Cardiorespiratory and cerebrovascular hemodynamics at sea-level and high altitude pre and post indomethacin.

Variable	*Condition*	*Pre*	*Post*	*DELTA pre post*	*pre vs post*	*SL vs HA pre post Δ*
HR (bpm)	SL	59 ± 9	62 ± 8	3	0.11	0.14
	HA	78 ± 26	68 ± 17	-10	0.41	
MAP (mmHg)	SL	90 ± 12	94 ± 12	4	0.44	0.5
	HA	96 ± 9	96 ± 9	0	0.91	
S_aO_2 (%)	SL	94 ± 10	91 ± 13	-3	0.47	0.28
	HA	79 ± 5	79 ± 6	0	0.91	
$P_{ET}O_2$ (mmHg)	SL	96 ± 8	99 ± 7	3	0.20	0.17
	HA	46 ± 3	45 ± 4	-1	0.56	
$P_{ET}CO_2$ (mmHg)	SL	39 ± 10	41 ± 4	2	0.57	0.35
	HA	28 ± 3	28 ± 3	0	0.81	
MCA_v ($cm.s^{-1}$)	SL	68 ± 9	52 ± 12	-16	0.009*	0.38
	HA	70 ± 15	61 ± 11	-9	0.22	
PI_{MCA} (a.u)	SL	0.85 ± 0.13	0.97 ± 0.17	0.12	0.14	0.59
	HA	0.65 ± 0.11	0.83 ± 0.11	0.18	0.003*	
ICA_{diam} (mm)	SL	5.0 ± 0.2	4.9 ± 0.7	-0.1	0.72	0.57
	HA	4.8 ± 0.4	4.9 ± 0.5	0.1	0.65	
ICAv ($cm.s^{-1}$)	SL	38.8 ± 10.1	30 ± 9	-9	0.07	0.7
	HA	39 ± 11.5	32 ± 7	-7	0.14	
Q_{ICA} ($ml.min^{-1}$)	SL	227 ± 68.1	174 ± 81.4	-53	0.04*	0.64
	HA	225 ± 66.5	184 ± 55.1	-41	0.004*	
PI_{ICA} (a.u)	SL	1.13 ± 0.24	1.04 ± 0.24	-0.09	0.32	0.8
	HA	1.28 ± 0.57	1.15 ± 0.32	-0.13	0.29	
DF_i (a.u)	SL	1.35 ± 0.24	1.09 ± 0.28	-0.26	0.07	0.18
	HA	1.92 ± 0.6	1.38 ± 0.29	-0.54	0.02*	
$CVRi_{MCA}$ ($mmHg.cm.s^{-1}$)	SL	1.35 ± 0.23	1.89 ± 0.53	0.54	0.03*	0.16
	HA	1.42 ± 0.34	1.6 ± 0.32	0.18	0.28	
$CVRi_{ICA}$ ($mmHg.ml.min^{-1}$)	SL	0.42 ± 0.11	0.69 ± 0.43	0.27	0.10	0.49
	HA	0.45 ± 0.12	0.56 ± 0.18	44	0.01*	
$CVCi_{MCA}$ ($cm.s.mmHg^{-1}$)	SL	0.76 ± 0.14	0.56 ± 0.14	-0.2	0.02*	0.21
	HA	0.73 ± 0.17	0.65 ± 0.13	-0.08	0.18	
$CVCi_{ICA}$ ($ml.min.mmHg^{-1}$)	SL	2.51 ± 0.56	1.87 ± 0.82	-0.64	0.03*	0.35
	HA	2.35 ± 0.63	1.97 ± 0.69	-0.38	0.01*	

HR: HEART RATE; MAP: MEAN ARTERIAL PRESSURE; $P_{ET}O_2$: PARTIAL PRESSURE OF END-TIDAL OXYGEN; $P_{ET}CO_2$: PARTIAL PRESSURE OF END-TIDAL CARBON DIOXIDE; MCAV: MIDDLE CEREBRAL ARTERY; $PI_{MCA\ \&\ ICA}$: MIDDLE CEREBRAL AND INTERNAL CAROTID ARTERY PULSITILITY INDEX; ICA_{DIAM}; INTERNAL CAROTID DIAMETER; ICAV; INTERNAL CAROTID ARTERY VELOCITY; Q_{ICA}; INTERNAL CAROTID ARTERY

FLOW; DF_I; DAMPING FACTOR INDEX; $CVR_{MCA\ \&\ ICA}$; *CEREBROVASCULAR RESISTANCE IN THE MIDDLE CEREBRAL AND INTERNAL CAROTID ARTERIES; $CVC_{MCA\ \&\ ICA}$; CEREBROVASCULAR RESISTANCE IN THE MIDDLE CEREBRAL AND INTERNAL CAROTID ARTERIES * INDICATES SIGNIFICANCE PRE AND POST DRUG, P<0.05 N=6; ** INDICATES SIGNIFICANCE BETWEEN THE PRE AND POST CHANGES AT SL AND HA, P < 0.05, N = 4.*

Cardiorespiratory Hemodynamics

At SL HR (p = 0.11), MAP (p = 0.44), S_aO_2 (p = 0.47), $P_{ET}O_2$ (p = 0.20), $P_{ET}CO_2$ (p = 0.57) did not vary significantly pre (59 ± 9 bpm; 90 ± 12 mmHg; 94 ± 10 %, 96 ± 8 mmHg, 39 ± 10 mmHg, respectively) to post (62 ± 8 bpm; 94 ± 12 mmHg; 91 ± 13 %; 99 ± 7 mmHg; 41 ± 4 mmHg respectively) INDO administration.

Similarly at HA, HR (p=0.41), MAP (p = 0.91), S_aO_2 (p = 0.91), $P_{ET}O_2$ (p = 0.56), $P_{ET}CO_2$ (p = 0.81) were not significantly different from pre (78 ± 26 bpm; 96 ± 9 mmHg; 79 ± 5 %; 46 ± 3 %; 28 ± 3 %, respectively) to post (68 ±17 bpm; 96 ± 9 mmHg; 79 ± 6 %; 45 ± 4 mmHg; 28 ± 3 mmHg, respectively) INDO administration.

Intracranial Hemodynamics

The MCA_v significantly decreased (p=0.009) post (52 ± 12 $cm.s^{-1}$) compared to pre (68 ± 9 $cm.s^{-1}$) INDO administration (**Figure 15**). At SL, PI_{MCA} did not change significantly from pre (0.85 ± 0.13 a.u) to post (0.97 ± 0.17 a.u) INDO administration (p = 0.14). An increased CVR_{MCA} was observed (p=0.03) post (1.89 ± 0.53 $mmHg^{-1}.cm.s^{-1}$) compared to pre (1.35 ± 0.23 $mmHg^{-1}.cm.s^{-1}$) INDO. In contrast, SL CVC_{MCA} significantly decreased (p=0.02) from pre (0.76 ± 0.14 $ml.min^{-1}.mmHg^{-1}$) to post (0.56 ± 0.14 $cm.s^{-1}.mmHg^{-1}$) INDO.

The changes in MCAv observed post (61 ± 11 cm.s-^{1}) INDO administration compared to pre (70 ± 15 cm.s-^{1}) were not significant (p = 0.22) at HA (**Figure 15**). However, PI_{MCA} at HA was greater post (0.83 ± 0.11 a.u) compared to pre (0.65 ± 0.11 a.u) INDO administration (p=0.003). The changes in CVR_{MCA} (p = 0.28) and CVC_{MCA} (0.18) were not significantly different pre (1.42 ± 0.34 cm.s.mmHg^{-1}; 0.73 ± 0.17 ml.min.mmHg^{-1}) compared to post (1.6 ± 0.32 cm.s.mmHg^{-1}) INDO administration.

No differences between the SL and HA intracranial. responses following INDO administration were observed (Table 2).

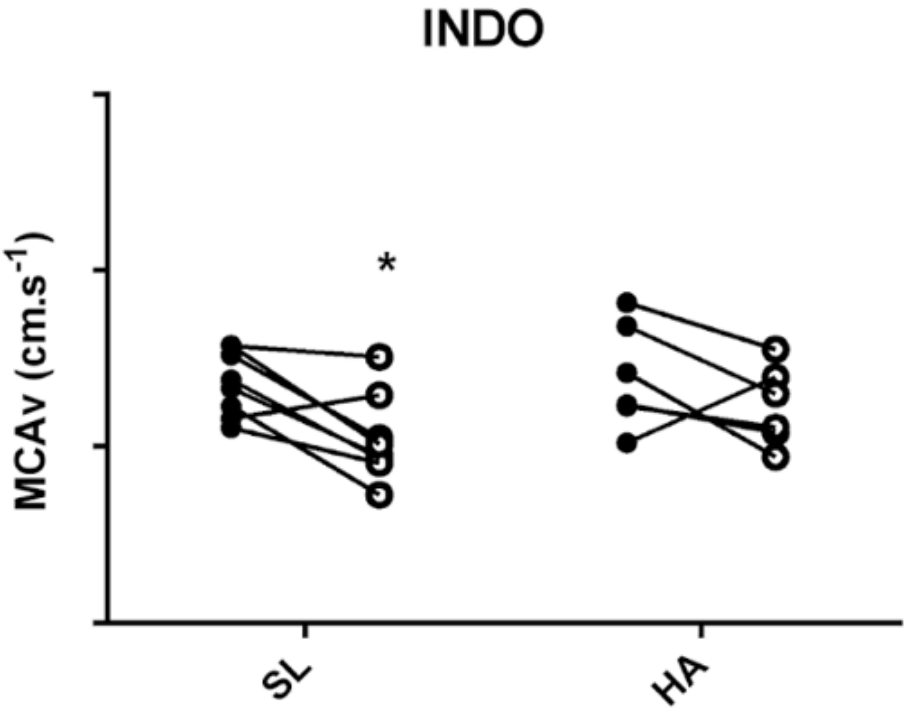

Figure 15. The middle cerebral artery velocity (MCA_v cm.s^{-1}) at sea level (SL) and high altitude (HA; 5050 m above SL) pre (closed circles) and post (open circles) indomethacin (INDO).
* Illustrates a difference post drug compared to pre drug (p<0.05): ** illustrates that the change score between pre to post drug was different between SL and HA, p<0.05.

Extracranial Hemodynamics

At SL ICA_{diam} ($p = 0.14$), ICA_v ($p = 0.07$), and PI_{ICA} (0.32) did not change significantly pre (0.5 ± 0.02 mm; 38.8 ± 10.1cm.s^{-1}; 1.13 ± 0.24 a.u respectively) to post (0.49 ± 0.07 mm; 30 ± 9 cm.s^{-1}; 1.04 ± 0.24 a.u) INDO. Despite this, SL Q_{ICA} was observed to be decreased pre (227 ± 68.1 ml.min^{-1}) compared to post (174 ± 81.4 ml.min^{-1}) INDO administration ($p=0.04$) (**Figure 16**). CVR_{ICA} did not change significantly at SL pre (0.42 ± 0.11 mmHmg.ml.min^{-1}) compared to post (0.69 ± 0.43 mmHmg.ml.min^{-1}) INDO administration. In contrast, CVC_{ICA} a significant ($p=0.03$) decrease was observed pre (2.51 ± 0.56 ml.min $mmHg^{-1}$) -post (1.87 ± 0.82 ml.min $mmHg^{-1}$) INDO at SL.

Similarly, at HA ICA_{diam}, ICA_v, and PI_{ICA} did not change significantly pre (0.48 ± 0.04 mm; 39 ± 11.5 cm.s^{-1}; 1.28 ± 0.57 a.u)-post (0.49 ± 0.05 mm; 32 ± 7 cm.s^{-1}; 1.15 ± 0.32 a.u) INDO. However, Q_{ICA} at HA decreased HA pre (225 ± 66.5 ml.min^{-1}) compared to post (184 ± 55.1 ml.min^{-1}) INDO ($p=0.004$). Whereas an increase ($p=0.01$) in CVR_{ICA} was observed at HA pre (0.45 ± 0.12 mmHmg.ml^{-1}.min^{-1}) compared to post (0.56 ± 0.18 mmHmg.ml^{-1}.min^{-1}) INDO administration. In contrast, a significant ($p=0.01$) decrease in CVC_{ICA} was observed at HA pre (2.35 ± 0.63 ml.min^{-1}.$mmHg^{-1}$) compared to post (1.97 ± 0.69 ml.min^{-1}.$mmHg^{-1}$) INDO administration.

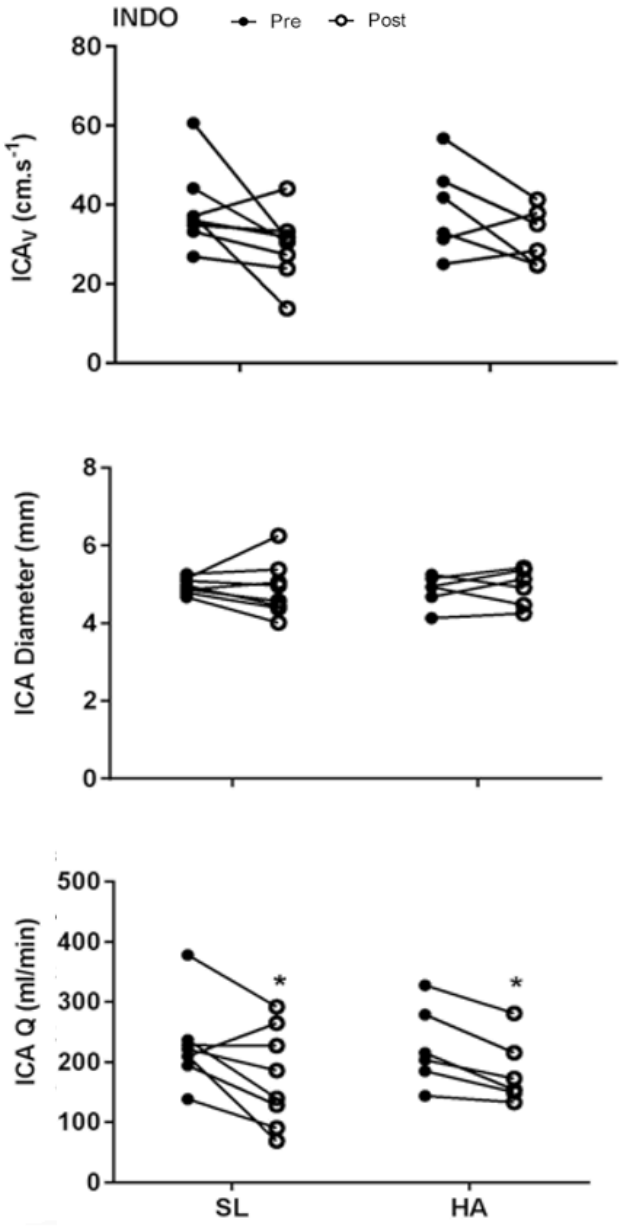

Figure 16. Extracranial artery velocity (ICA_v cm.s^{-1}), diameter (ICA_{diam} mm), and flow (Q_{ICA} ml.min^{-1}) pre/ indomethacin (INDO). ICA_v (cm.s^{-1}), ICA_{diam} (mm) and Q_{ICA} (ml.min^{-1}) at sea level (SL) and high altitude (HA; 5050m above SL) pre (closed circles) and post (open circles) INDO.* Illustrates a difference post drug compared to pre drug ($p<0.05$): ** illustrates that the change score between pre to post drug was different between SL and HA, $p<0.05$.

Proximal to Distal Hemodynamics

At SL the decrease in DFi from pre (1.35 ± 0.24 a.u) to post (1.09 ± 0.28 a.u) INDO ($p = 0.07$) was not observed to be significant. However, at HA a significant decrease in DFi pre (1.92 ± 0.6 a.u) compared to post (1.38 ± 0.29 a.u) was observed ($p = 0.02$) (**Figure 17**).

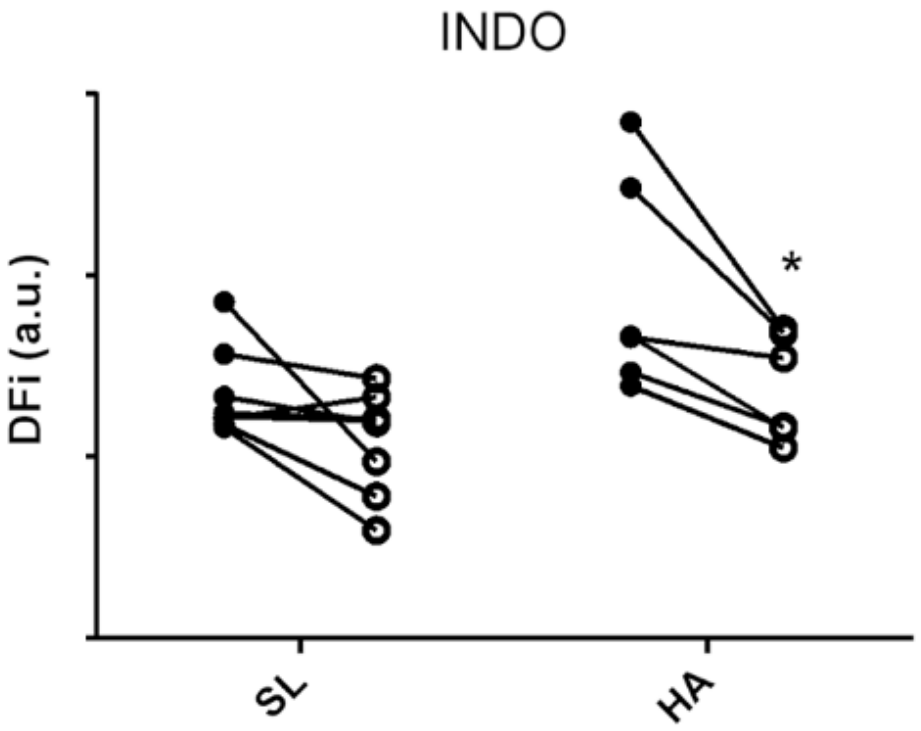

Figure 17. DFi (a.u) at sea level (SL) and high altitude (HA; 5050m above SL) pre (closed circles) and post (open circle) indomethacin (INDO). * Illustrates a difference post drug compared to pre drug ($p<0.05$): ** illustrates that the change score between pre to post drug was different between SL and HA, $p<0.05$. DFi (a.u) was not significantly changed post INDO at SL. DFi (a.u) significantly increased post INDO at HA.

4.4. Discussion

Based on our findings, at SL hemodynamic DFi is influenced by increased vascular resistances associated with hypocapnic vasoconstrictions. In contrast, the maintained DFI at HA following

DOB+ACZ is likely related to the reduced vascular resistances when CBF is increased. In contrast prostaglandin mediated reductions in CBF negatively impact HA DFi but not at SL.

Following DOB infusion PI_{ICA} increased at sea level and high altitude, which was expected as DOB increases cardiac contractility (beta-1 receptor agonist). However, CBF (Q_{ICA}) only increased at HA following DOB+ACZ. In contrast, DFi was only altered at SL, not during HA. The change in DFi at SL and the lack of DFi response at HA were contrary to our hypothesis. At SL change in DFi may be due to changes in cerebrovascular resistance distal to the MCA_v, possibly a product of CO_2 mediated vasoconstrictions. At HA the changes in DFi also appear linked to changes in cerebrovascular resistance but as a product of pharmacological induced metabolic acidosis. Following INDO administration, CBF decreased both at SL and HA, an expected response due to non-selective cyclooxygenase inhibition triggering smooth muscles contractions. However, PI and DFi were only altered at HA following INDO, changes we did not observe at SL. Despite decreases in CBF at SL and HA, the lack of SL DFi response contrasts with our original hypothesis. Although, the reduction in DFi at HA was consistent with our original hypothesis. Increased resistance at the level of the ICA and not the MCA suggest that INDO may have impacted the large extracranial to intracranial vasomotor damping factors more so than vessels distal to the intracranial vessels at HA.

One of the unexpected findings in this study was the lack of increase in CBF following DOB administration at SL. It is worth noting that DOB administration at SL, resulted in significant hypocapnia (-3 mmHg). Because the brain is sensitive to changes in CO_2, and a ~2.75% decrease in CBF is expected per mmHg reduction in $PaCO_2$ a potential counter vasoconstriction, caused

by hypocapnia may have blocked the hypothesized DOB mediated CBF increase by a total of 8.25% (Lucas et al., 2011). When we consider that the DOB+ACZ increases in CBF at HA was ~12%, it is feasible to infer that DOB did have an impact on SL CBF but was countered by hyperventilation induced hypocapnia. Because $PI_{MCA\&ICA}$ increased at SL following DOB without any compensatory alterations to cerebrovascular resistance, we interpret the reduction in DFi to the result of conflicting hemodynamics factors. Specifically DOB mediated increases in CBF as well as hypocapnic mediated vasoconstriction. Future studies should investigate the influence of DOB on cerebrovascular hemodynamics while controlling for changes in $PaCO_2$.

It has been well demonstrated that CBF increases upon ascent to HA to ensure constant cerebral oxygen delivery. This increase is achieved through systemic compensations such as increased heart rate, ventilation, and blood pressure (Hoiland et al., 2018; Severinghaus et al., 1963; Willie et al., 2014). At HA following DOB+ACZ administration heart rate (6.5%) and CBF (12.9%) increased as hypothesized. Although hypoxic induced hyperventilation leads to hypocapnic vasoconstriction this mechanism can be counterbalanced by hypoxic vasodilation (Ainslie & Subudhi., 2014; Lucas et al., 2011). The degree of hypoxic vasodilation in the face of hypocapnic vasoconstriction is a product of hypoxic severity and the degree of metabolic acclimation (Willie et al., 2014; Lucas et al., 2011). Considering the increase in CBF following beta adrenergic stimulation in combination of metabolic acidosis it is probable that DOB+ACZ at HA provided a compounding cerebrovascular stimulus. More importantly, the maintained DFi following DOB+ACZ suggest that the hemodynamic stress was well managed. We interpret the maintained DFi at HA to be a product of a reduced CVR_{MCA} and highlights the importance of upstream microvascular compensations. In a comprehensive review, Caldwell et al., (2021) discuss how

hypercapnia and acidosis are influential in triggering precapillary and capillary vasodilation's in the brain, both at SL and HA. This microvascular vasodilation provides mechanistic insight into how cerebrovascular CO_2 sensitivities may play a compensatory role in hemodynamic damping. Specifically, the observed reduction in CVR_{MCA} following DOB+ACZ may have mitigated the hemodynamic PI burden originating in the ICA by providing a more compliant microvascular environment. We interpret this compliant compensatory response as a important mechanistic buffering of extra to intracranial PI's (i.e., maintained PI_{MCA} and DFi). This contrasts with the results observed at SL, where DFi was reduced when $PI_{ICA\ and\ MCA}$ were increased following DOB. The lack of any observed change in CVR at SL suggest that no microvascular benefit was provided. Unfortunately, our experimental design limits our ability to determine if the different SL and HA hemodynamic responses were caused by HA or ACZ. Regardless, at HA it appears that following DOB+ACZ administration the brain may gain a greater capacity to deal with hemodynamic stress. Coupled with the results of Burgess et al., 2018, DOB+ACZ appears to provide beneficial hemodynamic regulation at HA.

Impaired prostaglandin control of smooth muscle caused by non-selective cyclooxygenase inhibition (INDO) triggers smooth muscle contractions and consequently alters arterial tone (Ruan et al., 2010). In the brain, this manifests as a reduced CBF, however does not impact cerebrovascular reactivity to PaO_2 and $PaCO_2$ both at SL and HA (Hoiland et al., 2015). The aim of this investigation was to quantify if a reduced prostaglandin mediated smooth muscle control altered cerebrovascular hemodynamic damping at SL and HA. At SL, increases in cerebrovascular resistance downstream from the MCA appear to provide sufficient hemodynamic regulation to maintain extracranial to intracranial DFi. In contrast at HA, cyclooxygenase

inhibition appears to have caused extracranial hemodynamic adjustments in resistance, however these adjustments were insufficient to maintain DFi, resulting in a reduced hemodynamic buffering. Unfortunately, the experimental design limits our ability to explain why INDO altered extracranial resistance and not intracranial cranial resistances. Additionally, it is not possible to discern if HA cerebrovascular regulation provoked responses distal to the MCA that were counterbalanced to the extracranial changes in resistance. While it is possible that INDO altered vascular compliance distal to the intracranial vessels, we are unable to determine if this triggered caused the ICA to have more prominent role in regulation cerebrovascular resistance. Regardless, considering that DFi is reduced at HA following INDO administration our data suggests that INDO impacts cerebrovascular resistance downstream of the ICA, and negatively impacts hemodynamic buffering. Future studies should aim to quantify whether the reduced resting DFi results in a greater hemodynamic transmittance during dynamic tasks that cause changes in arterial blood gases and pressures. This information may provide important details pertaining to whether cyclooxygenase inhibition makes the brain more susceptible to HA related illness due to enhanced hemodynamic stress.

Limitations

A major limitation of this study is the limited completers (n=4) for pairwise comparisons. Pre to post drug comparisons where non-parametric (n=6 at SL, n=6 at HA) as there were different participants. Participants drop out was further influenced by emergency illness and acute mountain sickness, both which required descent. Further, our sample lacked sufficient diversity to compared pharmacological mediated cerebrovascular regulation in males and females. Additionally, our data was only performed in lowland people not Indigenous to the HA region.

Future studies should include equal representation of males and females, as well as consider the hemodynamic regulation people Indigenous to HA regions. Smirl et al., 2014 assess measures of static and dynamic cerebral autoregulation in lowlander and HA Indigenous people and observed no difference in cerebral autoregulation. The nature of extreme high altitude expeditions is both physiologically and logistically challenging, which has limited the interpretability of this research. Future studies that increase the sample size, as well as the diversity of the population will provide greater ecological validity.

Considering this is a secondary analysis, future studies that are designed specifically to investigate DOB, DOB+ACZ and INDO on cerebrovascular hemodynamics are needed. One experimental arm that is missing from this data set is a SL DOB+ACZ data collection. Pilot work in the initial SL experimentation indicated that ACZ did not influence resting CBF, and because of logistical consideration and in respect of participants time was excluded from initial experimentation. Because of this, it is not possible to determine if the DOB+ACZ benefits in cerebrovascular damping are a product of this combination of drugs at HA, or if the cerebrovascular benefits are purely in response to ACZ. Additionally, our findings only provide a measure of the acute short-term impact of pharmacological cerebrovascular regulation. Longitudinal studies that assess these impacts during HA ascension, acclimation to HA, as well the prolonged use in treating HA illness is needed.

In consideration of all studies that rely on TCD measures it is necessary to discuss the limitations associated with using TCD derived measures to assess CBF. While TCD provides reliable velocity trace, with superior temporal resolution its ability to provide volumetric hemodynamic

quantification is limited by the lack of cross-sectional area measures. The solution in recent years has been to include vascular Duplex ultrasound to collect velocity and diameter measures contemporaneously in the vessels distal to the intracranial vessels of interest. Although this provides us with the capacity to access volumetric CBF flow into the brain, the lack of intracranial diameter measures with TCD remains a limitation as we are unable to determine if pulsatile changes in diameter influence our hemodynamic assessments. Data collected using transcranial color doppler ultrasound may prove to be a useful measure of acclimatory hemodynamic changes (Willie et al., ascension paper), yet its use in dynamic cerebral assessment uncertain.

This study was also performed at rest and may have limited application to understand how dynamic systemic and cerebrovascular hemodynamics are influenced physiologically demanding tasks that provoke further changes in blood pressure, arterial blood gases, metabolism, and neurogenic activity. Smith et al., 2014 demonstrated that global cerebrovascular resistance was lower during maximal intensity exercise compared to sea-level, which is similar to what was observed during DOB+ACZ. Smith et al., 2014 did not assess the influence of DOB+ACZ on cerebrovascular hemodynamics during exercise, however if our findings were superimposed, it is plausible that DOB+ACZ during exercise may have a hyper additive benefit resulting in a more compliant cerebrovascular response during exercise.

4.5. Summary

Collectively this study provides important details pertaining to how pharmacologically induced increases and decreases in CBF impact the brains' ability to manage hemodynamic stress. As

mentioned above, based on our findings at SL hemodynamic DFi is influenced by increased vascular resistances while the maintained DFI at HA following DOB+ACZ is likely related to reduced vascular resistances. In contrast cyclooxygenase mediated reductions in CBF negatively impact DFi at HA but not at SL.

For future studies exploring whether the cerebrovascular compliance mechanisms demonstrated in this study underlie the etiology of altitude-related illness is of particular interest. Further, future studies should aim to specifically investigate the effects of DOB, DOB+ACZ and INDO on cerebrovascular hemodynamics during dynamic tests in larger sample populations. These studies could provide greater insight into the mechanisms of cerebrovascular damping. Studies that aim to explore cerebrovascular regulation should include measures of extra- to intracranial cerebrovascular damping if they wish to have a comprehensive understanding of the hemodynamic forces involved in maintaining adequate CBF.

Chapter 5 Summary and Significance

The following section aims to summarize the primary findings associated with this thesis, address the significance of these findings to the research question proposed, as well as discuss the limitations and future directions of research that will help to improve the findings and interpretations derived from this research.

5.1. Discussion

The influence of upstream and downstream resistances on hemodynamic stress in cerebral arteries has been difficult to assess until recently. The experimental chapter in this thesis present the outcomes from two experimental designs aiming to quantify how the brain deals with hemodynamic stress when CBF is altered pharmacologically at SL and HA. The primary finding from these experiments support previous views that downstream microvascular resistance is extremely important in determining the effectiveness of the cerebral vasculature to buffer hemodynamic stress both at SL and HA. Additionally, the influence of carbon dioxide and vascular smooth muscles cells were revealed to be important modulators of cerebrovascular hemodynamic stress. Specifically, the balance of hypocapnic vasoconstriction as well as $PaCO_2$ arterial tissue gradients in countering or supporting hemodynamic buffering will be discussed in the following paragraphs. Additionally, details pertaining to the role prostaglandins play in regulating hemodynamic stress will be discussed.

The effect of DOB on CBF is somewhat unclear, as some studies suggest it reduces CBF despite increasing heart rate, blood pressure, and cardiac output. Previous studies have observed an increase in external carotid artery flow following DOB administration and suggested that the

external carotid artery was a major contributor to the reduction in CBF, as the authors suggest facial capacitance served to shunt the hemodynamic stress away from the brain as a potential cerebrovascular protective mechanism (Ogoh., 2017). Unfortunately, this recent study by Ogoh et al., (2017) did not provide any measure of $PaCO_2$. The potential for $PaCO_2$ to provoke a counter cerebrovascular stimulus following DOB administration is significant and has potential micro and macrovascular influences via increased resistance. Regardless, we hypothesized that DOB would increase CBF due to its impact on systemic blood flow as a beta-1 receptor agonist at SL and HA. The observations in chapter 4 did not reveal a significant change in CBF at SL similar to what Ogoh et al., (2017) observed. What is more, a reduction in $P_{ET}CO_2$ was observed following DOB administration. Considering that the brain is highly sensitive to changes in CO_2 (a ~2.75% decrease in CBF per mmHg reduction in $PaCO_2$) (Lucas et al., 2011), the lack of an observable change in CBF following DOB administration may be because the hypocapnic (- 3 mmHg) vasoconstriction triggered a counter reduction in CBF of approximately 11.7% (Lucas et al., 2011). Since CBF was not observed to fall below baseline values, it is reasonable to suggest that the hypothesized increase in CBF following DOB did occur but was not observed because of the counterbalanced hypocapnic vasoconstriction. However, an increased PI in both the MCA and ICA was observed in support of an increased hemodynamic response following DOB administration at SL. Our main finding following the DOB mediated increase in PI at SL was the reduction in DFi. Despite no change in CBF the increased PI was not buffered as well prior to DOB at SL. Despite, the evidence pertaining to increased hemodynamics stress following DOB at SL, the lack of change in ICA and MCA CVR makes it difficult to determine the degree to which downstream microvascular responses impacted the reduction in DFi. However, our findings would suggest that the perspectives outlined by Ogoh et al., (2017) regarding

extracranial facial circulation compensating for hemodynamic changes instigated by DOB are not completely sufficient. As previously mentioned, interpretations from the experimental chapter suggest that DOB administration at SL does provoke extra and intracranial hemodynamic stress, which results in a reduction in DFi. This is achieved because of our attempts to measure hemodynamics between extra and intracranial cerebrovascular segments.

At HA following DOB+ACZ there was an increase in heart rate, PI_{ICA}, and CBF_{ICA} and MCAv. Also, introduce resistance findings here. Coupled with the influence of HA (i.e., different HR response; significant increase in MCAv and ICAv at HA, the DOB+ACZ responses is intriguing because it indicates that increased CBF does not appear to modulate damping, at least when resistance distal to the MCA is reduced. Comparing HA vs SL DFi measures suggest that the key to maintaining healthy damping is a product of a reduced resistance / increased conductance. Thus, it may represent that the brain when exposed to the combination of DOB+ACZ was capable of dealing with any provoked hemodynamic stress. The increase in HR with DOB+ACZ and trend towards DOB+ACZ increasing MAP at HA suggests that cardiac hemodynamics did increase, but the cerebral vasculature maintained a similar hemodynamic buffering. At HA ACZ may have provided microvascular hemodynamics support, as it helped to balance acid-base balances at the neurovascular unit inhibiting carbonic anhydrase activity (Caldwell et al., 2021). Additionally, enhanced renal excretion of bicarbonate over time reset systemic acid base balances, helping to stabilize ventilation and consequently arterial oxygen saturation (Cain & Dunn., 1966; Leaf & Goldfarb., 2007; Teppema et al., 2007). No SL ACZ data was presented in this thesis, yet pilot testing revealed no impact of ACZ on CBF by itself. Research observations pertaining to ACZ responses on CBF are conflicting. For example, Hauge et al., (1988) observed

no change in CBF but an increase in MCAv following ACZ administration. Interpretating these differential responses would indicate that the increased MCAv was in response to a vasoconstriction in the MCA following ACZ. Pilot testing in our lab prior to the 2012 expedition revealed similar maintenance of CBF during SL ACZ, yet it remains o be observed if MCA diameter changes following ACZ. However, Okazawa et al., (2001) using PET observed regional increases in CBF attributed to vasodilatory responses in the microvasculature. The data collected in this thesis would not be sufficient to infer microvascular vasodilation at SL, however our HA response when ACZ is presented in combination with DOB would. Further research investigating these responses is required.

During hypoxia, ACZ acts on smooth muscles by inhibiting carbonic anhydrases. Because carbonic-anhydrases catalyze the reaction $CO_2 + OH^- \rightleftarrows HCO3^-$, thereby accelerating equilibration of the acid-base buffer system, inhibition via ACZ induces metabolic acidosis causing vasodilation of the cerebral arterioles, reducing distal cerebrovascular resistance (Okazawa et al., 2001; Rasmussen & Boedtkjer., 2017; Teppema et al., 2007). A study by Domoki et al., (2008) in pigs found ACZ induced pial arterial vasodilation and increased cortical perfusion, similar to the effects of hypercapnia, and the pial arterioles saw a greater impact from acid-base balance than prostaglandin or other NO mediated mechanisms.

Our results discussed in Chapter 4 suggest, that when DOB+ACZ are administered together an increase in cardiac output (upstream macrovasculature) and decrease in downstream resistance (cerebral microvasculature) promote an increase CBF (**Figure 18**). In contrast to SL responses, DFi at HA was maintained despite a similar increase in PI. The reduction in CVR_{MCA} following

DOB+ACZ indicates that factors at or distal to the MCA provided beneficial hemodynamic support serving to mitigate increases in pulsatile flow. Our interpretation of these SL and HA findings in regard to the relationship between changes in PI and resistance indicate more compliant vessels will result in less pulsatile transmission. Future studies aiming to identify interventions that preserve cerebrovascular compliance with aging are needed. Additionally, future studies investigating damping factors in the posterior circulation would also be beneficial to understanding how other intracranial pathways are involved in mitigating pulsatile hemodynamic stress.

Indomethacin acts by non-selectively blocking COX, impairing prostaglandin synthesis and a pathway involved in NO mediated smooth muscle function. This modest NO inhibition likely attenuates vasodilatory function consequently reducing CBF and compliance along the extra to intracranial vascular segment. The observation of the reduced DFi following INDO application at HA and the SL DFi supports this. At SL INDO reduces CBF, likely through the increased resistance and decreased conductance observed at the MCA. Also, there were no observable changes in PI at either the MCA or ICA at SL.

Considering that CVR_{MCA} increased at SL there are several potential interpretations (**Figure 18**). First, given that the reduction in DFi (~19%) at SL was not observed to be significant, CVR_{MCA} had a opposite and optimal benefit on hemodynamic buffering compared to HA where DFi was significantly reduced (~40%). Therefore, increases in CVR_{ICA} observed at HA were not sufficient to mitigate reductions in DFi which contrasts with the benefits of an increased CVR_{MCA} on DFi responses at SL. However, interaction analysis did not reveal differential

responses in DFi at SL and HA. Thus, a second, and contrasting, interpretation might suggest that the lack of statistical significance yet trending 19% reduction in DFi at SL was merely an issue of insufficient statistical power. A post hoc power calculation aiming to achieve a 90% power would requires 18 participants to achieve statistical significance for the DFi response observed at SL. If the secondary statistical interpretation was further interrogated, it is plausible that attenuations in cerebrovascular compliance (i..e, lower DFi) between the extra and intracranial segments and the segments distal to the MCA would be significant at SL and HA. Shoemaker et al. (2023) compared MCA_v and microvascular hemodynamics during a normoxic hypotensive stimulus (i.e., lower body negative pressure) using diffuse correlation spectroscopy. The authors observed that intracranial responses at or proximal to the MCA help to reduce the hypotensive hemodynamic insult in the cerebral microvasculature. While speculative because this thesis did not measure microvascular responses to changes in blood pressure, our results suggest that INDO may mitigate the extracranial to intracranial buffering. Future studies, with a larger sample, should investigate dynamic hypo- and hypertensive fluctuations in BP with and without INDO administration to gain a better understanding of cerebrovascular hemodynamic damping and its implications to HA acclimation and healthy aging at SL.

While the reduction in Q_{ICA} (18%) following INDO at HA was largely due to the reduction in ICA_v (17%). In contrast, the reduction in MCA_v was 13%, suggesting the increased ICA_{res} observed at HA is likely the result of a vasoconstrictive phenomenon between the ICA and MCA. Because no change in resistance was observed beyond the MCA, coupled with the mismatch in percentage change in velocity and flow, there may have been a MCA vasoconstriction. The potential for vasoconstriction along the ICA to MCA segment to negatively impact DFi at HA is

substantial. Despite our experimental design being insufficient to compare INDO and DOB+ACZ responses at HA, the vascular damping benefits observed following DOB+ACZ (i.e., downstream reductions in resistance caused by microvascular recruitment) suggest that the reduction in DFi at SL was because of an inverse inadequate downstream microvascular response. Whether the 30% reduction in extra to intracranial DFi is further reduced distal to the MCA following INDO remains to be observed, both at rest and during dynamic cardiovascular stressors. Future studies should aim to characterize and compare the hemodynamic decay along the extracranial and intracranial segments using dynamic assessments as well using approaches that provide hemodynamic indexing in the microvasculature distal the circle of Willis. Shoemaker et al., (2023) compared MCA_v and microvascular hemodynamics during a hypotensive stimulus (i.e., lower body negative pressure) using diffuse correlation spectroscopy. Their findings indicate that the extracranial response helps to reduce the hypotensive hemodynamic transmission to the microvasculature. Unfortunately, our findings are unable to corroborate this. Future studies should investigate whether INDO mitigates extracranial hemodynamic buffering at SL and HA.

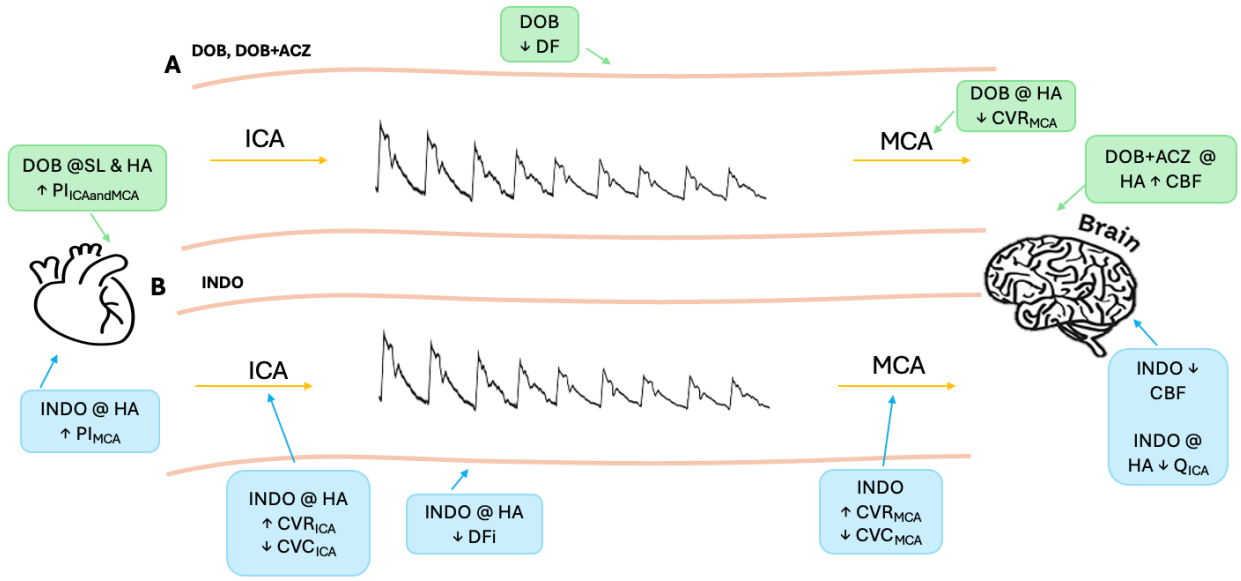

Figure 18. Hemodynamic changes observed at sea-level and high altitude following pharmacological interventions. Where the pharmacological interventions are DOB=Dobutamine, ACZ= Acetazolamide, INDO=Indomethacin. SL= Sea level, HA= High altitude. ICA = Internal carotid, MCA= Middle cerebral artery. Where hemodynamic changes are; PI=Pulsitility, CVR=Cerebrovascular resistance, CVC= Cerebrovascular conductance, Q=Flow, CBF= Cerebral blood flow, DFi=Damping factor index. (A) Shows the changes observed following DOB administration at SL and DOB+ACZ at HA. (B) Shows the changes observed following INDO administration at SL and HA.

5.2. Strengths and Limitations

As noted above, the greatest limitation of this thesis is the limited sample size (n=4, pairwise). Pre to post drug comparisons where non-parametric (n=6 at SL, n=6 at HA) as there were different participants. Participants drop out was due to emergency illness and acute mountain sickness, both which required descent. While the study required significant involvement from the participants, HA illness, and an emergency appendectomy further complicated the interpretability of this study by removing two participants that had completed SL testing. While a few points of speculation have been provided in above sections, each speculation considered statistical trends, and included post hoc power calculations to provide future studies quantitative support. Further, considering our low sample size, it is worth mentioning that our sample lacked sufficient

diversity to compared pharmacological mediated cerebrovascular regulation in males and females, as well as any potential regional and/or ethnic impacts on cerebrovascular responses. Additionally, our data was only performed in lowland people not people who are Indigenous to the HA region. Future studies should include equal representation of males and females, as well as consider the hemodynamic regulation people Indigenous to HA regions. Smirl et al., 2014 assess measures of static and dynamic cerebral autoregulation in lowlander and HA Indigenous people and observed no difference in cerebral autoregulation. Further, Tymko et al., (2022) found that Andean and Sherpa highlander populations have more acidic arterial blood, due to elevated arterial carbon dioxide and similar arterial bicarbonate compared with acclimatizing lowlanders at altitudes ≥4,300 m. The nature of extreme high-altitude expeditions is both physiologically and logistically challenging, which has limited the interpretability of this research. Future studies that increase the sample size, as well as the diversity of the population will provide greater ecological validity.

Considering this is a secondary analysis, more studies that are designed specifically to investigate DOB, DOB+ACZ and INDO on cerebrovascular hemodynamics are needed. One experimental arm that is missing from this data set is a SL ACZ, and a DOB+ACZ data collection. As mentioned above, pilot work in the initial SL experimentation indicated that ACZ did not influence resting CBF, and because of logistical consideration and in respect of participants time an ACZ experimental arm was excluded from initial experimentation in 2012. Because of this, it is not possible to determine if the DOB+ACZ benefits in cerebrovascular damping are a product of this combination of drugs at HA, or if the cerebrovascular benefits are purely in response to ACZ. Additionally, our findings only provide a measure of the acute short-

term impact of pharmacological cerebrovascular regulation. Longitudinal studies that assess these impacts during HA ascension, acclimation to HA, as well the prolonged use in treating HA illness is needed.

In consideration of all studies that rely on TCD measures it is necessary to discuss the limitations associated with using TCD derived measures to assess CBF. While TCD provides reliable velocity trace, with superior temporal resolution its ability to provide volumetric hemodynamic quantification is limited by the lack of cross-sectional area measures. The solution in recent years has been to include vascular Duplex ultrasound to collect velocity and diameter measures contemporaneously in the vessels distal to the intracranial vessels of interest. Although this provides us with the capacity to access volumetric CBF flow into the brain, the lack of intracranial diameter measures with TCD remains a limitation as we are unable to determine if pulsatile changes in diameter influence our hemodynamic assessments. Data collected using transcranial color doppler ultrasound may prove to be a useful measure of acclimatory hemodynamic changes (Willie et al., ascension paper), yet its use in dynamic cerebral assessment uncertain. The interpretation of our intracranial data was limited by the lack of diameter measures, although the discrepancy between the decrease in ICA flow (18%) and MCA velocity (13%) suggests MCA vasoconstriction following INDO at HA did occur. This contrasts with the SL data that indicates that the reduction in ICA flow was similar to the percent change in MCA velocity. Still in 2024, it remains difficult to assess intracranial diameters without the use of magnetic resonance imaging, which remains to be a continued difficulty to perform at HA.

This study was also performed at rest and may have limited application to understand how dynamic systemic and cerebrovascular hemodynamics are influenced physiologically demanding

tasks that provoke further changes in blood pressure, arterial blood gases, metabolism, and neurogenic activity. Smith et al., 2014 demonstrated that global cerebrovascular resistance was lower during maximal intensity exercise compared to sea-level, which is similar to what was observed during DOB+ACZ. Smith et al., 2014 did not assess the influence of DOB+ACZ on cerebrovascular hemodynamics during exercise, however if our findings were superimposed, it is plausible that DOB+ACZ during exercise may have a hyper additive benefit resulting in a more compliant cerebrovascular response during exercise. Maier., (2023) observed hemodynamic patterns in the brachial artery during handgrip exercise at altitude following beta, and alpha plus beta block. Their findings indicate an important autonomic relationship in the hemodynamic buffering in peripheral arteries. Further, because handgrip exercise is isolated to the lower arm and the body is stationary, steady insonation of intracranial arteries is easier to obtain. The impact of this handgrip protocol with alpha and beta block is an interesting direction for a future study.

5.3. Conclusion

Pulsitility increases with age often in parallel with vascular stiffening, which has been observed to reduce damping and increase the hemodynamic burden in cerebral vessels (Lefferts et al., 2020; Mitchell et al., 2011; Tarumi et al., 2014; Townsend et al., 2015). Reductions in cerebral vascular damping have recently been linked to increased risk of mild cognitive impairment and dementia (Bateman., 2004; Bateman et al., 2008; Zarrinkoob et al., 2016). Measures of peripheral vascular function are valuable for providing a large systemic view of vascular health however, measures of peripheral vascular function poorly reflect changes in cerebral hemodynamics (Claassen et al., 2021).

Traditional autoregulatory understanding credits the microvasculature with the mitigation of elevations in CBF in response to hypertensive stimuli (Kontos et al., 1978) by increasing downstream resistance. However, conduit arteries (e.g., carotids, ICA) have also been identified as playing a role in management of pulsitility (Tzeng et al., 2014; Willie et al., 2014). Further, impaired vasodilatory capacity, as seen following administration of INDO or in conditions such as hypertension, there is the risk of a harmful increase in transmission from the proximal to distal vasculature.

This thesis observed that increases in hemodynamic stress (i.e., PI), following DOB administration, when unaccompanied by increased extra and intracranial vascular resistances results in increased transmission illustrated by a reduced DFi. At HA, when DOB is administered with ACZ, the reduction in downstream resistance appears o provided hemodynamic protection resulting in a similar DFi. Conversely INDO led to a reduction in DFi at HA, and it remains to be determined if this reduced DFi has a negative influence on the microvasculature.

Further, the nature of expedition research in extreme conditions such as HA necessitate portability and easy to manage equipment. Both vascular Duplex and transcranial Doppler are portable and can be used offline, and the combination of these methods provides greater interpretability of the data as VDu provides diameter. Future expedition studies should include Colour Duplex for insonation of the MCA to access diameter data, and MRI to observe microvascular changes. Finally, a novel aspect of this thesis is the measurement of hemodynamics from the ICA to the MCA, rather than insonating at the common carotid which eliminates potential shunting to the ECA.

In summary, DFi is a promising measure of the ability for vasculature to manage pulsatile stress and provides valuable insight on vascular compliance. Hemodynamic measurements taken from the ICA-MCA using the combination of transcranial Doppler and vascular Duplex allow for a more direct measure of cerebrovascular extra-intracranial hemodynamics. The affordability and portability of this method, plus the non-invasive nature, has potential for wider clinical use. It would be exciting to see future studies investigate DFi as a potential measure of early detection for vascular and cerebrovascular disease in addition to further understanding of the cerebrovascular blood flow regulatory mechanisms outlined above.

Chapter 6 References

Aaslid, R. (1986). The Doppler Principle Applied to Measurement of Blood Flow Velocity in Cerebral Arteries. In Transcranial Doppler Sonography (pp. 22–38). Springer Vienna. https://doi.org/10.1007/978-3-7091-8864-4_3

Aaslid, R., Lindegaard, K. F., Sorteberg, W., & Nornes, H. (1989). Cerebral autoregulation dynamics in humans. Stroke, 20(1), 45–52. https://doi.org/10.1161/01.STR.20.1.45

Aaslid, R., Markwalder, T.-M., & Nornes, H. (1982). Noninvasive transcranial Doppler ultrasound recording of flow velocity in basal cerebral arteries. Journal of Neurosurgery, 57(6), 769–774. https://doi.org/10.3171/jns.1982.57.6.0769

Ainslie, P. N., & Duffin, J. (2009). Integration of cerebrovascular CO 2 reactivity and chemoreflex control of breathing: mechanisms of regulation, measurement, and interpretation. American Journal of Physiology-Regulatory, Integrative and Comparative Physiology, 296(5), R1473–R1495. https://doi.org/10.1152/ajpregu.91008.2008

Ainslie, P. N., & Ogoh, S. (2010). Regulation of cerebral blood flow in mammals during chronic hypoxia: a matter of balance. Experimental Physiology, 95(2), 251–262. https://doi.org/10.1113/expphysiol.2008.045575

Ainslie, P. N., & Poulin, M. J. (2004). Ventilatory, cerebrovascular, and cardiovascular interactions in acute hypoxia: regulation by carbon dioxide. Journal of Applied Physiology, 97(1), 149–159. https://doi.org/10.1152/japplphysiol.01385.2003

Ainslie, P. N., Shaw, A. D., Smith, K. J., Willie, C. K., Ikeda, K., Graham, J., & Macleod, D. B. (2014). Stability of cerebral metabolism and substrate availability in humans during hypoxia and hyperoxia. Clinical Science, 126(9), 661–670. https://doi.org/10.1042/CS20130343

Ainslie, P. N., & Subudhi, A. W. (2014). Cerebral Blood Flow at High Altitude. High Altitude Medicine & Biology, 15(2), 133–140. https://doi.org/10.1089/ham.2013.1138

Ajmani, R. S., Metter, E. J., Jaykumar, R., Ingram, D. K., Spangler, E. L., Abugo, O. O., & Rifkind, J. M. (2000). Hemodynamic changes during aging associated with cerebral blood flow and impaired cognitive function. Neurobiology of Aging, 21(2), 257–269. https://doi.org/10.1016/S0197-4580(00)00118-4

Alexander Monro. (1783). Observations on the Structure and Functions of the Nervous System, Illustrated with Tables. Lond Med J. , 113–135.

Arts, T., Onkenhout, L. P., Amier, R. P., van der Geest, R., van Harten, T., Kappelle, J., Kuipers, S., van Osch, M. J. P., van Bavel, E. T., Biessels, G. J., Zwanenburg, J. J. M., & Heart-Brain Connection Consortium. (2022). Non-Invasive Assessment of Damping of Blood Flow Velocity Pulsatility in Cerebral Arteries With MRI. Journal of Magnetic Resonance Imaging : JMRI, 55(6), 1785–1794. https://doi.org/10.1002/jmri.27989

Ashley, E., & Niebauer, J. (2004). Cardiology Explained. Remedica.

Avolio, A. (2013). Arterial Stiffness. Pulse, 1(1), 14–28. https://doi.org/10.1159/000348620

Barlinn, K., & Alexandrov, A. v. (2022). Transcranial Doppler Sonography. In Noninvasive Vascular Diagnosis (pp. 297–329). Springer International Publishing. https://doi.org/10.1007/978-3-030-60626-8_15

Barold, S. S. (2003). Willem Einthoven and the Birth of Clinical Electrocardiography a Hundred Years Ago. Cardiac Electrophysiology Review, 7(1), 99–104. https://doi.org/10.1023/A:1023667812925

Bateman, G. A. (2004). Pulse wave encephalopathy: a spectrum hypothesis incorporating Alzheimer's disease, vascular dementia and normal pressure hydrocephalus. Medical Hypotheses, 62(2), 182–187. https://doi.org/10.1016/S0306-9877(03)00330-X

Bateman, G. A., Levi, C. R., Schofield, P., Wang, Y., & Lovett, E. C. (2008). The venous manifestations of pulse wave encephalopathy: windkessel dysfunction in normal aging and senile dementia. Neuroradiology, 50(6), 491–497. https://doi.org/10.1007/s00234-008-0374-x

Baumgartner, R. W., Bärtsch, P., Maggiorini, M., Waber, U., & Oelz, O. (1994). Enhanced cerebral blood flow in acute mountain sickness. Aviation, Space, and Environmental Medicine, 65(8), 726–729.

Bayliss, W. M. (1902). On the local reactions of the arterial wall to changes of internal pressure. The Journal of Physiology, 28(3), 220–231. https://doi.org/10.1113/jphysiol.1902.sp000911

Belz, G. G. (1995). Elastic properties and Windkessel function of the human aorta. Cardiovascular Drugs and Therapy, 9(1), 73–83. https://doi.org/10.1007/BF00877747

Bernardi, L., Passino, C., Spadacini, G., Calciali, A., Robergs, R., Greene, R., Martignoni, E., Anand, I., & Appenzeller, O. (1998). Cardiovascular autonomic modulation and activity of carotid baroreceptors at altitude. Clinical Science, 95(5), 565–573. https://doi.org/10.1042/cs0950565

Berre, J., de Backer, D., Moraine, J.-J., Melot, C., Kahn, R. J., & Vincent, J.-L. (1997). Dobutamine increases cerebral blood flow velocity and jugular bulb hemoglobin saturation in septic patients. Critical Care Medicine, 25(3), 392–398. https://doi.org/10.1097/00003246-199703000-00004

Bishop, C. C., Powell, S., Rutt, D., & Browse, N. L. (1986). Transcranial Doppler measurement of middle cerebral artery blood flow velocity: a validation study. Stroke, 17(5), 913–915. https://doi.org/10.1161/01.STR.17.5.913

Brassard, P., Labrecque, L., Smirl, J. D., Tymko, M. M., Caldwell, H. G., Hoiland, R. L., Lucas, S. J. E., Denault, A. Y., Couture, E. J., & Ainslie, P. N. (2021). Losing the dogmatic view of cerebral autoregulation. Physiological Reports, 9(15). https://doi.org/10.14814/phy2.14982

Burgess, K. R., Lucas, S. J. E., Burgess, K. M. E., Sprecher, K. E., Donnelly, J., Basnet, A. S., Tymko, M. M., Day, T., Smith, K., Lewis, N., & Ainslie, P. N. (2018). Increasing cerebral blood flow reduces the severity of central sleep apnea at high altitude. Journal of Applied Physiology, 124(5), 1341–1348. https://doi.org/10.1152/japplphysiol.00799.2017

Caddy, H. T., Thomas, H. J., Kelsey, L. J., Smith, K. J., Doyle, B. J., & Green, D. J. (2023). Comparison of computational fluid dynamics with transcranial Doppler ultrasound in response to physiological stimuli. Biomechanics and Modeling in Mechanobiology. https://doi.org/10.1007/s10237-023-01772-9

Cain, S. M., & Dunn, J. E. (1966). Low doses of acetazolamide to aid accommodation of men to altitude. Journal of Applied Physiology, 21(4), 1195–1200. https://doi.org/10.1152/jappl.1966.21.4.1195

Caldwell, H. G., Carr, J. M. J. R., Minhas, J. S., Swenson, E. R., & Ainslie, P. N. (2021). Acid–base balance and cerebrovascular regulation. The Journal of Physiology, 599(24), 5337–5359. https://doi.org/10.1113/JP281517

Caldwell, H. G., Smith, K. J., Lewis, N. C. S., Hoiland, R. L., Willie, C. K., Lucas, S. J. E., Stembridge, M., Burgess, K. R., MacLeod, D. B., & Ainslie, P. N. (2021). Regulation of cerebral blood flow by arterial PCO 2 independent of metabolic acidosis at 5050 m. The Journal of Physiology, 599(14), 3513–3530. https://doi.org/10.1113/JP28144

Carr, J. M. J. R., Ainslie, P. N., Howe, C. A., Gibbons, T. D., Tymko, M. M., Steele, A. R., Hoiland, R. L., Vizcardo-Galindo, G. A., Patrician, A., Brown, C. v., Caldwell, H. G., & Tremblay, J. C. (2022). Brachial artery responses to acute hypercapnia: The roles of shear stress and adrenergic tone. Experimental Physiology, 107(12), 1440–1453. https://doi.org/10.1113/EP090690

Carr, J. M. J. R., Caldwell, H. G., & Ainslie, P. N. (2021). Cerebral blood flow, cerebrovascular reactivity and their influence on ventilatory sensitivity. Experimental Physiology, 106(7), 1425–1448. https://doi.org/10.1113/EP089446

Cassaglia, P. A., Griffiths, R. I., & Walker, A. M. (2008). Sympathetic nerve activity in the superior cervical ganglia increases in response to imposed increases in arterial pressure. American Journal of Physiology-Regulatory, Integrative and Comparative Physiology, 294(4), R1255–R1261. https://doi.org/10.1152/ajpregu.00332.2007

Chan, G. S. H., Ainslie, P. N., Willie, C. K., Taylor, C. E., Atkinson, G., Jones, H., Lovell, N. H., & Tzeng, Y.-C. (2011). Contribution of arterial Windkessel in low-frequency cerebral hemodynamics during transient changes in blood pressure. Journal of Applied Physiology, 110(4), 917–925. https://doi.org/10.1152/japplphysiol.01407.2010

Chandra, A., Li, W., Stone, C., Geng, X., & Ding, Y. (2017). The cerebral circulation and cerebrovascular disease I: Anatomy. Brain Circulation, 3(2), 45. https://doi.org/10.4103/bc.bc_10_17

Chiesa, S. T., Masi, S., Shipley, M. J., Ellins, E. A., Fraser, A. G., Hughes, A. D., Patel, R. S., Khir, A. W., Halcox, J. P., Singh-Manoux, A., Kivimaki, M., Celermajer, D. S., & Deanfield, J. E. (2019). Carotid artery wave intensity in mid- to late-life predicts cognitive decline: the Whitehall II study. European Heart Journal, 40(28), 2300–2309. https://doi.org/10.1093/eurheartj/ehz189

Cipolla, M. J. (2009). The Cerebral Circulation. Colloquium Series on Integrated Systems Physiology: From Molecule to Function, 1(1), 1–59. https://doi.org/10.4199/C00005ED1V01Y200912ISP002

Claassen, J. A. H. R., Thijssen, D. H. J., Panerai, R. B., & Faraci, F. M. (2021). Regulation of cerebral blood flow in humans: physiology and clinical implications of autoregulation. Physiological Reviews, 101(4), 1487–1559. https://doi.org/10.1152/physrev.00022.2020

Climie, R. E., Gallo, A., Picone, D. S., di Lascio, N., van Sloten, T. T., Guala, A., Mayer, C. C., Hametner, B., & Bruno, R. M. (2019). Measuring the Interaction Between the Macro- and Micro-Vasculature. Frontiers in Cardiovascular Medicine, 6. https://doi.org/10.3389/fcvm.2019.00169

Cloud, G. C. (2003). Diagnosis and management of vertebral artery stenosis. QJM, 96(1), 27–54. https://doi.org/10.1093/qjmed/hcg003

Cohen, P. J., Alexander, S. C., Smith, T. C., Reivich, M., & Wollman, H. (1967). Effects of hypoxia and normocarbia on cerebral blood flow and metabolism in conscious man. Journal of Applied Physiology, 23(2), 183–189. https://doi.org/10.1152/jappl.1967.23.2.183

Coverdale, N. (2015). Reactivity of the middle cerebral artery to carbon dioxide. The School of Graduate and Postdoctoral Studies. The University of Western Ontario. London, Ontario, Canada

Covic, A., & Siriopol, D. (2015). Pulse Wave Velocity Ratio. Hypertension, 65(2), 289–290. https://doi.org/10.1161/HYPERTENSIONAHA.114.04678

D'Alecy, L. G., Rose, C. J., & Sellers, S. A. (1979). Sympathetic modulation of hypercapnic cerebral vasodilation in dogs. Circulation Research, 45(6), 771–785. https://doi.org/10.1161/01.RES.45.6.771

Dalkara, T. (2015). Cerebral Microcirculation: An Introduction. In PanVascular Medicine (pp. 655–680). Springer Berlin Heidelberg. https://doi.org/10.1007/978-3-642-37078-6_29

Daneman, R., & Prat, A. (2015). The blood-brain barrier. Cold Spring Harbor Perspectives in Biology, 7(1), a020412. https://doi.org/10.1101/cshperspect.a020412

Davidge, S. T. (2001). Prostaglandin H Synthase and Vascular Function. Circulation Research, 89(8), 650–660. https://doi.org/10.1161/hh2001.098351

Dominelli, P. B., Wiggins, C. C., Baker, S. E., Shepherd, J. R. A., Roberts, S. K., Roy, T. K., Curry, T. B., Hoyer, J. D., Oliveira, J. L., & Joyner, M. J. (2020). Influence of high affinity haemoglobin on the response to normoxic and hypoxic exercise. The Journal of Physiology, 598(8), 1475–1490. https://doi.org/10.1113/JP279161

Donald, I., Macvicar, J., & Brown, T. G. (1958). Investigation of abdominal masses by pulsed ultrasound. The Lancet, 1188–1195.

Donato, A. J., Machin, D. R., & Lesniewski, L. A. (2018). Mechanisms of Dysfunction in the Aging Vasculature and Role in Age-Related Disease. Circulation Research, 123(7), 825–848. https://doi.org/10.1161/CIRCRESAHA.118.312563

Duan, W., Sehrawat, P., Balachandrasekaran, A., Bhumkar, A. B., Boraste, P. B., Becker, J. T., Kuller, L. H., Lopez, O. L., Gach, H. M., & Dai, W. (2020). Cerebral Blood Flow Is Associated with Diagnostic Class and Cognitive Decline in Alzheimer's Disease. Journal of Alzheimer's Disease, 76(3), 1103–1120. https://doi.org/10.3233/JAD-200034

DuBose, L. E., Voss, M. W., Weng, T. B., Kent, J. D., Dubishar, K. M., Lane-Cordova, A., Sigurdsson, G., Schmid, P., Barlow, P. B., & Pierce, G. L. (2017). Carotid β-stiffness index is associated with slower processing speed but not working memory or white matter integrity in healthy middle-aged/older adults. Journal of Applied Physiology (Bethesda, Md. : 1985), 122(4), 868–876. https://doi.org/10.1152/japplphysiol.00769.2016

Duvernoy, H. M., Delon, S., & Vannson, J. L. (1981). Cortical blood vessels of the human brain. Brain Research Bulletin, 7(5), 519–579. https://doi.org/10.1016/0361-9230(81)90007-1

Egnor, M., Zheng, L., Rosiello, A., Gutman, F., & Davis, R. (2002). A Model of Pulsations in Communicating Hydrocephalus. Pediatric Neurosurgery, 36(6), 281–303. https://doi.org/10.1159/000063533

Ehrenreich, D. L., Burns, R. A., Alman, R. W., & Fazekas, J. F. (1961). Influence of Acetazolamide on Cerebral Blood Flow. Archives of Neurology, 5(2), 227–232. https://doi.org/10.1001/archneur.1961.00450140109011

Faraci, F. M., Heistad, D. D., & Mayhan, W. G. (1987). Role of large arteries in regulation of blood flow to brain stem in cats. The Journal of Physiology, 387(1), 115–123. https://doi.org/10.1113/jphysiol.1987.sp016566

Farzam, K., & Abdullah, M. (2023). Acetazolamide. StatPearls Publishing.

Félétou, M. (2011). The Endothelium: Part 1: Multiple Functions of the Endothelial Cells—Focus on Endothelium-Derived Vasoactive Mediators. Morgan & Claypool Life Sciences.

Fog, M. (1938). The relationship between the blood pressure and the tonic regulation of pial arteries. Journal of Neurology, Neurosurgery & Psychiatry, 1(3), 187–197. https://doi.org/10.1136/jnnp.1.3.187

Friis, M. L., Paulson, O. B., & Hertz, M. M. (1980). Carbon dioxide permeability of the blood-brain barrier in man. Microvascular Research, 20(1), 71–80. https://doi.org/10.1016/0026-2862(80)90020-5

Giller, C. A., Bowman, G., Dyer, H., Mootz, L., & Krippner, W. (1993). Cerebral arterial diameters during changes in blood pressure and carbon dioxide during craniotomy. Neurosurgery, 32(5), 737–741; discussion 741-2.

Gosling, R. G., Dunbar, G., King, D. H., Newman, D. L., Side, C. D., Woodcock, J. P., Fitzgerald, D. E., Keates, J. S., & Macmillan, D. (1971). The Quantitative Analysis of Occlusive Peripheral Arterial Disease By a Non-Intrusive Ultrasonic Technique. Angiology, 22(1), 52–55. https://doi.org/10.1177/000331977102200109

Gosling, R. G., & King, D. H. (1974). Arterial assessment by Doppler-shift ultrasound. Proceedings of the Royal Society of Medicine, 67(6 Pt 1), 447–449.

Greitz, D. (1993). Cerebrospinal fluid circulation and associated intracranial dynamics. A radiologic investigation using MR imaging and radionuclide cisternography. Acta Radiologica. Supplementum, 386, 1–23.

Guelen, I., Westerhof, B. E., van der Sar, G. L., van Montfrans, G. A., Kiemeneij, F., Wesseling, K. H., & Bos, W. J. W. (2003). Finometer, finger pressure measurements with the possibility to reconstruct brachial pressure. Blood Pressure Monitoring, 8(1), 27–30. https://doi.org/10.1097/00126097-200302000-00006

Hackett, P. H., & Roach, R. C. (2001). High-Altitude Illness. New England Journal of Medicine, 345(2), 107–114. https://doi.org/10.1056/NEJM200107123450206

Hainsworth, R., Drinkhill, M. J., & Rivera-Chira, M. (2007). The autonomic nervous system at high altitude. Clinical Autonomic Research, 17(1), 13–19. https://doi.org/10.1007/s10286-006-0395-7

Hamberger, A., & Hydén, H. (1963). Inverse enzymatic changes in neurons and glia during increased function and hypoxia. The Journal of Cell Biology, 16(3), 521–525. https://doi.org/10.1083/jcb.16.3.521

Hauge, A., Nicolaysen, G., & Thoresen, M. (1983). Acute effects of acetazolamide on cerbral blood flow in man. Acta Physiologica Scandinavica, 117(2), 233–239. https://doi.org/10.1111/j.1748-1716.1983.tb07202.x

Heistad, D. D., Marcus, M. L., & Abboud, F. M. (1978). Role of Large Arteries in Regulation of Cerebral Blood Flow in Dogs. Journal of Clinical Investigation, 62(4), 761–768. https://doi.org/10.1172/JCI109187

Hoiland, R. L., Ainslie, P. N., Wildfong, K. W., Smith, K. J., Bain, A. R., Willie, C. K., Foster, G., Monteleone, B., & Day, T. A. (2015). Indomethacin-induced impairment of regional cerebrovascular reactivity: implications for respiratory control. The Journal of Physiology, 593(5), 1291–1306. https://doi.org/10.1113/jphysiol.2014.284521

Hoiland, R. L., Bain, A. R., Rieger, M. G., Bailey, D. M., & Ainslie, P. N. (2016). Hypoxemia, oxygen content, and the regulation of cerebral blood flow. American Journal of Physiology-Regulatory, Integrative and Comparative Physiology, 310(5), R398–R413. https://doi.org/10.1152/ajpregu.00270.2015

Hoiland, R. L., Fisher, J. A., & Ainslie, P. N. (2019). Regulation of the Cerebral Circulation by Arterial Carbon Dioxide. In Comprehensive Physiology (pp. 1101–1154). Wiley. https://doi.org/10.1002/cphy.c180021

Hoiland, R. L., Howe, C. A., Coombs, G. B., & Ainslie, P. N. (2018). Ventilatory and cerebrovascular regulation and integration at high-altitude. Clinical Autonomic Research : Official Journal of the Clinical Autonomic Research Society, 28(4), 423–435. https://doi.org/10.1007/s10286-018-0522-2

Hoiland, R. L., Robba, C., Menon, D. K., Citerio, G., Sandroni, C., & Sekhon, M. S. (2023). Clinical targeting of the cerebral oxygen cascade to improve brain oxygenation in patients with hypoxic–ischaemic brain injury after cardiac arrest. Intensive Care Medicine, 49(9), 1062–1078. https://doi.org/10.1007/s00134-023-07165-x

Huang, S. Y., McCullough, R. E., McCullough, R. G., Micco, A. J., Manco-Johnson, M., Weil, J. V., & Reeves, J. T. (1988). Usual clinical dose of acetazolamide does not alter cerebral blood flow velocity. Respiration Physiology, 72(3), 315–326. https://doi.org/10.1016/0034-5687(88)90090-4

Huang, S. Y., Moore, L. G., McCullough, R. E., McCullough, R. G., Micco, A. J., Fulco, C., Cymerman, A., Manco-Johnson, M., Weil, J. v., & Reeves, J. T. (1987). Internal carotid and vertebral arterial flow velocity in men at high altitude. Journal of Applied Physiology, 63(1), 395–400. https://doi.org/10.1152/jappl.1987.63.1.395

Hultgren, H. N. (1997). High altitude medicine. Hultgren Publications.

Humphrey, J. D., & Tellides, G. (2019). Central artery stiffness and thoracic aortopathy. American Journal of Physiology-Heart and Circulatory Physiology, 316(1), H169–H182. https://doi.org/10.1152/ajpheart.00205.2018

Jensen, J. B., Wright, A. D., Lassen, N. A., Harvey, T. C., Winterborn, M. H., Raichle, M. E., & Bradwell, A. R. (1990). Cerebral blood flow in acute mountain sickness. Journal of Applied Physiology, 69(2), 430–433. https://doi.org/10.1152/jappl.1990.69.2.430

Jensen, K., J Ohrström, Cold, G. E., & Astrup, J. (1991). The effects of indomethacin on intracranial pressure, cerebral blood flow and cerebral metabolism in patients with severe head injury and intracranial hypertension. Acta Neurochirurgica, 108(3–4), 116–121. https://doi.org/10.1007/BF01418518

Johnston, A. J., Steiner, L. A., Gupta, A. K., & Menon, D. K. (2003). Cerebral oxygen vasoreactivity and cerebral tissue oxygen reactivity. British Journal of Anaesthesia, 90(6), 774–786. https://doi.org/10.1093/bja/aeg104

Jordan, J., Shannon, J. R., Diedrich, A., Black, B., Costa, F., Robertson, D., & Biaggioni, I. (2000). Interaction of Carbon Dioxide and Sympathetic Nervous System Activity in the Regulation of Cerebral Perfusion in Humans. Hypertension, 36(3), 383–388. https://doi.org/10.1161/01.HYP.36.3.383

Kabat, H., Anderson, J. P., & Rossen, R. (1943). Acute arrest of cerebral circulation in man. Archives of Neurology & Psychiatry, 50(5), 510. https://doi.org/10.1001/archneurpsyc.1943.02290230022002

Kallenberg, K., Bailey, D. M., Christ, S., Mohr, A., Roukens, R., Menold, E., Steiner, T., Bärtsch, P., & Knauth, M. (2007). Magnetic Resonance Imaging Evidence of Cytotoxic Cerebral Edema in Acute Mountain Sickness. Journal of Cerebral Blood Flow & Metabolism, 27(5), 1064–1071. https://doi.org/10.1038/sj.jcbfm.9600404

Kety, S. S., & Schmidt, C. F. (1948a). The effects of altered arterial tensions of carbon dioxide and oxygen on cerebral blood flow and cerebral oxygen consumption of normal young. Journal of Clinical Investigation, 27(4), 484–492. https://doi.org/10.1172/JCI101995

Kety, S. S., & Schmidt, C. F. (1948b). The nitrous oxide method for the quantitative determination of cerebral blood flow in man: theory, procedure and normal values. The Journal of Clinical Investigation, 27(4), 476–483. https://doi.org/10.1172/JCI101994

Koep, J. L., Taylor, C. E., Coombes, J. S., Bond, B., Ainslie, P. N., & Bailey, T. G. (2022). Autonomic control of cerebral blood flow: fundamental comparisons between peripheral and cerebrovascular circulations in humans. The Journal of Physiology, 600(1), 15–39. https://doi.org/10.1113/JP281058

Kohn, J. C., Lampi, M. C., & Reinhart-King, C. A. (2015). Age-related vascular stiffening: causes and consequences. Frontiers in Genetics, 06. https://doi.org/10.3389/fgene.2015.00112

Kohn, J. C., Zhou, D. W., Bordeleau, F., Zhou, A. L., Mason, B. N., Mitchell, M. J., King, M. R., & Reinhart-King, C. A. (2015). Cooperative Effects of Matrix Stiffness and Fluid Shear Stress on Endothelial Cell Behavior. Biophysical Journal, 108(3), 471–478. https://doi.org/10.1016/j.bpj.2014.12.023

Kontos, H. A., Wei, E. P., Navari, R. M., Levasseur, J. E., Rosenblum, W. I., & Patterson, J. L. (1978). Responses of cerebral arteries and arterioles to acute hypotension and hypertension. American Journal of Physiology-Heart and Circulatory Physiology, 234(4), H371–H383. https://doi.org/10.1152/ajpheart.1978.234.4.H371

Korte, N., Nortley, R., & Attwell, D. (2020). Cerebral blood flow decrease as an early pathological mechanism in Alzheimer's disease. Acta Neuropathologica, 140(6), 793–810. https://doi.org/10.1007/s00401-020-02215-w

Krishnaswamy, A., Klein, J. P., & Kapadia, S. R. (2010). Clinical cerebrovascular anatomy. Catheterization and Cardiovascular Interventions, 75(4), 530–539. https://doi.org/10.1002/ccd.22299

Lacolley, P., Regnault, V., & Laurent, S. (2020). Mechanisms of Arterial Stiffening. Arteriosclerosis, Thrombosis, and Vascular Biology, 40(5), 1055–1062. https://doi.org/10.1161/ATVBAHA.119.313129

Lafave, H. C., Zouboules, S. M., James, M. A., Purdy, G. M., Rees, J. L., Steinback, C. D., Ondrus, P., Brutsaert, T. D., Nysten, H. E., Nysten, C. E., Hoiland, R. L., Sherpa, M. T., & Day, T. A. (2019). Steady-state cerebral blood flow regulation at altitude: interaction between oxygen and carbon dioxide. European Journal of Applied Physiology, 119(11–12), 2529–2544. https://doi.org/10.1007/s00421-019-04206-6

Larsen, F. S., Olsen, K. S., Hansen, B. A., Paulson, O. B., & Knudsen, G. M. (1994). Transcranial Doppler is valid for determination of the lower limit of cerebral blood flow autoregulation. Stroke, 25(10), 1985–1988. https://doi.org/10.1161/01.STR.25.10.1985

Lassen, N. A. (1959). Cerebral Blood Flow and Oxygen Consumption in Man. Physiological Reviews, 39(2), 183–238. https://doi.org/10.1152/physrev.1959.39.2.183

Lassen, N. A. (1985). Normal Average Value of Cerebral Blood Flow in Younger Adults is 50 ml/100 g/min. Journal of Cerebral Blood Flow & Metabolism, 5(3), 347–349. https://doi.org/10.1038/jcbfm.1985.48

Lassen, N. A., Ingvar, D. H., & Skinhøj, E. (1978). Brain Function and Blood Flow. Scientific American, 239(4), 62–71. https://doi.org/10.1038/scientificamerican1078-62

Lawley, J. S., Levine, B. D., Williams, M. A., Malm, J., Eklund, A., Polaner, D. M., Subudhi, A. W., Hackett, P. H., & Roach, R. C. (2016). Cerebral spinal fluid dynamics: effect of hypoxia and implications for high-altitude illness. Journal of Applied Physiology, 120(2), 251–262. https://doi.org/10.1152/japplphysiol.00370.2015

Leaf, D. E., & Goldfarb, D. S. (2007). Mechanisms of action of acetazolamide in the prophylaxis and treatment of acute mountain sickness. Journal of Applied Physiology, 102(4), 1313–1322. https://doi.org/10.1152/japplphysiol.01572.2005

Lefferts, W. K., DeBlois, J. P., Augustine, J. A., Keller, A. P., & Heffernan, K. S. (2020). Age, sex, and the vascular contributors to cerebral pulsatility and pulsatile damping. Journal of Applied Physiology, 129(5), 1092–1101. https://doi.org/10.1152/japplphysiol.00500.2020

Lefferts, W. K., & Smith, K. J. (2021). Let's talk about sex, let's talk about pulsatility, let's talk about all the good things and the bad things of MCAv. Journal of Applied Physiology (Bethesda, Md. : 1985), 130(6), 1672–1674. https://doi.org/10.1152/japplphysiol.00215.2021

Leier, C. v. (1983). Drugs Five Years Later. Annals of Internal Medicine, 99(4), 490. https://doi.org/10.7326/0003-4819-99-4-490

Lenfant, C., Torrance, J. D., & Reynafarje, C. (1971). Shift of the O2-Hb dissociation curve at altitude: mechanism and effect. Journal of Applied Physiology, 30(5), 625–631. https://doi.org/10.1152/jappl.1971.30.5.625

Lenfant, C., Torrance, J., English, E., Finch, C. A., Reynafarje, C., Ramos, J., & Faura, J. (1968). Effect of altitude on oxygen binding by hemoglobin and on organic phosphate levels. The Journal of Clinical Investigation, 47(12), 2652–2656. https://doi.org/10.1172/JCI105948

Levine, B. D., & Zhang, R. (2008). Comments on Point:Counterpoint: Sympathetic activity does/does not influence cerebral blood flow. Journal of Applied Physiology, 105(4), 1369–1373. https://doi.org/10.1152/japplphysiol.zdg-8199.pcpcomm.2008

Lucas, S. (2016). The Pharmacology of Indomethacin. Headache: The Journal of Head and Face Pain, 56(2), 436–446. https://doi.org/10.1111/head.12769

Lucas, S. J. E., Burgess, K. R., Thomas, K. N., Donnelly, J., Peebles, K. C., Lucas, R. A. I., Fan, J., Cotter, J. D., Basnyat, R., & Ainslie, P. N. (2011). Alterations in cerebral blood flow and cerebrovascular reactivity during 14 days at 5050 m. The Journal of Physiology, 589(3), 741–753. https://doi.org/10.1113/jphysiol.2010.192534

Lucas, S. J. E., Tzeng, Y. C., Galvin, S. D., Thomas, K. N., Ogoh, S., & Ainslie, P. N. (2010). Influence of Changes in Blood Pressure on Cerebral Perfusion and Oxygenation. Hypertension, 55(3), 698–705. https://doi.org/10.1161/HYPERTENSIONAHA.109.146290

Luks, A. M., Swenson, E. R., & Bärtsch, P. (2017). Acute high-altitude sickness. European Respiratory Review, 26(143), 160096. https://doi.org/10.1183/16000617.0096-2016

Mackenzie, I. S. (2002). Assessment of arterial stiffness in clinical practice. QJM, 95(2), 67–74. https://doi.org/10.1093/qjmed/95.2.67

Maier, L. (2023). Communities and Collections Graduate Studies and Research, Faculty of / Theses and Dissertations Usage 12 views 30 downloads Vascular Reactivity to Rhythmic Handgrip at Altitude.

Majerus, T. C., Dasta, J. F., Bauman, J. L., Danziger, L. H., & Ruffolo, R. R. (1989). Dobutamine: Ten Years Later. Pharmacotherapy: The Journal of Human Pharmacology and Drug Therapy, 9(4), 245–259. https://doi.org/10.1002/j.1875-9114.1989.tb04133.x

Marini, S., Georgakis, M. K., & Anderson, C. D. (2021). Interactions Between Kidney Function and Cerebrovascular Disease: Vessel Pathology That Fires Together Wires Together. Frontiers in Neurology, 12, 785273. https://doi.org/10.3389/fneur.2021.785273

Mattos, J. D., Campos, M. O., Rocha, M. P., Mansur, D. E., Rocha, H. N. M., Garcia, V. P., Batista, G., Alvares, T. S., Oliveira, G. v., Souza, M. v., Videira, R. L. R., Rocha, N. G., Secher, N. H., Nóbrega, A. C. L., & Fernandes, I. A. (2019). Human brain blood flow and metabolism during isocapnic hyperoxia: the role of reactive oxygen species. The Journal of Physiology, 597(3), 741–755. https://doi.org/10.1113/JP277122

Matz, R. L., Schott, C., Stoclet, J. C., & Andriantsitohaina, R. (2000). Age-related endothelial dysfunction with respect to nitric oxide, endothelium-derived hyperpolarizing factor and cyclooxygenase products. Physiological Research, 49(1), 11–18.

Mayo Clinic. (2023, December 1). Indomethacin (Oral Route).

Mazzeo, R. S., Child, A., Butterfield, G. E., Mawson, J. T., Zamudio, S., & Moore, L. G. (1998). Catecholamine response during 12 days of high-altitude exposure (4,300 m) in women. Journal of Applied Physiology, 84(4), 1151–1157. https://doi.org/10.1152/jappl.1998.84.4.1151

Mercadante, A., & Raja, A. (2023). Anatomy, Arteries. StatPearls Publishing.

Mertes, H., Sawada, S. G., Ryan, T., Segar, D. S., Kovacs, R., Foltz, J., & Feigenbaum, H. (1993). Symptoms, adverse effects, and complications associated with dobutamine stress echocardiography. Experience in 1118 patients. Circulation, 88(1), 15–19. https://doi.org/10.1161/01.CIR.88.1.15

Millasseau, S. C., Stewart, A. D., Patel, S. J., Redwood, S. R., & Chowienczyk, P. J. (2005). Evaluation of Carotid-Femoral Pulse Wave Velocity. Hypertension, 45(2), 222–226. https://doi.org/10.1161/01.HYP.0000154229.97341.d2

Mitchell, G. F., van Buchem, M. A., Sigurdsson, S., Gotal, J. D., Jonsdottir, M. K., Kjartansson, Ó., Garcia, M., Aspelund, T., Harris, T. B., Gudnason, V., & Launer, L. J. (2011). Arterial stiffness, pressure and flow pulsatility and brain structure and function: the Age, Gene/Environment Susceptibility – Reykjavik Study. Brain, 134(11), 3398–3407. https://doi.org/10.1093/brain/awr253

Miyazaki, M., & Kato, K. (1965). Measurement of Cerebral Blood Flow by Ultrasonic Doppler Technique : THEORY. Japanese Circulation Journal, 29(4), 375–382. https://doi.org/10.1253/jcj.29.375

Møller, K., Paulson, O. B., Hornbein, T. F., Colier, W. N. J. M., Paulson, A. S., Roach, R. C., Holm, S., & Knudsen, G. M. (2002). Unchanged Cerebral Blood Flow and Oxidative Metabolism after Acclimatization to High Altitude. Journal of Cerebral Blood Flow & Metabolism, 22(1), 118–126. https://doi.org/10.1097/00004647-200201000-00014

Moore, L. G. (2000). Comparative human ventilatory adaptation to high altitude. Respiration Physiology, 121(2–3), 257–276. https://doi.org/10.1016/S0034-5687(00)00133-X

Moppett, I. K., & Mahajan, R. P. (2004). Transcranial Doppler ultrasonography in anaesthesia and intensive care. British Journal of Anaesthesia, 93(5), 710–724. https://doi.org/10.1093/bja/aeh205

Morioka, T., Mori, K., & Emoto, M. (2021). Is Stiffness Parameter β Useful for the Evaluation of Atherosclerosis?~ Its Clinical Implications, Limitations, and Future Perspectives ~. Journal of Atherosclerosis and Thrombosis, 28(5), 435–453. https://doi.org/10.5551/jat.RV17047

Mosso, A. (1880). Sulla circolazione del sangue nel cervello dell'uomo. Ricerche Sfigmografia.

Munjal, A., & Allam, AE. (2023, January). Indomethacin. StatPearls Publishing.

Muskat, J. C., Rayz, V. L., Goergen, C. J., & Babbs, C. F. (2021). Hemodynamic modeling of the circle of Willis reveals unanticipated functions during cardiovascular stress. Journal of Applied Physiology, 131(3), 1020–1034. https://doi.org/10.1152/japplphysiol.00198.2021

Naeije, R. (2010). Physiological Adaptation of the Cardiovascular System to High Altitude. Progress in Cardiovascular Diseases, 52(6), 456–466. https://doi.org/10.1016/j.pcad.2010.03.004

Nagai, Y., Helwegen, J., Fleg, J. L., Kemper, M. K., Earley, C. J., Rywik, T. M., Wijn, P., & Metter, E. J. (1999). Decay index: a new carotid Doppler waveform measure associated with the Windkessel function of elastic arteries. Ultrasound in Medicine & Biology, 25(9), 1371–1376. https://doi.org/10.1016/S0301-5629(99)00100-3

Naqvi, J., Yap, K. H., Ahmad, G., & Ghosh, J. (2013). Transcranial Doppler Ultrasound: A Review of the Physical Principles and Major Applications in Critical Care. International Journal of Vascular Medicine, 2013, 1–13. https://doi.org/10.1155/2013/629378

Nijboer, J. A., Dorlas, J. C., & Mahieu, H. F. (1981). Photoelectric plethysmography-some fundamental aspects of the reflection and transmission methods. Clinical Physics and Physiological Measurement, 2(3), 205–215. https://doi.org/10.1088/0143-0815/2/3/004

Numan, T., Bain, A. R., Hoiland, R. L., Smirl, J. D., Lewis, N. C., & Ainslie, P. N. (2014). Static autoregulation in humans: a review and reanalysis. Medical Engineering & Physics, 36(11), 1487–1495. https://doi.org/10.1016/j.medengphy.2014.08.001

Ogoh, S., Moralez, G., Washio, T., Sarma, S., Hieda, M., Romero, S. A., Cramer, M. N., Shibasaki, M., & Crandall, C. G. (2017). Effect of increases in cardiac contractility on cerebral blood flow in humans. American Journal of Physiology-Heart and Circulatory Physiology, 313(6), H1155–H1161. https://doi.org/10.1152/ajpheart.00287.2017

Okazawa, H., Yamauchi, H., Sugimoto, K., Toyoda, H., Kishibe, Y., & Takahashi, M. (2001). Effects of Acetazolamide on Cerebral Blood Flow, Blood Volume, and Oxygen Metabolism: A Positron Emission Tomography Study with Healthy Volunteers. Journal of Cerebral Blood Flow & Metabolism, 21(12), 1472–1479. https://doi.org/10.1097/00004647-200112000-00012

Olusanya, O. (2023). General Principles of Ultrasound (pp. 5–18). https://doi.org/10.1007/978-3-031-32462-8_2

Overgaard, C. B., & Džavík, V. (2008). Inotropes and Vasopressors. Circulation, 118(10), 1047–1056. https://doi.org/10.1161/CIRCULATIONAHA.107.728840

Panerai, R. B. (1998). Assessment of cerebral pressure autoregulation in humans - a review of measurement methods. Physiological Measurement, 19(3), 305–338. https://doi.org/10.1088/0967-3334/19/3/001

Paralikar, S. (2012). High altitude pulmonary edema-clinical features, pathophysiology,

prevention and treatment. Indian Journal of Occupational and Environmental Medicine, 16(2), 59. https://doi.org/10.4103/0019-5278.107066

Paralikar, S., & Paralikar, J. (2010). High-altitude medicine. Indian Journal of Occupational and Environmental Medicine, 14(1), 6. https://doi.org/10.4103/0019-5278.64608

Peacock, A. J. (1998). ABC of oxygen: Oxygen at high altitude. BMJ, 317(7165), 1063–1066. https://doi.org/10.1136/bmj.317.7165.1063

Powers, W. J. (2003). Cerebral Blood Flow Measurement with Positron Emission Tomography. In Cerebral Blood Flow (pp. 217–225). Springer Berlin Heidelberg. https://doi.org/10.1007/978-3-642-56036-1_16

Purkayastha, S., & Sorond, F. (2012). Transcranial Doppler ultrasound: technique and application. Seminars in Neurology, 32(4), 411–420. https://doi.org/10.1055/s-0032-1331812

Rasmussen, J. K., & Boedtkjer, E. (2018). Carbonic anhydrase inhibitors modify intracellular pH transients and contractions of rat middle cerebral arteries during CO 2 /HCO 3 – fluctuations. Journal of Cerebral Blood Flow & Metabolism, 38(3), 492–505. https://doi.org/10.1177/0271678X17699224

Rasmussen, M. (2005). Treatment of elevated intracranial pressure with indomethacin: Friend or foe? Acta Anaesthesiologica Scandinavica, 49(3), 341–350. https://doi.org/10.1111/j.1399-6576.2005.00647.x

Reeder, G. S., Currie, P. J., Hagler, D. J., Tajik, A. J., & Seward, J. B. (1986). Use of Doppler Techniques (Continuous-Wave, Pulsed-Wave, and Color Flow Imaging) in the Noninvasive Hemodynamic Assessment of Congenital Heart Disease. Mayo Clinic Proceedings, 61(9), 725–744. https://doi.org/10.1016/S0025-6196(12)62774-8

Rivera-Rivera, L. A., Cody, K. A., Eisenmenger, L., Cary, P., Rowley, H. A., Carlsson, C. M., Johnson, S. C., & Johnson, K. M. (2021). Assessment of vascular stiffness in the internal carotid artery proximal to the carotid canal in Alzheimer's disease using pulse wave velocity from low rank reconstructed 4D flow MRI. Journal of Cerebral Blood Flow and Metabolism : Official Journal of the International Society of Cerebral Blood Flow and Metabolism, 41(2), 298–311. https://doi.org/10.1177/0271678X20910302

Rosehart, A. C., Longden, T. A., Weir, N., Fontaine, J. T., Joutel, A., & Dabertrand, F. (2021). Prostaglandin E2 Dilates Intracerebral Arterioles When Applied to Capillaries: Implications for Small Vessel Diseases. Frontiers in Aging Neuroscience, 13. https://doi.org/10.3389/fnagi.2021.695965\

Ross, R. T. (1985). The random nature of cerebral mountain sickness. The Lancet, 325(8435), 990–991. https://doi.org/10.1016/S0140-6736(85)91771-4

Roy, C. S., & Sherrington, C. S. (1890). On the Regulation of the Blood-supply of the Brain. The Journal of Physiology, 11(1–2), 85-158.17. https://doi.org/10.1113/jphysiol.1890.sp000321

Ruan, Y. C., Zhou, W., & Chan, H. C. (2011). Regulation of Smooth Muscle Contraction by the Epithelium: Role of Prostaglandins. Physiology, 26(3), 156–170. https://doi.org/10.1152/physiol.00036.2010

Ruffolo, R. R. (1987). Review: The Pharmacology of Dobutamine. The American Journal of the Medical Sciences, 294(4), 244–248. https://doi.org/10.1097/00000441-198710000-00005

Sandoo, A., van Zanten, J. J. C. S. V., Metsios, G. S., Carroll, D., & Kitas, G. D. (2010). The endothelium and its role in regulating vascular tone. The Open Cardiovascular Medicine Journal, 4, 302–312. https://doi.org/10.2174/1874192401004010302

Schöning, M., & Hartig, B. (1996). Age Dependence of Total Cerebral Blood Flow Volume from Childhood to Adulthood. Journal of Cerebral Blood Flow & Metabolism, 16(5), 827–833. https://doi.org/10.1097/00004647-199609000-00007

Schubert, T., Santini, F., Stalder, A. F., Bock, J., Meckel, S., Bonati, L., Markl, M., & Wetzel, S. (2011). Dampening of blood-flow pulsatility along the carotid siphon: does form follow function? AJNR. American Journal of Neuroradiology, 32(6), 1107–1112. https://doi.org/10.3174/ajnr.A2426

Secknus, M.-A., & Marwick, T. H. (1997). Evolution of Dobutamine Echocardiography Protocols and Indications: Safety and Side Effects in 3,011 Studies Over 5 Years. Journal of the American College of Cardiology, 29(6), 1234–1240. https://doi.org/10.1016/S0735-1097(97)00039-9

Serrador, J. M., Picot, P. A., Rutt, B. K., Shoemaker, J. K., & Bondar, R. L. (2000). MRI Measures of Middle Cerebral Artery Diameter in Conscious Humans During Simulated Orthostasis. Stroke, 31(7), 1672–1678. https://doi.org/10.1161/01.STR.31.7.1672

Severinghaus, J. W., Chiodi, H., Eger I, E. I., Brandstater, B., & Hornbein, T. F. (1966). Cerebral Blood Flow In Man at High Altitude. Circulation Research, 19(2), 274–282. https://doi.org/10.1161/01.RES.19.2.274

Shirwany, N. A., & Zou, M. (2010). Arterial stiffness: a brief review. Acta Pharmacologica Sinica, 31(10), 1267–1276. https://doi.org/10.1038/aps.2010.123

Shoemaker, L. N., Wilson, L. C., Lucas, S. J. E., Machado, L., Walker, R. J., & Cotter, J. D. (2021). Indomethacin markedly blunts cerebral perfusion and reactivity, with little cognitive consequence in healthy young and older adults. The Journal of Physiology, 599(4), 1097–1113. https://doi.org/10.1113/JP280118

Smirl, J. D., Lucas, S. J. E., Lewis, N. C. S., duManior, G. R., Smith, K. J., Bakker, A., Basnyat, A. S., & Ainslie, P. N. (2014). Cerebral Pressure–Flow Relationship in Lowlanders and Natives at High Altitude. Journal of Cerebral Blood Flow & Metabolism, 34(2), 248–257. https://doi.org/10.1038/jcbfm.2013.178

Smirl, JD. (2015). The relationship between arterial blood pressure and cerebral blood flow : insights into aging, altitude and exercise.

Smith, K. J., & Ainslie, P. N. (2017). Regulation of cerebral blood flow and metabolism during exercise. Experimental Physiology, 102(11), 1356–1371. https://doi.org/10.1113/EP086249

Smith, K. J., MacLeod, D., Willie, C. K., Lewis, N. C. S., Hoiland, R. L., Ikeda, K., Tymko, M. M., Donnelly, J., Day, T. A., MacLeod, N., Lucas, S. J. E., & Ainslie, P. N. (2014). Influence of high altitude on cerebral blood flow and fuel utilization during exercise and recovery. The Journal of Physiology, 592(24), 5507–5527. https://doi.org/10.1113/jphysiol.2014.281212

Steinback, C. D., & Poulin, M. J. (2016). Influence of Hypoxia on Cerebral Blood Flow Regulation in Humans (pp. 131–144). https://doi.org/10.1007/978-1-4899-7678-9_9

Strandgaard, S., & Paulson, O. B. (1984). Cerebral autoregulation. Stroke, 15(3), 413–416. https://doi.org/10.1161/01.STR.15.3.413

Subasi, A. (2019). Biomedical Signals. In Practical Guide for Biomedical Signals Analysis Using Machine Learning Techniques (pp. 27–87). Elsevier. https://doi.org/10.1016/B978-0-12-817444-9.00002-7

Subudhi, A. W., Fan, J., Evero, O., Bourdillon, N., Kayser, B., Julian, C. G., Lovering, A. T., & Roach, R. C. (2014). AltitudeOmics: effect of ascent and acclimatization to 5260 m on regional cerebral oxygen delivery. Experimental Physiology, 99(5), 772–781. https://doi.org/10.1113/expphysiol.2013.075184

Sugawara, M., Niki, K., Ohte, N., Okada, T., & Harada, A. (2009). Clinical usefulness of wave intensity analysis. Medical & Biological Engineering & Computing, 47(2), 197–206. https://doi.org/10.1007/s11517-008-0388-x

Suleyman, H., Albayrak, A., Bilici, M., Cadirci, E., & Halici, Z. (2010). Different Mechanisms in Formation and Prevention of Indomethacin-induced Gastric Ulcers. Inflammation, 33(4), 224–234. https://doi.org/10.1007/s10753-009-9176-5

Summ, O., & Evers, S. (2013). Mechanism of Action of Indomethacin in Indomethacin-Responsive Headaches. Current Pain and Headache Reports, 17(4), 327. https://doi.org/10.1007/s11916-013-0327-x

Tacon, C. L., McCaffrey, J., & Delaney, A. (2012). Dobutamine for patients with severe heart failure: a systematic review and meta-analysis of randomised controlled trials. Intensive Care Medicine, 38(3), 359–367. https://doi.org/10.1007/s00134-011-2435-6

Tarumi, T., Khan, M. A., Liu, J., Tseng, B. M., Parker, R., Riley, J., Tinajero, C., & Zhang, R. (2014). Cerebral Hemodynamics in Normal Aging: Central Artery Stiffness, Wave Reflection, and Pressure Pulsatility. Journal of Cerebral Blood Flow & Metabolism, 34(6), 971–978. https://doi.org/10.1038/jcbfm.2014.44

Teppema, L. J., Balanos, G. M., Steinback, C. D., Brown, A. D., Foster, G. E., Duff, H. J., Leigh, R., & Poulin, M. J. (2007). Effects of Acetazolamide on Ventilatory, Cerebrovascular, and Pulmonary Vascular Responses to Hypoxia. American Journal of Respiratory and Critical Care Medicine, 175(3), 277–281. https://doi.org/10.1164/rccm.200608-1199OC

Thomas, K. N., Lewis, N. C. S., Hill, B. G., & Ainslie, P. N. (2015). Technical recommendations for the use of carotid duplex ultrasound for the assessment of extracranial blood flow. American Journal of Physiology-Regulatory, Integrative and Comparative Physiology, 309(7), R707–R720. https://doi.org/10.1152/ajpregu.00211.2015

Townsend, R. R., Wilkinson, I. B., Schiffrin, E. L., Avolio, A. P., Chirinos, J. A., Cockcroft, J. R., Heffernan, K. S., Lakatta, E. G., McEniery, C. M., Mitchell, G. F., Najjar, S. S., Nichols, W. W., Urbina, E. M., Weber, T., & American Heart Association Council on Hypertension. (2015). Recommendations for Improving and Standardizing Vascular Research on Arterial Stiffness: A Scientific Statement From the American Heart Association. Hypertension (Dallas, Tex. : 1979), 66(3), 698–722. https://doi.org/10.1161/HYP.0000000000000033

Tremblay, J. C., & Ainslie, P. N. (2021). Global and country-level estimates of human population at high altitude. Proceedings of the National Academy of Sciences, 118(18). https://doi.org/10.1073/pnas.2102463118

Tuttle, R. R., & Mills, J. (1975). Dobutamine: development of a new catecholamine to selectively increase cardiac contractility. Circulation Research, 36(1), 185–196. https://doi.org/10.1161/01.RES.36.1.18

Tymko, M. M., Ainslie, P. N., & Smith, K. J. (2018). Evaluating the methods used for measuring cerebral blood flow at rest and during exercise in humans. European Journal of Applied Physiology, 118(8), 1527–1538. https://doi.org/10.1007/s00421-018-3887-y

Tymko, M. M., Willie, C. K., Howe, C. A., Hoiland, R. L., Stone, R. M., Tymko, K., Tymko, C., MacLeod, D., Anholm, J. D., Gasho, C., Villafuerte, F., Vizcardo-Galindo, G., Figueroa-Mujica, R., Day, T. A., Bird, J. D., Foster, G. E., Steinback, C. D., Brugniaux, J. v., Champigneulle, B., … Ainslie, P. N. (2022). Acid-base balance at high altitude in lowlanders and indigenous highlanders. Journal of Applied Physiology, 132(2), 575–580. https://doi.org/10.1152/japplphysiol.00757.2021

Tzeng, Y. C., MacRae, B. A., Ainslie, P. N., & Chan, G. S. H. (2014). Fundamental relationships between blood pressure and cerebral blood flow in humans. Journal of Applied Physiology, 117(9), 1037–1048. https://doi.org/10.1152/japplphysiol.00366.2014

Tzeng, Y.-C., & Ainslie, P. N. (2014). Blood pressure regulation IX: cerebral autoregulation under blood pressure challenges. European Journal of Applied Physiology, 114(3), 545–559. https://doi.org/10.1007/s00421-013-2667-y

Uppal, T., & Mogra, R. (2010). RBC motion and the basis of ultrasound Doppler instrumentation. Australasian Journal of Ultrasound in Medicine, 13(1), 32–34. https://doi.org/10.1002/j.2205-0140.2010.tb00216.x

Valdueza, J. M., Balzer, J. O., Villringer, A., Vogl, T. J., Kutter, R., & Einhäupl, K. M. (1997). Changes in blood flow velocity and diameter of the middle cerebral artery during hyperventilation: assessment with MR and transcranial Doppler sonography. AJNR. American Journal of Neuroradiology, 18(10), 1929–1934.

van Bortel, L. M., de Backer, T., & Segers, P. (2016). Standardization of Arterial Stiffness Measurements Make Them Ready for Use in Clinical Practice: Table 1. American Journal of Hypertension, 29(11), 1234–1236. https://doi.org/10.1093/ajh/hpw084

van Bussel, B. C., Schouten, F., Henry, R. M., Schalkwijk, C. G., de Boer, M. R., Ferreira, I., Smulders, Y. M., Twisk, J. W., & Stehouwer, C. D. (2011). Endothelial Dysfunction and Low-Grade Inflammation Are Associated With Greater Arterial Stiffness Over a 6-Year Period. Hypertension, 58(4), 588–595. https://doi.org/10.1161/HYPERTENSIONAHA.111.174557

Verbree, J., Bronzwaer, A.-S. G. T., Ghariq, E., Versluis, M. J., Daemen, M. J. A. P., van Buchem, M. A., Dahan, A., van Lieshout, J. J., & van Osch, M. J. P. (2014). Assessment of middle cerebral artery diameter during hypocapnia and hypercapnia in humans using ultra-high-field MRI. Journal of Applied Physiology, 117(10), 1084–1089. https://doi.org/10.1152/japplphysiol.00651.2014

Vrselja, Z., Brkic, H., & Curic, G. (2015). Arterial tree asymmetry reduces cerebral pulsatility. Medical Hypotheses, 85(5), 622–627. https://doi.org/10.1016/j.mehy.2015.07.030

Vrselja, Z., Brkic, H., Mrdenovic, S., Radic, R., & Curic, G. (2014). Function of Circle of Willis. Journal of Cerebral Blood Flow & Metabolism, 34(4), 578–584. https://doi.org/10.1038/jcbfm.2014.7

Wagenseil, J. E., & Mecham, R. P. (2012). Elastin in Large Artery Stiffness and Hypertension. Journal of Cardiovascular Translational Research, 5(3), 264–273. https://doi.org/10.1007/s12265-012-9349-8

Wang, Y.-X., & Fitch, R. (2004). Vascular Stiffness: Measurements, Mechanisms and Implications. Current Vascular Pharmacology, 2(4), 379–384. https://doi.org/10.2174/1570161043385448

Watson, N. A., Beards, S. C., Altaf, N., Kassner, A., & Jackson, A. (2000). The effect of hyperoxia on cerebral blood flow: a study in healthy volunteers using magnetic resonance phase-contrast angiography. European Journal of Anaesthesiology, 17(3), 152–159. https://doi.org/10.1046/j.1365-2346.2000.00640.x

Webb, K. L., Dominelli, P. B., Baker, S. E., Klassen, S. A., Joyner, M. J., Senefeld, J. W., & Wiggins, C. C. (2022). Influence of High Hemoglobin-Oxygen Affinity on Humans During Hypoxia. Frontiers in Physiology, 12. https://doi.org/10.3389/fphys.2021.763933

Westerhof, N., Lankhaar, J.-W., & Westerhof, B. E. (2009). The arterial Windkessel. Medical & Biological Engineering & Computing, 47(2), 131–141. https://doi.org/10.1007/s11517-008-0359-2

Wielicka, M., Neubauer-Geryk, J., Kozera, G., & Bieniaszewski, L. (2020). Clinical application of pulsatility index. Medical Research Journal, 5(3), 201–210. https://doi.org/10.5603/MRJ.a2020.0016

Williams, L. R., & Leggett, R. W. (1989). Reference values for resting blood flow to organs of man. Clinical Physics and Physiological Measurement, 10(3), 187–217. https://doi.org/10.1088/0143-0815/10/3/001

Willie, C. K., Colino, F. L., Bailey, D. M., Tzeng, Y. C., Binsted, G., Jones, L. W., Haykowsky, M. J., Bellapart, J., Ogoh, S., Smith, K. J., Smirl, J. D., Day, T. A., Lucas, S. J., Eller, L. K., & Ainslie, P. N. (2011). Utility of transcranial Doppler ultrasound for the integrative assessment of cerebrovascular function. Journal of Neuroscience Methods, 196(2), 221–237. https://doi.org/10.1016/j.jneumeth.2011.01.011

Willie, C. K., Eller, L. K., & Ainslie, P. N. (2012). New Directions in the Dynamic Assessment of Brain Blood Flow Regulation. In Applied Aspects of Ultrasonography in Humans. InTech. https://doi.org/10.5772/31483

Willie, C. K., MacLeod, D. B., Smith, K. J., Lewis, N. C., Foster, G. E., Ikeda, K., Hoiland, R. L., & Ainslie, P. N. (2015). The Contribution of Arterial Blood Gases in Cerebral Blood Flow Regulation and Fuel Utilization in Man at High Altitude. Journal of Cerebral Blood Flow & Metabolism, 35(5), 873–881. https://doi.org/10.1038/jcbfm.2015.4

Willie, C. K., Smith, K. J., Day, T. A., Ray, L. A., Lewis, N. C. S., Bakker, A., Macleod, D. B., & Ainslie, P. N. (2014). Regional cerebral blood flow in humans at high altitude: gradual ascent and 2 wk at 5,050 m. Journal of Applied Physiology, 116(7), 905–910. https://doi.org/10.1152/japplphysiol.00594.2013

Willie, C. K., Stembridge, M., Hoiland, R. L., Tymko, M. M., Tremblay, J. C., Patrician, A., Steinback, C., Moore, J., Anholm, J., Subedi, P., Niroula, S., McNeil, C. J., McManus, A., MacLeod, D. B., & Ainslie, P. N. (2018). UBC-Nepal Expedition: An experimental overview of the 2016 University of British Columbia Scientific Expedition to Nepal Himalaya. PLOS ONE, 13(10), e0204660. https://doi.org/10.1371/journal.pone.0204660

Willie, C. K., Tzeng, Y., Fisher, J. A., & Ainslie, P. N. (2014). Integrative regulation of human brain blood flow. The Journal of Physiology, 592(5), 841–859. https://doi.org/10.1113/jphysiol.2013.268953

Wilson, M. H., Edsell, M. E., Davagnanam, I., Hirani, S. P., Martin, D. S., Levett, D. Z., Thornton, J. S., Golay, X., Strycharczuk, L., Newman, S. P., Montgomery, H. E., Grocott, M. P., & Imray, C. H. (2011). Cerebral Artery Dilatation Maintains Cerebral Oxygenation at Extreme Altitude and in Acute Hypoxia—An Ultrasound and MRI Study. Journal of Cerebral Blood Flow & Metabolism, 31(10), 2019–2029. https://doi.org/10.1038/jcbfm.2011.81

Wohlfahrt, P., Krajčoviechová, A., Seidlerová, J., Mayer, O., Bruthans, J., Filipovský, J., Laurent, S., & Cífková, R. (2013). Arterial stiffness parameters: How do they differ? Atherosclerosis, 231(2), 359–364. https://doi.org/10.1016/j.atherosclerosis.2013.10.006

Wolff, H. G. (1936). The cerebral circulation . Physiological Reviews, 16(4), 545–596.

Woodman, R. J., Playford, D. A., Watts, G. F., Cheetham, C., Reed, C., Taylor, R. R., Puddey, I. B., Beilin, L. J., Burke, V., Mori, T. A., & Green, D. (2001). Improved analysis of brachial artery ultrasound using a novel edge-detection software system. Journal of Applied Physiology, 91(2), 929–937. https://doi.org/10.1152/jappl.2001.91.2.929

World Health Organization (WHO). (2023, March 15). Dementia.

Xing, C.-Y., Tarumi, T., Liu, J., Zhang, Y., Turner, M., Riley, J., Tinajero, C. D., Yuan, L.-J., & Zhang, R. (2017). Distribution of cardiac output to the brain across the adult lifespan. Journal of Cerebral Blood Flow & Metabolism, 37(8), 2848–2856. https://doi.org/10.1177/0271678X16676826

Xu, F., Liu, P., Pascual, J. M., Xiao, G., & Lu, H. (2012). Effect of hypoxia and hyperoxia on cerebral blood flow, blood oxygenation, and oxidative metabolism. Journal of Cerebral Blood Flow and Metabolism : Official Journal of the International Society of Cerebral Blood Flow and Metabolism, 32(10), 1909–1918. https://doi.org/10.1038/jcbfm.2012.93

Xu, F., Uh, J., Brier, M. R., Hart, J., Yezhuvath, U. S., Gu, H., Yang, Y., & Lu, H. (2011). The Influence of Carbon Dioxide on Brain Activity and Metabolism in Conscious Humans. Journal of Cerebral Blood Flow & Metabolism, 31(1), 58–67. https://doi.org/10.1038/jcbfm.2010.153

Xu, X., Wang, B., Ren, C., Hu, J., Greenberg, D. A., Chen, T., Xie, L., & Jin, K. (2017). Age-related Impairment of Vascular Structure and Functions. Aging and Disease, 8(5), 590–610. https://doi.org/10.14336/AD.2017.0430

Zarrinkoob, L., Ambarki, K., Wåhlin, A., Birgander, R., Carlberg, B., Eklund, A., & Malm, J. (2016). Aging alters the dampening of pulsatile blood flow in cerebral arteries. Journal of Cerebral Blood Flow & Metabolism, 36(9), 1519–1527. https://doi.org/10.1177/0271678X16629486

Zarrinkoob, L., Ambarki, K., Wåhlin, A., Birgander, R., Eklund, A., & Malm, J. (2015). Blood Flow Distribution in Cerebral Arteries. Journal of Cerebral Blood Flow & Metabolism, 35(4), 648–654. https://doi.org/10.1038/jcbfm.2014.241

Zhang, R., Behbehani, K., & Levine, B. D. (2009). Dynamic pressure–flow relationship of the cerebral circulation during acute increase in arterial pressure. The Journal of Physiology, 587(11), 2567–2577. https://doi.org/10.1113/jphysiol.2008.168302

Zhang, T., Niu, H., Liu, Y., Cai, L., Liu, D., Zhao, E., Li, M., Liu, W., Li, J., Qiao, P., Zheng, W., Ren, P., & Wang, Z. (2023). Dobutamine-induced alternations in cerebral blood flow of healthy adults: a 3D pseudocontinuous arterial spin labeling study. BMC Medicine, 21(1), 238. https://doi.org/10.1186/s12916-023-02928-1

Zieman, S. J., Melenovsky, V., & Kass, D. A. (2005). Mechanisms, Pathophysiology, and Therapy of Arterial Stiffness. Arteriosclerosis, Thrombosis, and Vascular Biology, 25(5), 932–943. https://doi.org/10.1161/01.ATV.0000160548.78317.29g/10.1161/01.ATV.0000160548.78317.29

Appendix

Appendix A

```
data=INDOSL

mean(data$MAP[data$Time==4])-mean(data$MAP[data$Time==2])

mean(data$MCAv[data$Time==4])-mean(data$MCAv[data$Time==2])

mean(data$`MCA PI`[data$Time==4])-mean(data$`MCA PI`[data$Time==2])

mean(data$SaO2[data$Time==4])-mean(data$SaO2[data$Time==2])

mean(data$PetO2[data$Time==4])-mean(data$PetO2[data$Time==2])

mean(data$PETCO2[data$Time==4])-mean(data$PETCO2[data$Time==2])

mean(data$Diameter[data$Time==4])-mean(data$Diameter[data$Time==2])

mean(data$`ICA V`[data$Time==4])-mean(data$`ICA V`[data$Time==2])

mean(data$`ICA Q`[data$Time==4])-mean(data$`ICA Q`[data$Time==2])

mean(data$`ICA PI`[data$Time==4])-mean(data$`ICA PI`[data$Time==2])

mean(data$DF[data$Time==4])-mean(data$DF[data$Time==2])

data=Dobutamine_SL_and_HA

Post=mean(data$MAP[data$Time==4])/mean(data$MCAv[data$Time==4])
Pre= mean(data$MAP[data$Time==2])/mean(data$MCAv[data$Time==2])

Post-Pre

Post=mean(data$MAP[data$Time==4])/mean(data$`ICA Q`[data$Time==4])
Pre= mean(data$MAP[data$Time==2])/mean(data$`ICA Q`[data$Time==2])

Post-Pre

Post=mean(data$MCAv[data$Time==4])/mean(data$MAP[data$Time==4])
Pre= mean(data$MCAv[data$Time==2])/mean(data$MAP[data$Time==2])

Post-Pre

Post=mean(data$`ICA Q`[data$Time==4])/mean(data$MAP[data$Time==4])
Pre= mean(data$`ICA Q`[data$Time==2])/mean(data$MAP[data$Time==2])

Post-Pre
```

Appendix A. R studio package: Pre high altitude minus pre sea-level changes scores

Appendix B

```
mean(data$HR[data$Time==4])-mean(data$HR[data$Time==3])

mean(data$MAP[data$Time==4])-mean(data$MAP[data$Time==3])

mean(data$MCAv[data$Time==4])-mean(data$MCAv[data$Time==3])

mean(data$`MCA PI`[data$Time==4])-mean(data$`MCA PI`[data$Time==3])

mean(data$SaO2[data$Time==4])-mean(data$SaO2[data$Time==3])

mean(data$PetO2[data$Time==4])-mean(data$PetO2[data$Time==3])

mean(data$PETCO2[data$Time==4])-mean(data$PETCO2[data$Time==3])

mean(data$Diameter[data$Time==4])-mean(data$Diameter[data$Time==3])

mean(data$`ICA V`[data$Time==4])-mean(data$`ICA V`[data$Time==3])

mean(data$`ICA Q`[data$Time==4])-mean(data$`ICA Q`[data$Time==3])

mean(data$`ICA PI`[data$Time==4])-mean(data$`ICA PI`[data$Time==3])

mean(data$DF[data$Time==4])-mean(data$DF[data$Time==3])
```

Appendix B. R-studio package: Pre-post high-altitude change scores.

Appendix C

```
analysis=t.test(data$HR[data$Time==3],data$HR[data$Time==4], paired=TRUE)
print(analysis)

analysis=t.test(data$MAP[data$Time==3],data$MAP[data$Time==4], paired=TRUE)
print(analysis)

analysis=t.test(data$MCAv[data$Time==3],data$MCAv[data$Time==4], paired=TRUE)
print(analysis)

analysis=t.test(data$`MCA PI`[data$Time==3],data$`MCA PI`[data$Time==4], paired=TRUE)
print(analysis)

analysis=t.test(data$SaO2[data$Time==3],data$SaO2[data$Time==4], paired=TRUE)
print(analysis)

analysis=t.test(data$PetO2[data$Time==3],data$PetO2[data$Time==4], paired=TRUE)
print(analysis)

analysis=t.test(data$PETCO2[data$Time==3],data$PETCO2[data$Time==4], paired=TRUE)
print(analysis)

analysis=t.test(data$Diameter[data$Time==3],data$Diameter[data$Time==4], paired=TRUE)
print(analysis)

analysis=t.test(data$`ICA V`[data$Time==3],data$`ICA V`[data$Time==4], paired=TRUE)
print(analysis)

analysis=t.test(data$`ICA Q`[data$Time==3],data$`ICA Q`[data$Time==4], paired=TRUE)
print(analysis)

analysis=t.test(data$`ICA PI`[data$Time==3],data$`ICA PI`[data$Time==4], paired=TRUE)
print(analysis)

analysis=t.test(data$DF[data$Time==3],data$DF[data$Time==4], paired=TRUE)
print(analysis)
```

Appendix C. R-studio package: Pre-post high altitude paired t-tests.

Appendix D

```
mean(data$MAP[data$Time==2])-mean(data$MAP[data$Time==1])

mean(data$MCAv[data$Time==2])-mean(data$MCAv[data$Time==1])

mean(data$`MCA PI`[data$Time==2])-mean(data$`MCA PI`[data$Time==1])

mean(data$SaO2[data$Time==2])-mean(data$SaO2[data$Time==1])

mean(data$PetO2[data$Time==2])-mean(data$PetO2[data$Time==1])

mean(data$PETCO2[data$Time==2])-mean(data$PETCO2[data$Time==1])

mean(data$Diameter[data$Time==2])-mean(data$Diameter[data$Time==1])

mean(data$`ICA V`[data$Time==2])-mean(data$`ICA V`[data$Time==1])

mean(data$`ICA Q`[data$Time==2])-mean(data$`ICA Q`[data$Time==1])

mean(data$`ICA PI`[data$Time==2])-mean(data$`ICA PI`[data$Time==1])

mean(data$DF[data$Time==2])-mean(data$DF[data$Time==1])
```

Appendix D. R-studio package: Pre-post sea-level change scores.

Appendix E

```
analysis=t.test(data$MAP[data$Time==1],data$MAP[data$Time==2], paired=TRUE)
print(analysis)

analysis=t.test(data$MCAv[data$Time==1],data$MCAv[data$Time==2], paired=TRUE)
print(analysis)

analysis=t.test(data$`MCA PI`[data$Time==1],data$`MCA PI`[data$Time==2], paired=TRUE)
print(analysis)

analysis=t.test(data$SaO2[data$Time==1],data$SaO2[data$Time==2], paired=TRUE)
print(analysis)

analysis=t.test(data$PetO2[data$Time==1],data$PetO2[data$Time==2], paired=TRUE)
print(analysis)

analysis=t.test(data$PETCO2[data$Time==1],data$PETCO2[data$Time==2], paired=TRUE)
print(analysis)

analysis=t.test(data$Diameter[data$Time==1],data$Diameter[data$Time==2], paired=TRUE)
print(analysis)

analysis=t.test(data$`ICA V`[data$Time==1],data$`ICA V`[data$Time==2], paired=TRUE)
print(analysis)

analysis=t.test(data$`ICA Q`[data$Time==1],data$`ICA Q`[data$Time==2], paired=TRUE)
print(analysis)

analysis=t.test(data$`ICA PI`[data$Time==1],data$`ICA PI`[data$Time==2], paired=TRUE)
print(analysis)

analysis=t.test(data$DF[data$Time==1],data$DF[data$Time==2], paired=TRUE)
print(analysis)
```

Appendix E. R-studio package: Pre to post sea-level paired t-test.

Appendix F

```
score=t.test(data$...2[data$...1==1],data$...2[data$...1==2])
print(score)

shapiro.test(data$...2)

wilcox.test(data$PETCO2[data$Time==1],data$PETCO2[data$Time==2])

mean(data$...2[data$...1==2])-mean(data$...2[data$...1==1],)
```

Appendix F. R-studio package: Shapiro-Wilk test.

Appendix G

The experimental chapter (i.e., chapter 4) was performed with approval for a secondary analysis from the University of Victoria 23-0629. The original study was approved by the University of British Columbia Ethics Committee, the Nepal Health Medical Research Council, and conformed to the standards set by the Declaration of Helsinki.

A version of the study presented in Chapter 4, “Mechanisms of cerebral artery compliance at sea-level and following acclimation to high altitude”. Underwood Destiny R1, Craig Tabitha V1, Smith, Brianne D1, Day Trevor2, Willie Chris K3, Lucas Samuel JE4, Burgess Keith R. 5,6, Ainslie Philip N2, Smith Kurt J1. I was responsible for all data analysis and interpretation, written presentation of results, and the conceptualization of the secondary analysis and manuscript preparation for submission to the Journal of Experimental Physiology in 2024.